65–13,886

GILBERT, Joel Sterling, 1935–
MEASUREMENT OF THE EXCHANGE OF RADIANT ENERGY BETWEEN PARALLEL WALLS.

The University of Oklahoma, Ph.D., 1965
Engineering, mechanical

University Microfilms, Inc., Ann Arbor, Michigan

THE UNIVERSITY OF OKLAHOMA

GRADUATE COLLEGE

MEASUREMENT OF THE EXCHANGE OF RADIANT ENERGY BETWEEN PARALLEL WALLS

A DISSERTATION

SUBMITTED TO THE GRADUATE FACULTY

in partial fulfillment of the requirements for the

degree of

DOCTOR OF PHILOSOPHY

BY

JOEL STERLING GILBERT

Norman, Oklahoma

1965

MEASUREMENT OF THE EXCHANGE OF RADIANT ENERGY

BETWEEN PARALLEL WALLS

APPROVED BY

J. J. Sone

C. M. Sliepcevich

Robert M. St. John

W. Kobach

C. W. Cook

DISSERTATION COMMITTEE

ABSTRACT

An experimental investigation was undertaken to determine at what spacing two congruent, parallel and directly opposed plane areas would approximate parallel surfaces of infinite extent in the determination of the net flux of radiant energy at either of the surfaces. Measurements were made of the net radiation from a 5.5 inch square located at the center of a 12 inch square plate opposing a similar 12 inch square plate.

The study was accomplished by designing and building an apparatus from which experimental data were secured. To evaluate the experimental results, two computational methods were used.

One of the computational methods was for infinite parallel geometry and the other was for finite plates. The application of the infinite parallel plane computation was found to be acceptable for the center portion of plates with spacings up to 0.5 inch for plates which were one foot square.

By placing aluminum foil around the border zone formed by the edges of the plates, infinite parallel walls could be simulated by plates which were one foot square at a spacing of 1.0 inch. By assuming surface temperature, reflectance, and radiosity constant in applying the lumped parameter method, a reasonable mathematical model was formed for the apparatus without aluminum around the border zone and with plate spacings up to 3.0 inches.

ACKNOWLEDGEMENTS

An expression of appreciation goes to all of those whose encouragement was important in the completion of this research.

Specific thanks goes to the following:

Dr. Tom J. Love, Jr., chairman of the committee, for his assistance.

The committee composed of Dr. C. H. Cook, Professor W. J. Ewbank, Dr. R. G. Fowler, Dr. D. G. Harden, Dr. C. M. Sliepcevich, and Dr. R. M. St. John for their suggestions and comments.

Mr. W. A. Munter, Mr. E. Z. Million, and Mr. Earl Finch for their assistance.

My wife, Evelyn, and children, Sharon Lynn and Brian Joel for their patience.

Funding for the research was provided by the Aerospace Research Laboratories, Office of Aerospace Research, United States Air Force. A National Science Foundation grant GP-360 provided the funds for a major portion of the equipment.

TABLE OF CONTENTS

TABLE OF CONTENTS (continued)

LIST OF TABLES

LIST OF ILLUSTRATIONS

LIST OF ILLUSTRATIONS (continued)

LIST OF ILLUSTRATIONS (continued)

MEASUREMENT OF THE EXCHANGE OF RADIANT ENERGY BETWEEN PARALLEL WALLS

CHAPTER I

STATEMENT OF THE PROBLEM

The need for an improved understanding of radiant heat transfer in a scattering, absorbing, and emitting medium is important. Specific examples of the transmission of radiant energy being altered by media having local inhomogeneities are the cases of fibrous thermal insulation material between two parallel walls and of luminous particles in the exhaust gases of a solid propellant rocket. Another example would be the particles of ablative material near the heat shield of a spacecraft during re-entry.

An analysis for considering the radiant energy exchange in various media was proposed by Love (1).[1] In his analysis the equation for the transfer of radiant energy for a scattering, absorbing, and emitting medium was simplified by restricting the method to axially symmetric, plane parallel geometry. The assumption of infinite, parallel walls was necessary in order to provide a reasonable solution to the

---

[1]Numbers in parentheses refer to items in the bibliography.

equation of radiant transfer. To assist in the evaluation of any computational analysis, some experimental observations should be made and compared with computed values. Because of the assumption of plane parallel geometry, any walls or planes used in an experimental apparatus would be required to be infinite in length and width. The infinite extent of the walls dictates that the net flux at either surface would not be a function of the distance between the surfaces. Because creating an environment which exactly satisfies the assumption of infinite, parallel walls would be impossible, the effect of finite plates on the results of an experimental study involving a medium between plates was required.

This research effort measured the exchange of radiant energy between infinite parallel walls without a medium between the plates. Hence, the object of this experimental investigation was to determine how closely infinite plane walls could be approximated by finite plates. As the original objective involved the experimental study of the transfer of radiant energy through particulate media, a discussion of the major problems connected with the generation of the desired medium is given in Appendix A, together with the development of the equipment. Radiant energy measurements involving particulate media were not made; hence, the major research effort was concerned with an environment without particles.

A logical extension of this study would be a measurement of net flux at either of the two surfaces bounding a scattering, absorbing, and emitting medium for comparison with the computed values of net radiant exchange.

A careful search of the literature found no experimental work reporting the net radiant flux at one of the surfaces of two, finite, parallel walls which were maintained at different temperatures. An experiment suggested by Worthing (2) was closely related to this research as he proposed that the rate of transfer of energy by radiation between two parallel plates be used to determine the total hemispherical emittance of the plates. By using the same material for both surfaces, only one emittance value would exist, and by knowing the net energy transfer rate and the surface temperatures, the value of emittance could then be computed. In his proposed experiment, the spacing of the plates would be extremely small with no provision for altering the spacing.

Purpose Of This Work

The primary objective of this experimental investigation was to measure the exchange of radiant energy between two congruent, parallel, and directly opposed plane areas. Tests were conducted to determine if the equipment would give reproducible data with the walls at a fixed spacing. In evaluating the effect of spacing of the walls on the exchange of radiant energy, three positions were selected for the walls.

The second objective was to determine if infinite, parallel plates could be simulated by placing aluminum foil around the border zone of the plates. Some experimental observations were made in the presence of a sandblasted stainless steel shield between the original walls.

The third objective was to make a comparison between the experimental values and the computed values of net radiant flux. By using the computational method for infinite, parallel plates, the object was to determine how closely infinite plane walls could be approximated by finite plates. The two remaining methods used were for finite plates. By also using the finite computations for comparison, a technique was available for describing the radiant transfer of energy at large plate spacings.

CHAPTER II

LITERATURE SURVEY

This survey of the literature covers two general areas. First is the measurement or the determination of the net radiant energy exchange between two walls. Problems involving radiant heat transfer require a knowledge of surface properties which are characterized by values of emittance. The second topic covers various surface emittances.

Net Radiant Exchange

All the experimental approaches in the literature involved measuring the emittance of various surfaces and then calculating the net radiant exchange between the surfaces. An experiment proposed by Worthing (2) suggested measuring the net radiant exchange of energy of parallel walls and from these results calculating the total hemispherical emittance.

Chapman (3), in his text on heat transfer, covers most of the traditional concepts of radiant transfer. In a text to be published, Love (4) has extended these concepts to provide a solution to specific engineering problems. Another topic presented by Love (1) is a method for computing the net radiative heat transfer between parallel, diffusely reflecting, and emitting surfaces bounding absorbing, scattering, and emitting media.

Typical of other theoretical approaches to specific radiative problems is the paper by Sparrow, Gregg, Szel, and Manos (5) for analysis of radiation between simply arranged gray surfaces.

An interesting computation by Branstetter (6), for the net radiant heat flow between two infinite, parallel, tungsten plates compiled by summing the monochromatic energy exchange, yields fluxes ranging from approximately 8 to 25 percent greater than the results of gray-body computations based on the same emissivity data. Goodman (7) made a similar study using aluminum walls and Inconel walls. He found that assuming the plates to be gray bodies introduced an error of 2 to 29 percent in the computed heat transfer rate.

Surface Emittance

There is but one surface whose radiating characteristics are known from theoretical considerations, the black body. These radiation characteristics are completely determined by the temperature of the black body and certain experimental constants. Hence, the radiation properties of all real surfaces must be determined experimentally.

The most complete single source of information is the 1960 Thermal Radiation Properties Survey by Gubareff, Janssen, and Torborg (8). Considering exclusively the emittance of stainless steels, Wood, Deem, and Lucks (9) have compiled a thorough listing of test data.

One of the total hemispherical emittance values used by this author was determined by Richmond and Harrison (10). The equipment and procedures used in making the above measurement was also discussed by Richmond and Harrison (11). Simmilar measurements were made by O'Sullivan and Wade (12) for Inconel and Inconel X. Total normal emissivity measurements on typical aircraft materials, including several of the stainless steels, were conducted by Snyder, Gier, and Dunkle (13). A comparison of measured total emittances with values computed from spectral measurements for 25 different samples, many of which were stainless steels, was made by Bevens, Gier, and Dunkle (14). Fletcher and Leppert (15) at Stanford University, using two concentric spheres, measured the total hemispherical emittance of Type 304 stainless steel. Ewbank, Townsend and Keutser (16) conducted a similar experiment at the University of Oklahoma using Type 302 stainless steel which had been sandblasted.

Clauss (17) contains many papers and discussions on emittance measurements presented during the first symposium on "Surface Effects On Spacecraft Materials" held in May, 1959 at Palo Alto, California. Of general interest are the final two references. Maki and Plyler (18) discuss a method of measuring normal spectral emissivities in the infrared region from 1 to 13 microns. The apparatus described by Maki, Stair, and Johnston (19) was for similar measurements, but it included coatings or oxides which tightly adhere to metals.

CHAPTER III

DEVELOPMENT OF EQUATIONS

The expression for net radiative flux for infinite, parallel planes which are diffuse is a basic equation found in most heat transfer texts.

$$Q = \frac{\sigma \left(T_2^4 - T_4^4 \right)}{\left(\frac{1}{\epsilon_2} \right) + \left(\frac{1}{\epsilon_4} \right) - 1} \qquad (3.1)$$

The total hemispherical emittance values were assumed constant with respect to temperature.

The locations of the temperatures and of the values of emittance are given in Figure 1 together with the geometry for the computations. To provide consistency in the definitions of the symbols, those suggested by Love (4) were used, see Appendix B.

As it was probable that at large spacings infinite parallel planes could not be closely approximated with finite walls, two other computational methods were considered. By assuming that the walls represented two sides of an enclosure, with the other four sides formed by the open space around the edges of the plates, another method of determining the net radiant flux at either surface was available, see Figure 2.

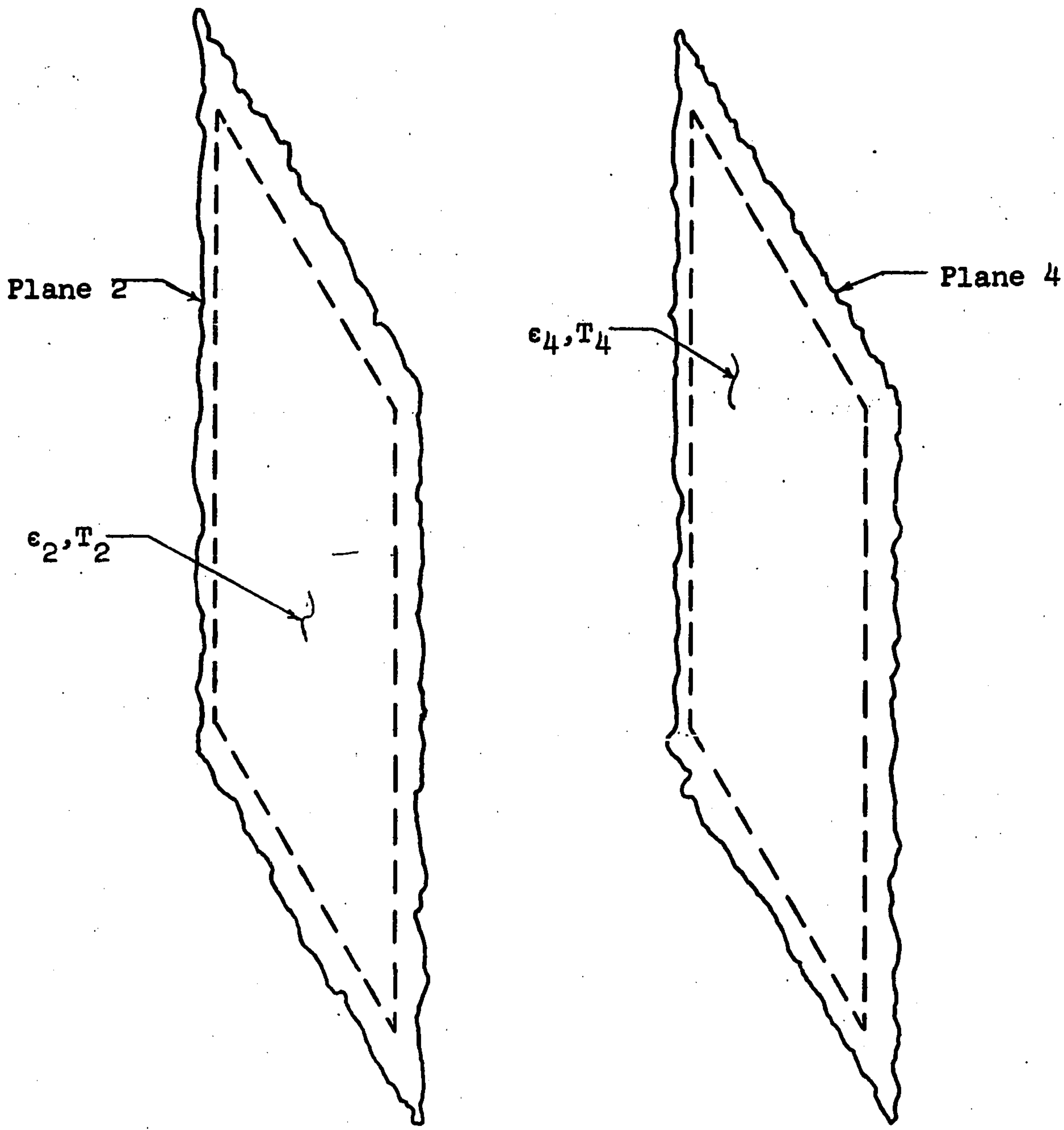

Figure 1

Infinite Parallel Planes

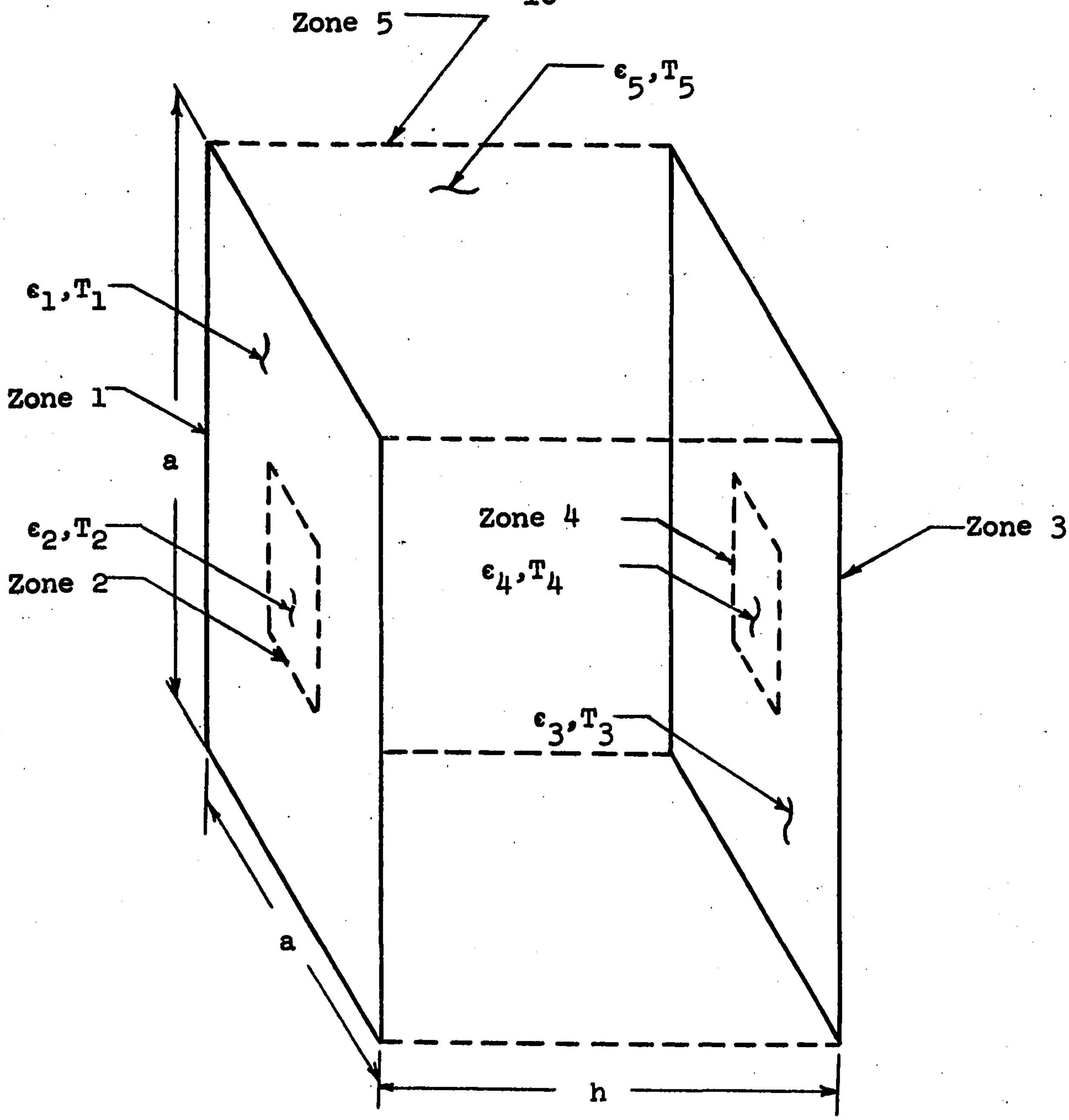

Figure 2

Geometry for Finite Parallel Planes With Zones for Lumped System Approximation

This second method, the lumped parameter system, uses the concept of radiosity which is defined as the flux leaving a surface due to the energy emitted from that surface and the energy reflected from it. The basic monochromatic equation for the lumped parameter method is given as

$$R_{\nu,i} = \pi\epsilon_{\nu,i} I_{b,\nu}(T_i) + \rho_{\nu,i} \sum_{j=1}^{n} R_{\nu,j} F_{ij} \tag{3.2}$$

The term containing $I_{b,\nu}$ in equation 3.2 represents the energy emitted from surface i, while the second term is the energy reflected from surface i due to the emission of radiant energy from all of the other surfaces.

The configuration factor, F_{ij}, is defined by the following expression:

$$F_{ij} = \frac{1}{\pi A_i} \iiiint_{A_i A_j} \frac{\cos \varphi_i \cos \varphi_j \, dA_i \, dA_j}{r_{ij}^2} \tag{3.3}$$

The locations of the polar angle, φ, and other terms are given in Figure 3.

Diffuse reflectance was assumed, and the definition of black body intensity was used; therefore, the surfaces were defined as gray surfaces, and equation 3.2 is rewritten as

$$R_i = \epsilon_i \sigma T_i^4 + \rho_i \sum_{j=1}^{n} R_j F_{ij} \tag{3.4}$$

In the application of the lumped parameter system to the parallel plate problem, the geometry was thought of as an

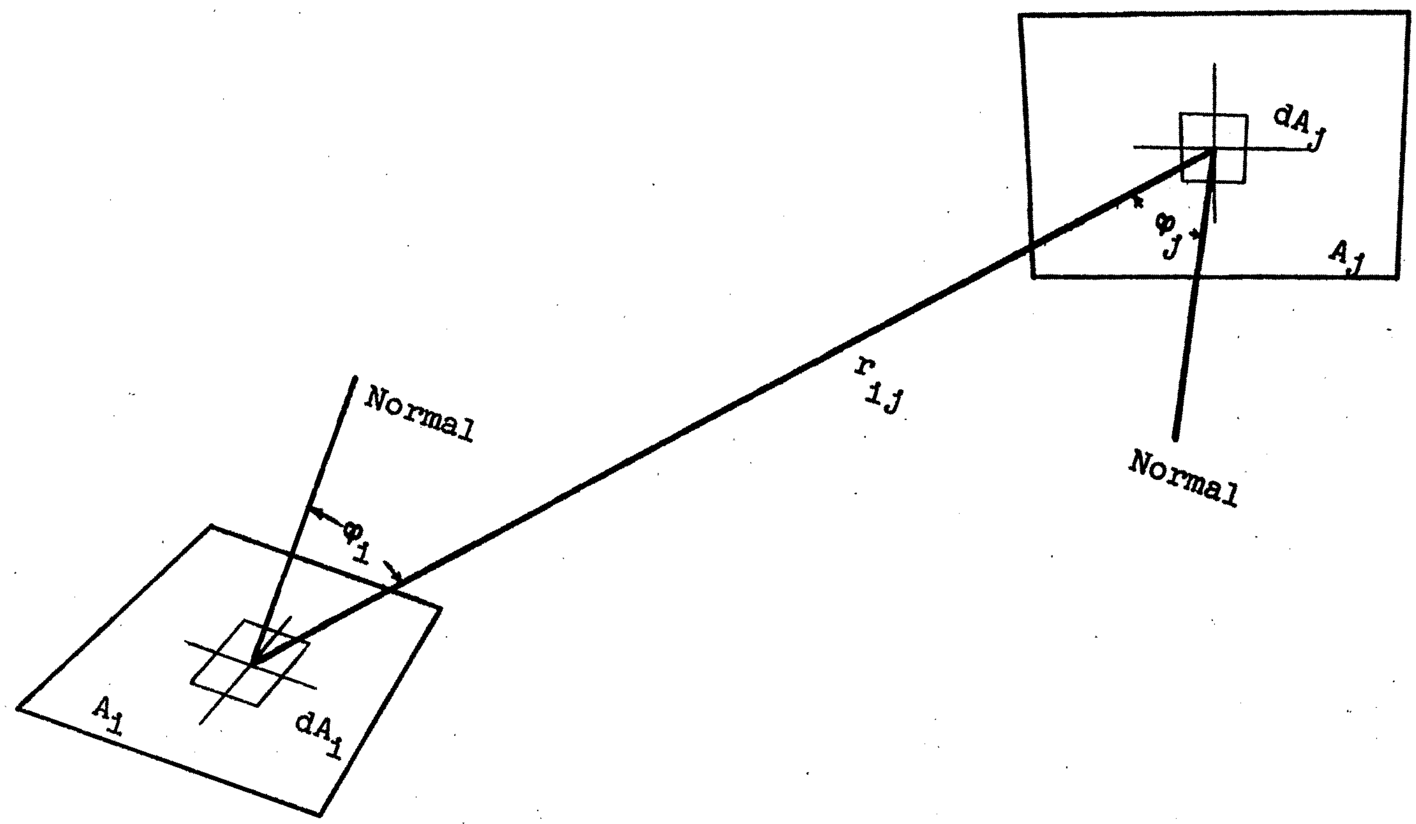

Figure 3
A Sketch Showing Polar Angles Used in Shape Factors

enclosure divided into a finite number of areas. This method was distinguished from the third and last computation by the assumption that the parameters, surface temperature, reflectance, and radiosity were assumed constant over each area or zone.

Writing equation 3.4 in matrix form using a matrix inversion yields:

$$\left[R_i \right] = \left[\frac{\delta_{ij}}{\rho_i} - F_{ij} \right]^{-1} \left[\frac{\epsilon_i}{\rho_i} \sigma T_i^4 \right] \tag{3.5}$$

The Kronecker Delta, δ_{ij}, is defined as follows:

$$\delta_{ij} = 0 \qquad i \neq j$$
$$\delta_{ij} = 1 \qquad i = j$$

The determination of the net flux at any surface of the enclosure is given by

$$Q_i = R_i - \sum_{j=1}^{n} R_j F_{ij} \tag{3.6}$$

or in terms of only the properties of one surface

$$Q_i = \frac{\epsilon_i}{\rho_i} (\sigma T_i^4 - R_i) \tag{3.7}$$

where a positive Q_i represents an energy loss from the surface. If the reflectance is 0, then equation 3.4 and equation 3.6 must be used in place of equation 3.5 and equation 3.7 because of division by 0.

The third and final computation which can be performed in the determination of the net flux was by the method of quadrature. The geometry was again that of two parallel surfaces with the details shown in Figure 4. The basic radiosity equation for the quadrature method is as follows:

$$R(x_p, y_q) = \epsilon\sigma T^4 + \frac{\rho h^2}{\pi} \sum_{r=1}^{n} \sum_{s=1}^{n} \frac{W_r W_s R(x_r, y_s)}{[(x_p - x_r)^2 + (y_q - y_s)^2 + h^2]^2} \tag{3.8}$$

The weight factors of the Gaussian quadrature are the W's, and the ordinates are the x's and y's.

To simplify the handling of this problem, equation 3.8 is converted to a nondimensional radiosity equation. This transformation is accomplished by

$$X_s = \frac{x_s}{a}, \qquad H = \frac{h}{a}$$
$$Y_s = \frac{y_s}{a}, \qquad B(X,Y) = \frac{R(x,y)}{\epsilon\sigma T^4} \tag{3.9}$$

Because only the energy leaving one of the surfaces was required in the determination of the radiosity at that surface, the effect of the temperature at the other surface is considered in equation 3.10 only.

$$B_2(X_p, Y_q) = 1 + \frac{\rho_2 a^4 H^2}{\pi} \sum_{r=1}^{n} \sum_{s=1}^{n} \frac{W_r W_s B_4(X_r, Y_s)}{[a^2(X_p - X_r)^2 + a^2(Y_q - Y_s)^2 + H^2]^2} \tag{3.10}$$

$$B_4(X_r, Y_s) = \frac{\rho_4 a^4 H^2}{\pi} \sum_{p=1}^{n} \sum_{q=1}^{n} \frac{W_p W_q B_2(X_p, Y_q)}{[a^2(X_p - X_r)^2 + a^2(Y_q - Y_s)^2 + H^2]^2} \tag{3.11}$$

Equations 3.10 and 3.11 were combined to form the radiosity at surface 2.

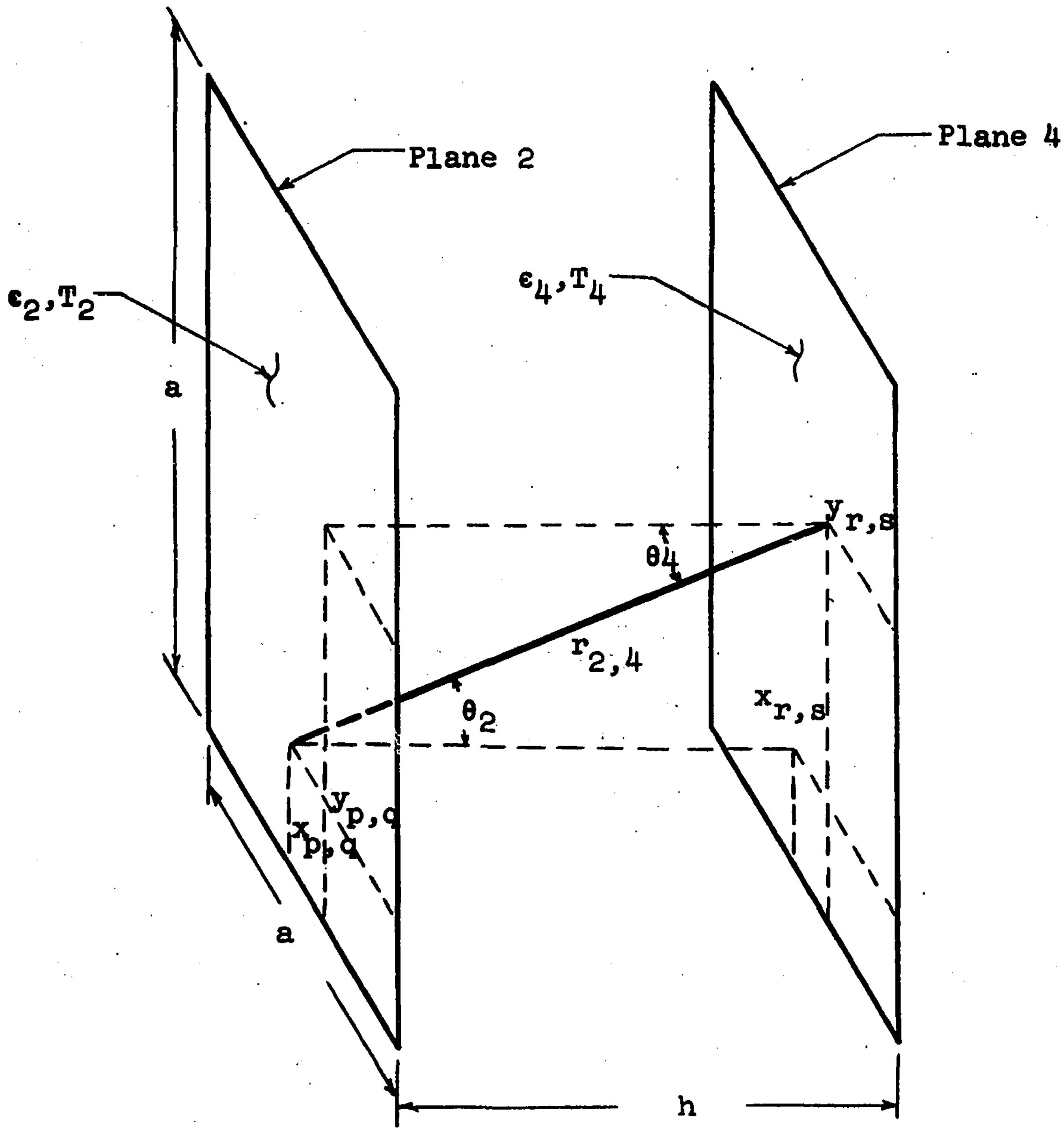

Figure 4

Geometry for Finite Parallel Planes for Variable Radiosity Calculation

$$R_2 = \epsilon_2 \sigma T_2^4 B_2(X_p, Y_q) + \epsilon_4 \sigma T_4^4 B_4(X_r, Y_s) \tag{3.12}$$

Knowing the radiosity at surface 2, the net flux can be found by using equation 3.7. As n is increased in equations 3.10 and 3.11 from 3 to 4, for example, the number of simultaneous equations increases from 18 to 32. Results for n = 1, 2, 3, and 4 will be discussed in the chapter on calculated results. Thus, the three methods used for computing values to compare with the experimental data have been outlined. When a shield was placed between the two walls, the infinite, parallel plane method and the lumped parameter method were used in computing the net radiant flux.

CHAPTER IV

EQUIPMENT DESIGN AND DESCRIPTION

The design criteria used in accomplishing the objective of this research were as follows:

1. The material selected for the faces of the walls was required to withstand elevated temperatures in a moderate vacuum environment. The selection was also restricted to surfaces similar to materials for which total hemispherical emittance values were known.
2. The vacuum between the two plates was required to be sufficiently high to eliminate convective heating effects to allow for the measurement of radiant heat flux only.

Selection of Surfaces and Emittance Values

A stainless steel surface met the requirement of withstanding elevated temperatures in a moderate vacuum environment. Also the gaseous content of a stainless metal tends to be lower than that of other materials. Type 302 stainless steel, the material used in this research, is listed in Table 1 for comparison with other stainless steels for which emittance values are available.

The total hemispherical emittance is the amount of

TABLE 1

COMPOSITION OF SURFACES

Stainless Steel Type No.	C	Mn Max.	P Max.	S Max.	Si Max.	Cr	Ni	Mo	Other Elements
302	0.15 Max.	2.00	0.045	0.030	1.00	17.00 19.00	8.00 10.00		
321	0.08 Max.	2.00	0.045	0.030	1.00	17.00 19.00	9.00 12.00		Ti 5 x C min.
430	0.12 Max.	1.00	0.040	0.030	1.00	14.00 18.00			
Inconel Nominal Composition	0.06	0.25		0.007	0.25	15.0	77.0		Cu 0.2 Fe 7.0

radiant energy emitted, per unit area and time, expressed as a function of the energy emitted by a black body or complete radiator under the same conditions. The total hemispherical emittance of a specimen is altered by its internal structure, chemical composition, surface texture, and thickness if it is not completely opaque. To achieve the required diffuse surface condition, the plates were sandblasted as described in the section on surface preparation. The sandblasting procedure was the same as the technique used by Richmond and Harrison (10) in preparing samples of stainless steel Types 321, 430, and Inconel. Even with the large variation in composition between Inconel and Type 321 stainless steel, the total hemispherical emittance ranged from 0.50 to 0.65 for all the data points from 400°F to 1450°F. Richmond and Harrison (10) found that for the three alloys considered the surface condition of the metal had more effect on the total hemispherical emittance of the unoxidized and uncoated specimen than did the composition of the alloys. An estimated total hemispherical emittance value of 0.535 was selected from the data available for Type 321 stainless steel because of its similarity to Type 302 which was used in this research work.

An independent measurement was made by Avco Corporation in Tulsa, Oklahoma, using samples supplied by the author. These results are discussed in Appendix C and illustrated in Figure 5. These measurements give almost identical results for two samples of Type 302 stainless steel. From a plot of

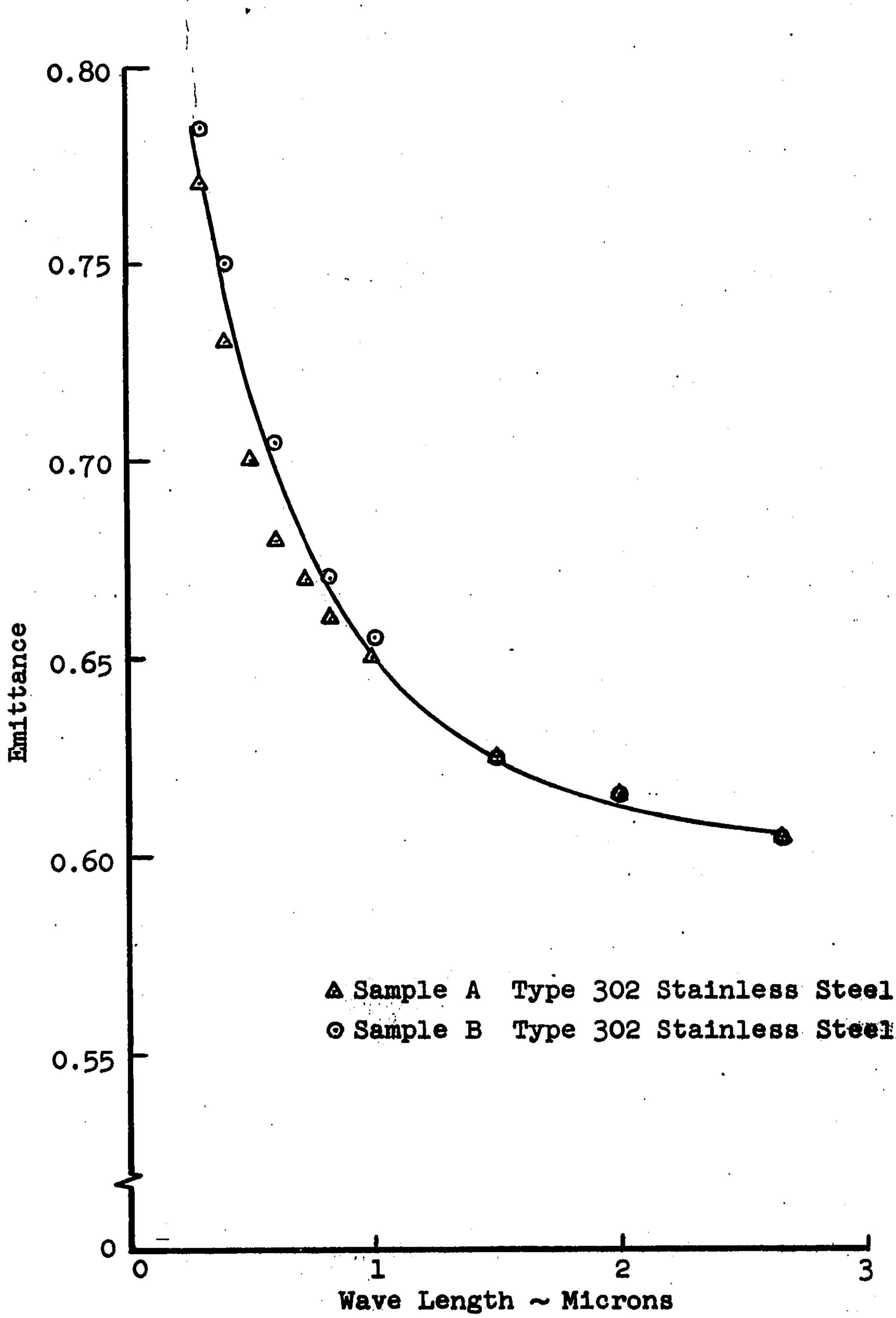

Figure 5
Spectral Emittance of Surfaces

the spectral emissive power in Figure 6 and the computed data in Appendix D, the region of maximum spectral flux density occurs between a wavelength of 3.5 for T = 1500°R and a wavelength of 6.0 for T = 1000°R. Thus, if Figure 6 could be extended, the expected total hemispherical emittance for the region of maximum flux would be between $\epsilon = 0.60$ and $\epsilon = 0.55$. However, it is not known at what temperature these tests were conducted.

Fletcher and Lippert (15) made basic emittance measurements of machined Type 304 stainless steel. The experimental apparatus consisted of two concentric spheres. The inner sphere, which was 1 1/2 inches in diameter, served as the high-temperature emitting material. The 18 inch diameter outer sphere served as the absorber and as a pressure vessel. The results reported by Fletcher and Lippert show a gradual decrease in total hemispherical emittance from approximately 0.4 at 400°F to approximately 0.3 at 1000°F.

Ewbank, Townsend, and Keutzer (16) constructed an apparatus similar to the one built by Fletcher and Lippert (15) and performed emittance measurements on sandblasted Type 302 stainless steel. At 589°F the total hemispherical emittance was determined to be 0.556. The emittance values ranged from 0.671 at 312°F to 0.476 at 765°F. The reading at 589°F was determined at the most stable thermal conditions, according to Ewbank et al.

In summary, the value of emittance equal to 0.556 was used in all of the final computations as it was a measured

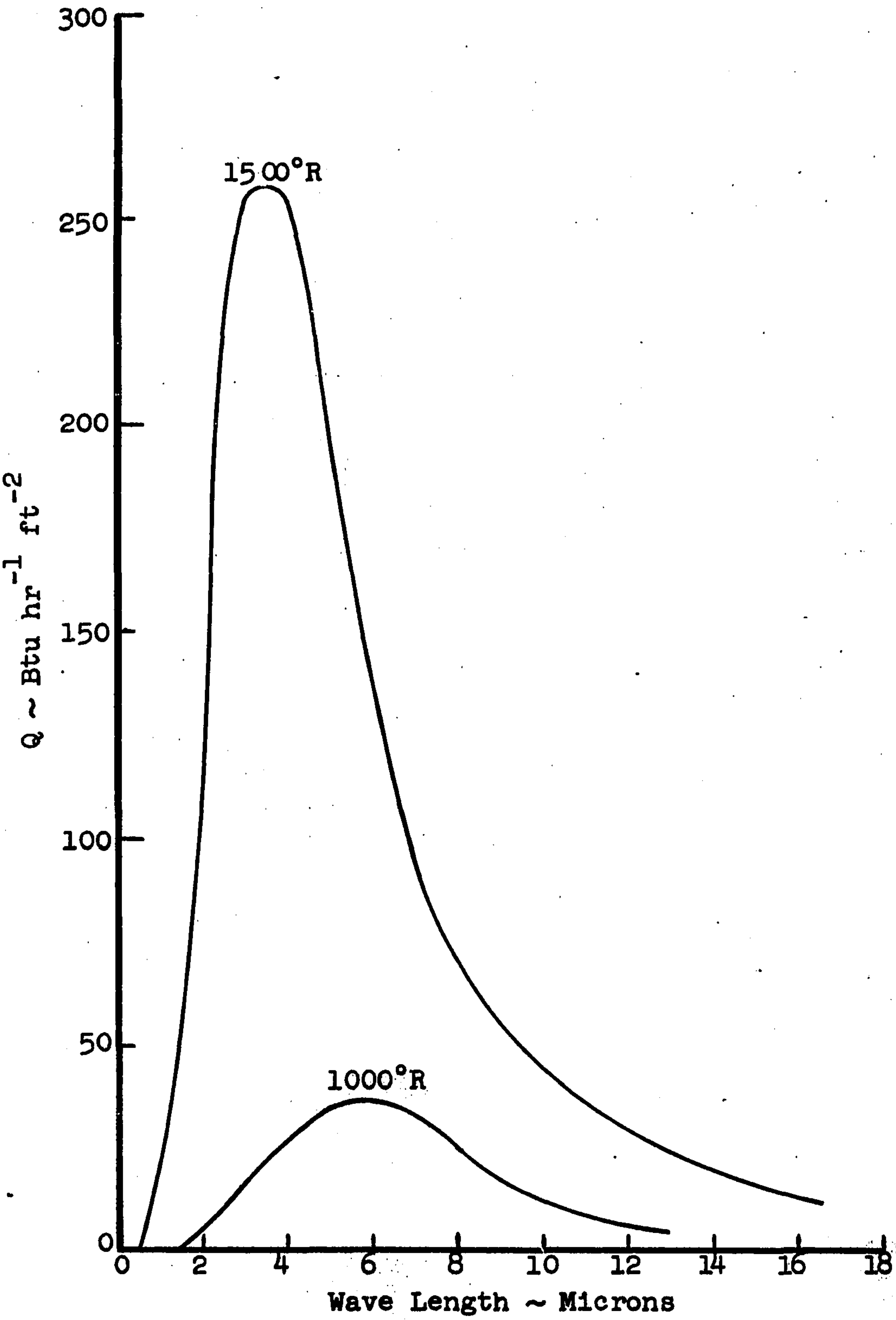

Figure 6
Monochromatic Emissive Power of Surfaces

value of emittance of the material used in the experiment. For comparison, some of the computations were carried out for $\epsilon = 0.535$. A constant value of emittance was chosen because the value of emittance as a function of temperature has not been established.

Convective Effects

A search of the literature, together with the calculations made in Appendix E, show that operations below 1×10^{-4} torr eliminate all significant amounts of energy being transferred by convective heating. Also, the thermal accommodation coefficient, which measures the effectiveness of the energy exchange at the surface, was assumed to be unity, in accordance with the literature. This assumption, together with the calculations in Appendix E, based on the theoretical approach of Rohsenow and Choi (20), was used in energy flux calculations plotted in Figure 7 for Run No. 1.

Since similar experiments were not found in the literature, the design of the experimental equipment was patterned after many ideas found in descriptions of vacuum resistance furnaces. This design evolved by first considering the most desirable type of apparatus and then modifying it to that which could be obtained with the resources available. Specific equipment used is listed in Appendix F.

Equipment Requirements

1. The heater and other parts of the apparatus which were not to be cooled were restricted to materials

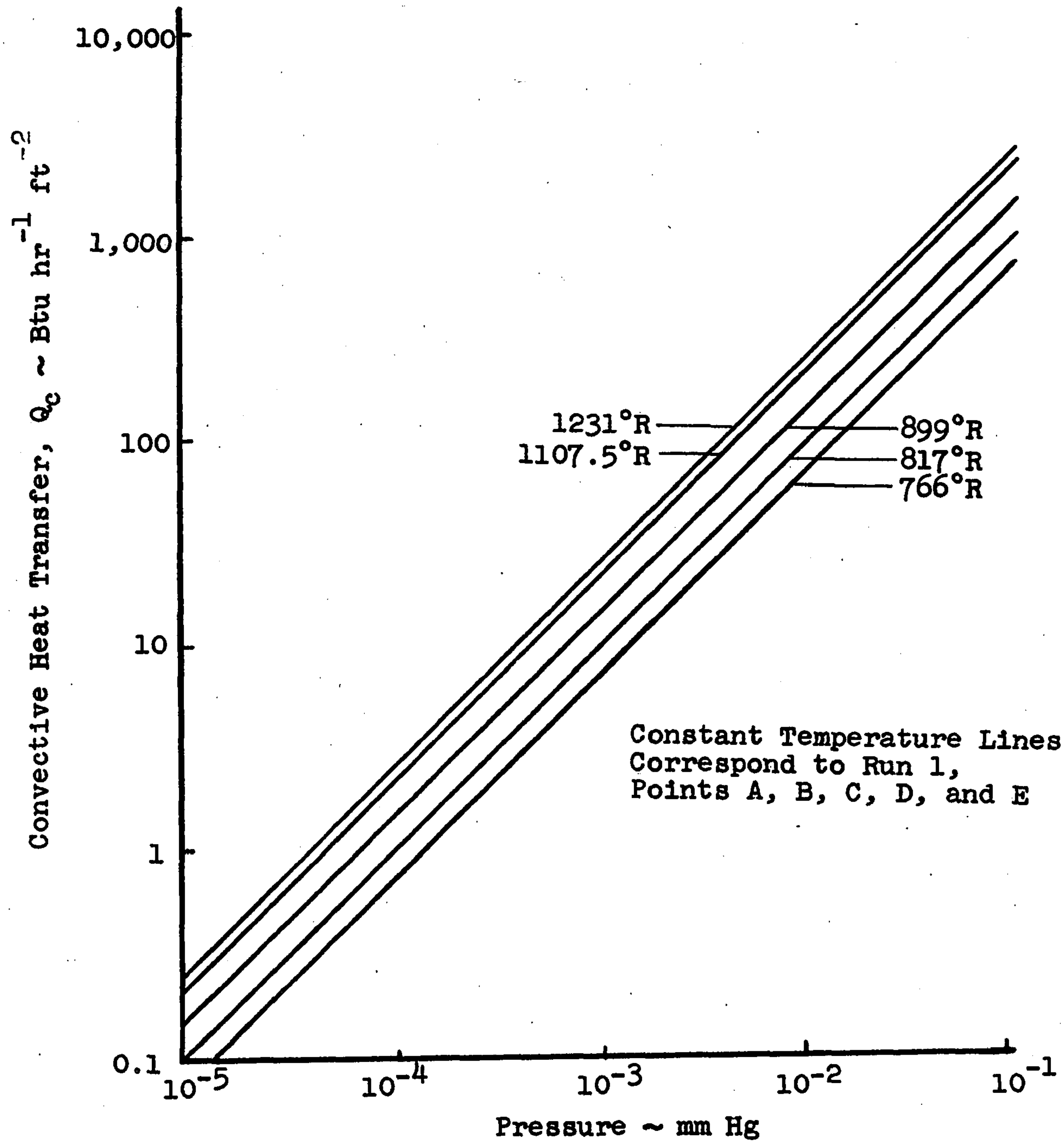

Figure 7

Convective Heating Effects

of construction which could be heated in a vacuum.

2. Because in all of the computations the directional effects of radiant heat transfer were neglected, the surfaces of the hot and cold plates were required to be diffuse.
3. The plates had to be located such that they were flat, parallel, and exactly opposite to each other with the distance between them variable.
4. The ability to measure the energy exchange at one of the surfaces was implied by the computational methods.
5. Instrumentation was desired for maintaining and measuring steady state temperatures while checking the uniformity of the surface temperatures.
6. To allow for variations in the tests which could be conducted, the faces of the plates were required to be removable such that new surfaces could be substituted.

Vacuum System

The National Research Corporation, Model 3307, Pumping System was selected from among systems and components available from five major vacuum equipment manufacturers because the National Research Corporation System was the only one which met the following requirements.

1. The system had to be able to create and maintain a vacuum of 1×10^{-6} torr or better without using liquid nitrogen.

2. Gases entering the chamber due to leakage and the permeability of the system, together with gases released inside the chamber because of desorption and volatilization, create a gas pumping requirement for the vacuum pumps which is in addition to the gases occupying the volume of the chamber. The system was required to have sufficient pumping capacity to remove the gases in excess of the chamber pumping requirement.
3. The system was required to have the highest pumping speed per unit cost within economic considerations.

The description of the vacuum apparatus illustrated by the schematic in Figure 8 and the photographs in Figure 9 and Figure 10 is followed by a discussion of the estimated gas pumping requirements.

The mechanical pump used to rough pump the chamber and to back-pump the diffusion pump is the gas ballasted, two-stage type. Backstreaming of diffusion pump oil into the vacuum chamber was reduced by 98 to 99 percent by a large copper washer which was water cooled and which rested directly on top of the diffusion pump. The diffusion pump was typical of most metal pumps, but it also had an ejector stage which prevented gas bursts from stalling the pump.

For measuring the vacuum conditions in the spool, a gauge control unit provided for measurements from 1 torr to 1×10^{-7} torr. A thermocouple gauge was used for reading to 1×10^{-3} torr; an ionization gauge, which could not be

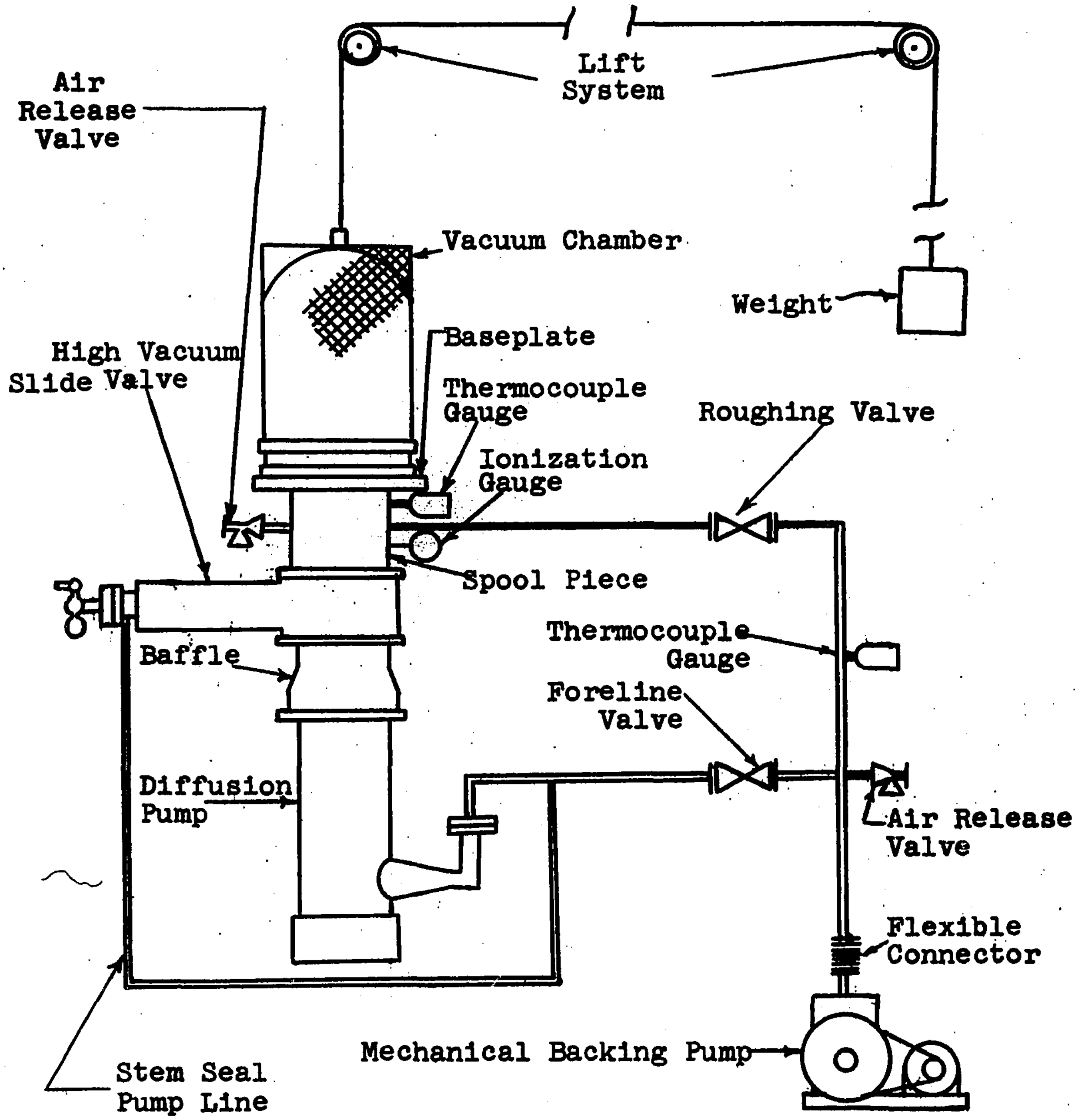

Figure 8

Vacuum Pumping System

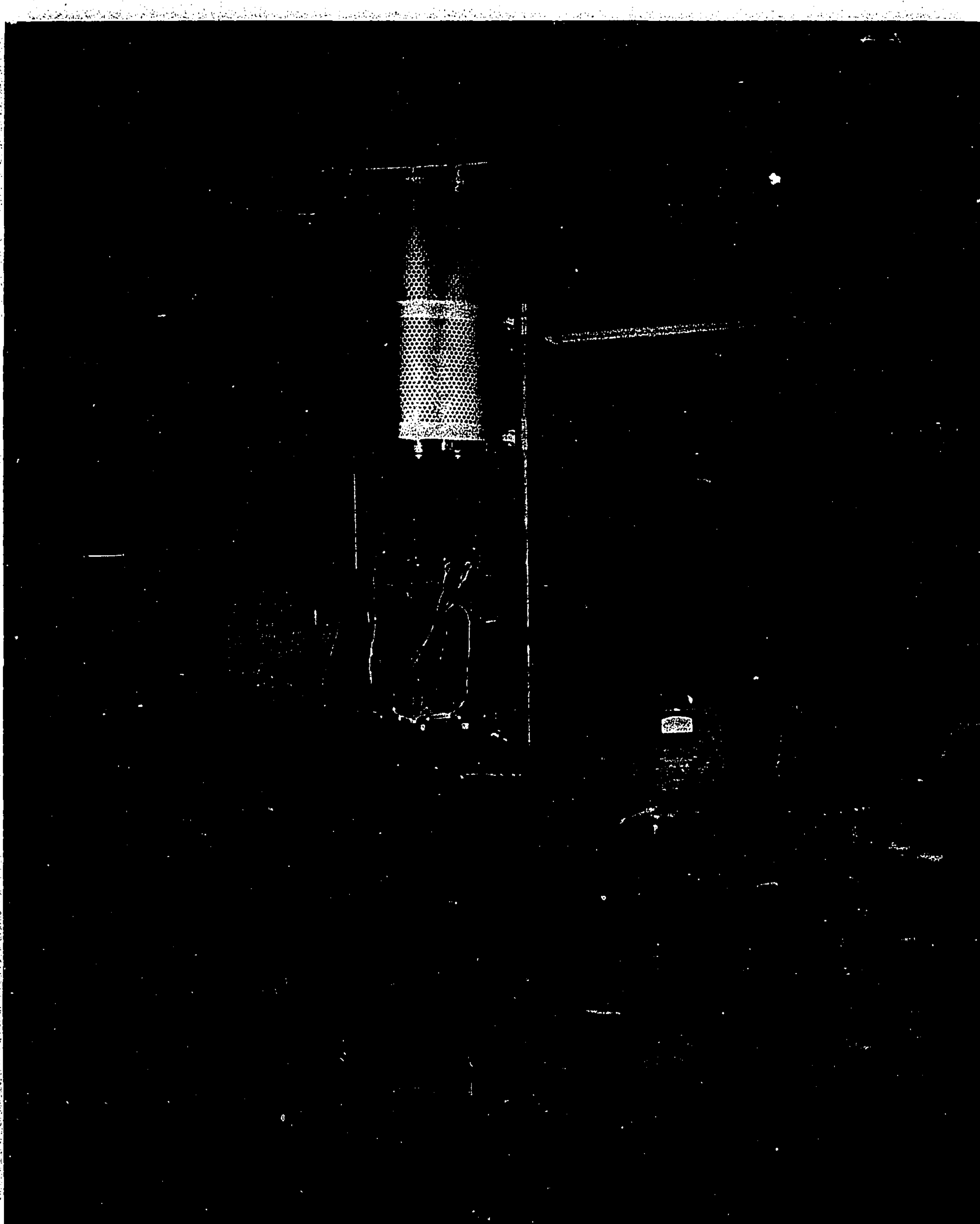

Figure 9

Experimental System

Figure 10

Vacuum Chamber Fixtures

operated above 5×10^{-3} torr, was used down to 1×10^{-7} torr.

In addition to two air release valves, the valves on the rough pumping line and the foreline were bellow valves. A cast aluminum slide valve was used in separating the chamber from the diffusion pump.

A circular chevron liquid nitrogen baffle was located between the diffusion pump and the slide valve. It was never used during actual testing because an improved vacuum was not needed. Pressures below 1×10^{-7} torr were observed when liquid nitrogen was added. For an accurate reading in this range, improved gauging would be necessary.

A 13/16 inch thick, Type 304 stainless steel baseplate with a 32 rms surface finish or better as shown in Figure 11 was designed. Appropriate feed throughs, see Figure 12, were used in making connections to the inside of the vacuum chamber.

An 18 inch diameter by 30 inch high Pyrex bell jar was used as the chamber because of its desirability as a vacuum material. It was not recommended that the bell jar be heated above 300°F during the partial removal of absorbed gases. It was also necessary that the heat be evenly distributed to prevent undue stress on the glass. The heating process can be accomplished satisfactorily using infrared heat lamps.

A bell jar, L-shaped, Viton A, elastomer gasket was used between the ground edge of the bell jar and the baseplate. Dow Corning high vacuum grease was used only between

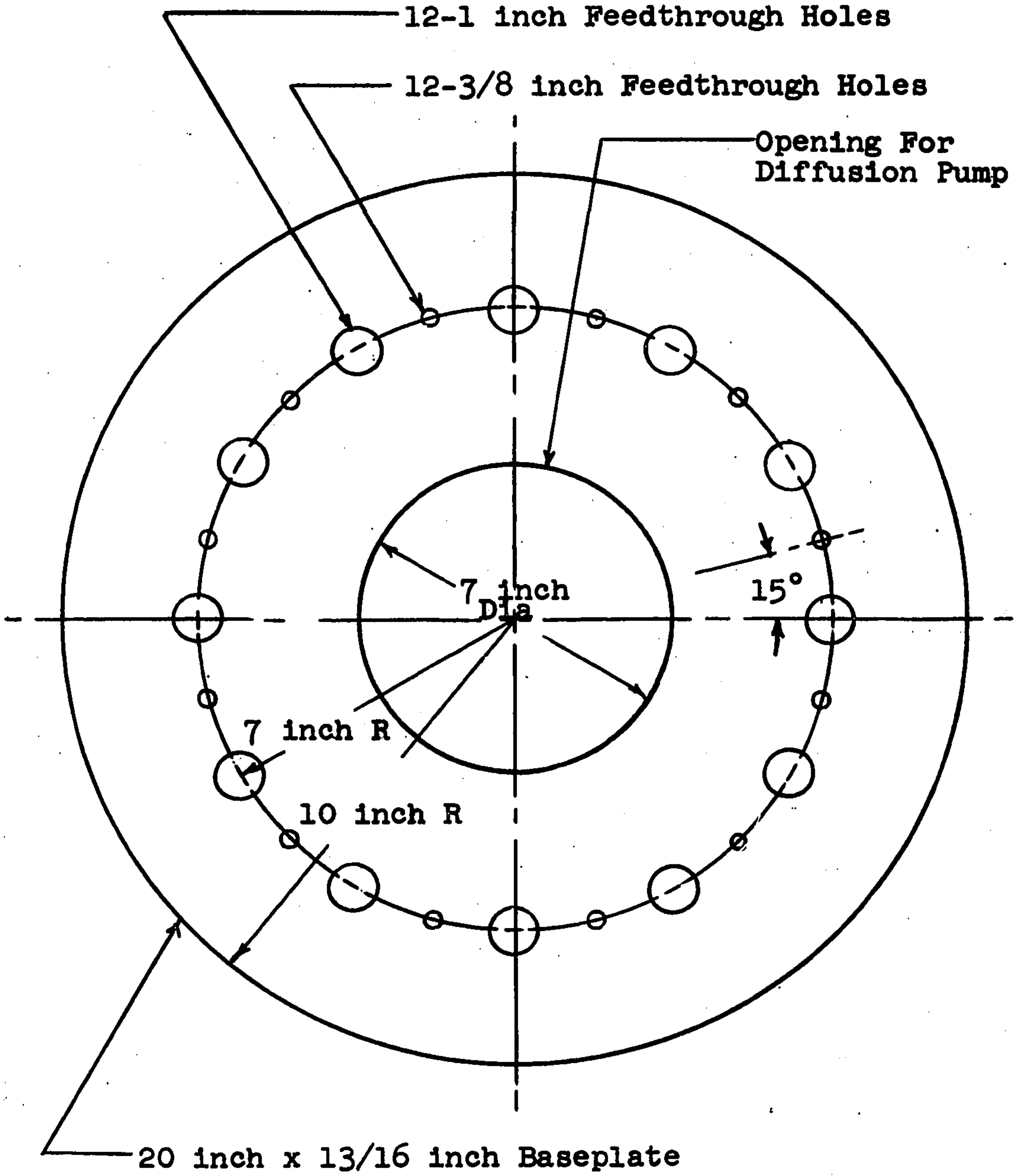

Figure 11

A Sketch of the Baseplate Openings

Vacuum Side

(Inside of Chamber)

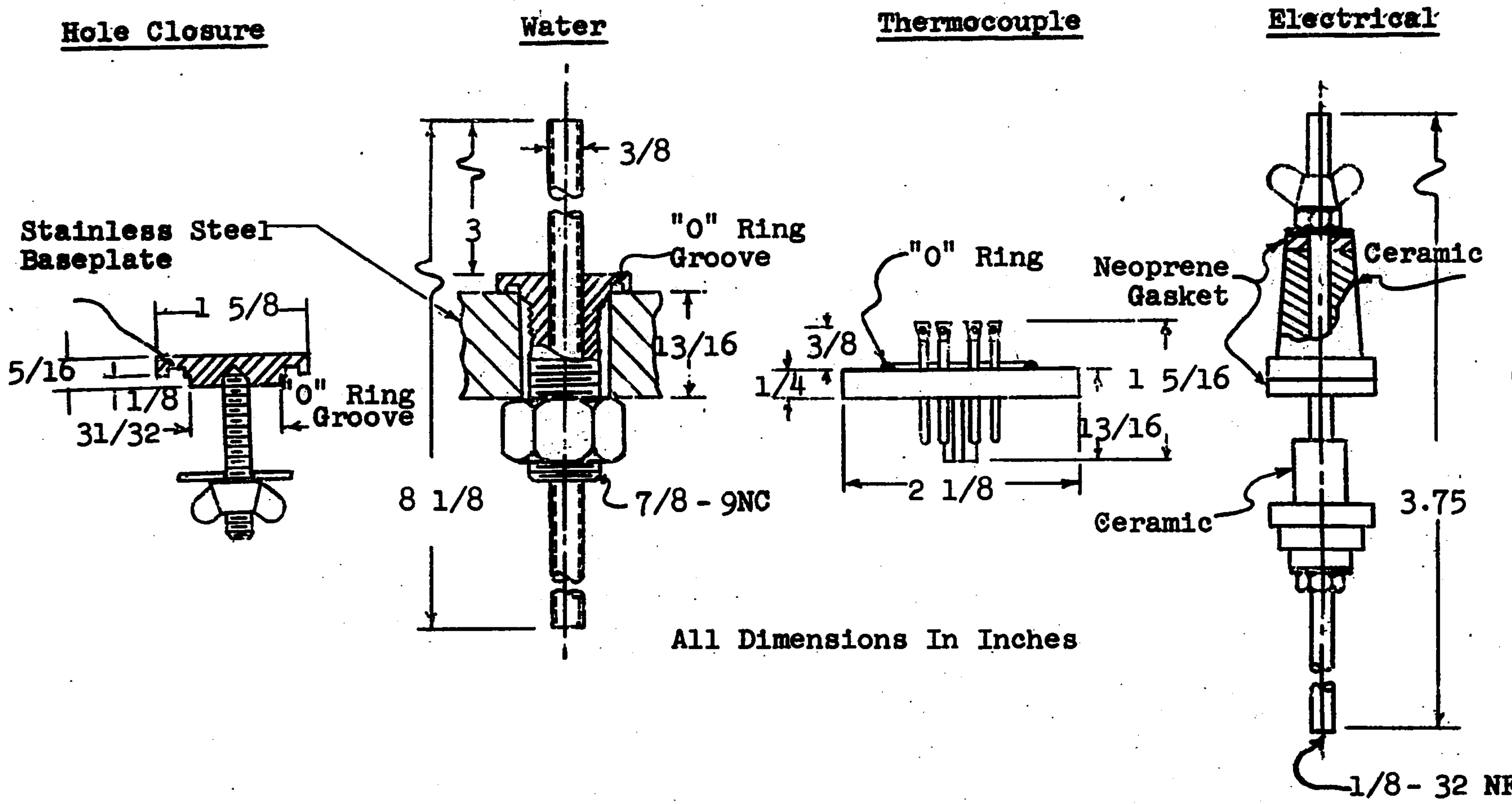

Figure 12

Vacuum Feedthroughs for Baseplate

the gasket and the bell jar and not between the gasket and the baseplate. The vacuum chamber was thus made up of the bell jar with an elastomer gasket on its base, sealing against the stainless steel baseplate, see Figure 13. The feed throughs, vacuum gauges, and diffusion pump sealed all of the openings to form the vacuum enclosure.

Acetone was used as a universal cleaner on the baseplate, bell jar, and other fixtures. It was not used on the gasket materials.

A bell jar guard of a perforated aluminum sheet was around the sides of the bell jar with an aluminum plate over the top. The guard provided a means by which the bell jar could be lifted and protected against possible damage. It also protected the personnel and equipment should an accidental implosion occur.

A hoist arrangement was provided by a system of steel cables and pullies with a counter balance to facilitate the raising and lowering of the bell jar for good access to the test fixtures.

The two factors considered in choosing a diffusion pump oil were: 1. the ultimate pressure required; and 2. the possibility of the boiler being exposed to the atmosphere while at an elevated temperature.

Silicone oil, Dow Corning 704, can be exposed to hot air without serious damage because it does not decompose as a hydrocarbon does. As the vapor pressure of Dow Corning 704 is approximately 1×10^{-8} torr, it met all the requirements

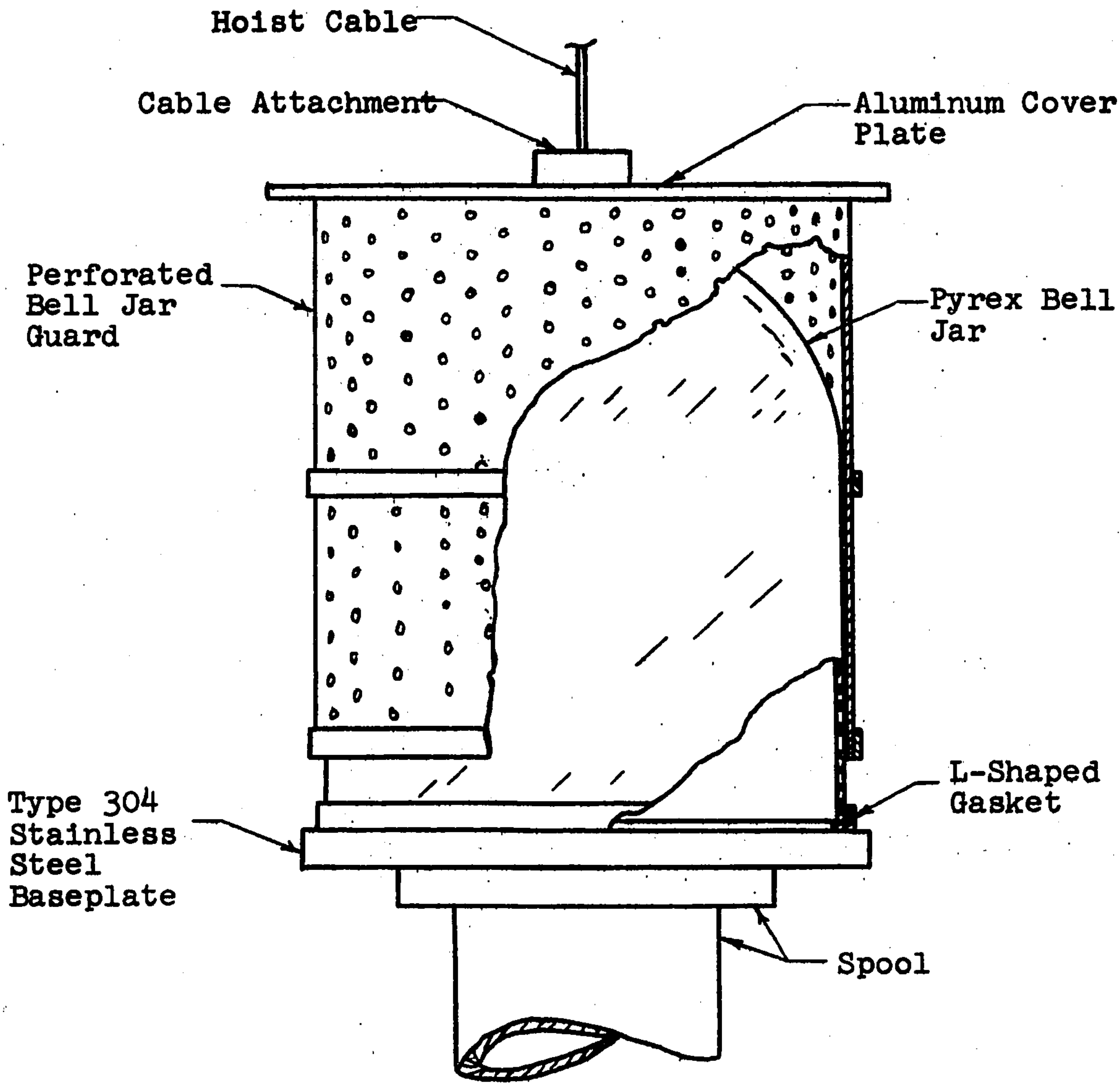

Figure 13

A Sketch of the Vacuum Chamber

and hence was used in the diffusion pump.

Excessive vibration of the system was encountered, which is typical of systems with mechanical pumps mechanically coupled to the vacuum apparatus. Consistent with good vacuum design practice, a 1 1/2 inch diameter copper tubing, 3 feet long, was used to allow placing the mechanical pump away from the system, thus allowing for the coupling of the mechanical pump directly to the floor for better dissipation of the vibrational energy. Also an additional 3 inch section of high vacuum, flexible rubber tubing was added between the pump and the tubing.

Vacuum System Pumping Requirements

The materials used in the construction of the vacuum chamber and the fixtures for the chamber were important as they were a source for a significant portion of the gas which was liberated inside the chamber upon the removal of the initial volume of gas. All of the materials listed in Table 2 were found to be adequate for the combination of vacuum and thermal environments in which they were used. Four possible sources of gas for the system were desorption, permeability, volatilization, and leakage.

Desorption is the process of removing a gas from a solid surface known as an adsorbent. Gases are held on surfaces by chemisorption, involving valence forces, and by physisorption, involving Van der Waals forces. Desorption of the heater was effective as the maximum temperatures of

TABLE 2

MATERIALS USED IN VACUUM CHAMBER

ITEM	MATERIAL	THERMAL ENVIRONMENT	COMMENT
Hot Plate		1007°F Maximum	
	a. 18-8 series stainless steel bolts and nuts		Initial gas content lower than mild steel. Its hydrogen permeability remains low even at elevated temperatures. Superior corrosion resistance to that of mild steel.
	b. Type 302 stainless steel sheet		
	c. Type 321 stainless steel sheet		
	d. Nickel chrome wire		Properties similar to stainless steel.
	e. Ceramic plate		Maximum operating temperature of 1832°F at atmospheric pressure.
	f. Pyrex plate		Annealing temperature 1050°F
Cold Plate		91.5°F Maximum	
	a. Mild steel plate		Acceptable if temperature is not excessively high.
	b. Cadmium plated mild steel plate		Not recommended for service below 10^{-6} torr.

TABLE 2 (continued)

MATERIALS USED IN VACUUM CHAMBER

ITEM	MATERIAL	THERMAL ENVIRONMENT	COMMENT
	c. Neoprene gasket		Not recommended for service below 10^{-6} torr.
	d. Type 302 stainless steel sheet		
	e. Scotch-Weld structural adhesive		Non-volatile thermosetting film adhesive at atmospheric pressure.
	f. Copper tubing		Resists oxidation.
	g. Monel coupling body		Acceptable vacuum properties.
	h. Brass coupling nut		Acceptable vacuum properties if not heated. If heated, it then breaks down due to the zinc content.
	i. Dow Corning silicone grease		Not recommended for service below 10^{-6} torr.
Chamber		180°F Maximum	
	a. Pyrex bell jar		Maximum service temperature 302°F.

TABLE 2 (continued)

MATERIALS USED IN VACUUM CHAMBER

ITEM	MATERIAL	THERMAL ENVIRONMENT	COMMENT
	b. Viton gasket		A fluorinated elastomer with low vapor pressure and permeability which can be baked at 392°F. Vacuums of 10^{-8} torr can be achieved with it.
	c. Dow Corning silicone grease		
Fixtures		Probably above 180°F	
	a. Mild steel		
Thermocouples		1007°F Maximum	
	a. Chromel wire		Acceptable vacuum properties.
	b. Alumel wire		Acceptable vacuum properties.
	c. Fiberglas insulation		Acceptable vacuum properties.
Baseplate		Slightly above room temperature	
	a. Type 304 stainless steel plate		

TABLE 2 (continued)

MATERIALS USED IN VACUUM CHAMBER

ITEM	MATERIAL	THERMAL ENVIRONMENT	COMMENT
Feed throughs		Slightly above room temperature	
	a. Brass bolts and nuts		
	b. Glazed porcelain		
	c. Copper wire		
	d. Ceramic insulators		

portions of the heater approached 1000°F. With ice water circulating in the cold plate, the plate acted as a shroud to adsorb or bind gas molecules to its surface. Whenever the ice bath temperature would rise, the vacuum would be decreased. The remaining fixtures were either at room temperature or just above due to energy loss from the heater to the surroundings.

As the major portion of the surface of the vacuum chamber was either the Pyrex glass bell jar or the 13/16 inch stainless steel baseplate, the permeabilities of only these two materials were considered. The computation discussed in Appendix G was performed to determine if the permeability of glass to helium gas was significant. Helium was considered as it has the highest permeation rate for passing through glass. From Steinherz (21), the permeation rate is expressed as follows for gases through nonmetals:

$F = (KAP/d)$

K = permeation constant, cm^2/sec

P = partial pressure difference, atm

d = wall thickness, cm

A = wall area, cm^2

From Appendix G the permeation rate was found to be 9.064×10^{-10} std atm ℓ/sec which was small enough to be negligible. The expression for the permeation rate of gases through metals is the same as the expression for gases through glass except that the partial pressure difference is raised to approximately the 1/2 power. According to Steinherz (21), the permeation constant for rare gases through metals is negligible. Hence, the stainless steel plate has negligible permeability.

Gases are liberated by substances due to a reduced pressure or an elevated temperature or both. Because most of the experimental data available on gas liberation properties of certain materials combine desorption, volatilization, and permeation together, meaningful calculations generally cannot be made for volatilization alone.

As only minor problems were encountered in obtaining the desired vacuum, there was no requirement to leak check with a device such as a commercial Mass-Spectrometer leak detector. The problem of pressure bursts due to air trapped in the stem seal of the slide valve was eliminated by removing the vacuum grease from between the two O-rings on the shaft and evacuating with the mechanical pump, see Figure 14. The cold plate was checked for leaks using a freon-12 gas at approximately 20 pounds per square inch pressure with a halogen leak detector to probe for leaks.

The proof of the validity of this design approach lay in the fact that the vacuum, attained consistently, ranged from approximately 1×10^{-6} torr to approximately 3×10^{-7} torr with the heater at its maximum and minimum temperatures respectively.

Heater and Controls

A requirement of the heater and the heater controls

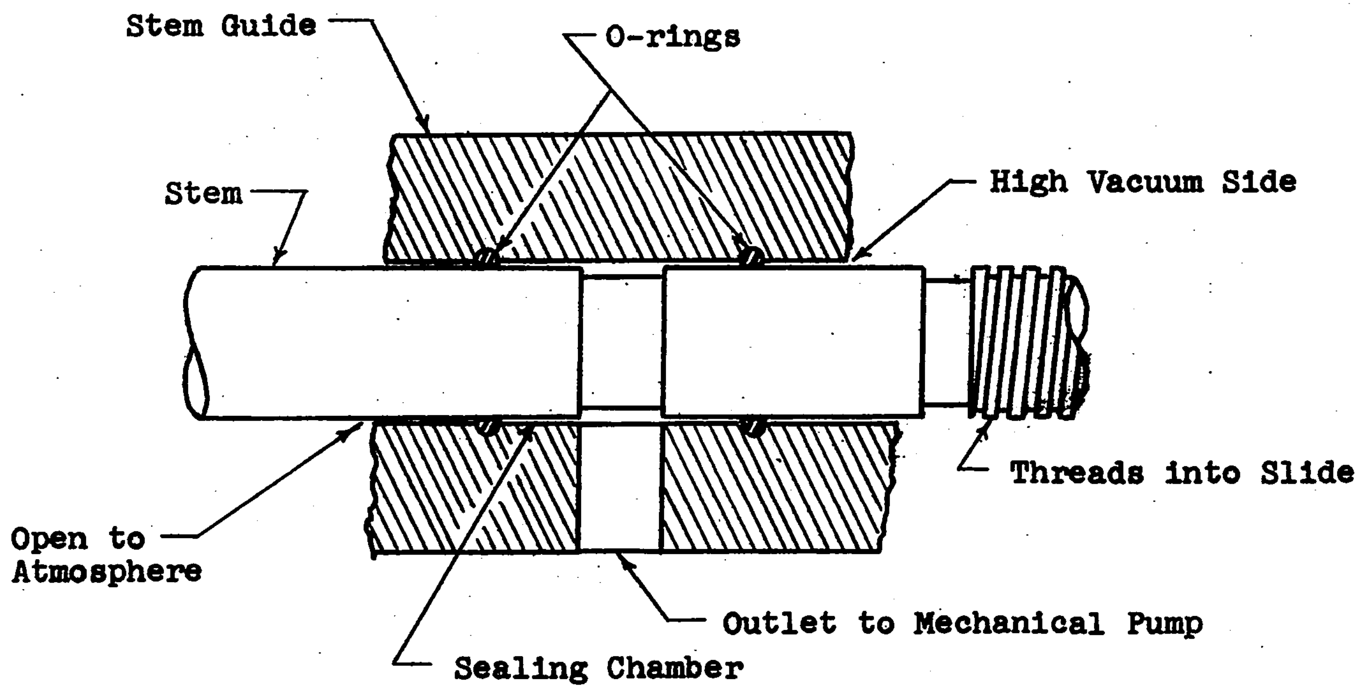

Figure 14

Section Through Slide Valve Stem Seal

is that the thermal inertia of the heater is such that a desired temperature can be reached in a reasonable period of time. Once this temperature has been reached, the system is thermally stable enough to maintain this temperature. An advantage of using stainless steel in the heater construction is its low thermal conductivity. Because of this property the heater components do not dissipate energy easily; thus, thermal equilibrium is more readily obtained. The poor conductivity also has the disadvantage of creating hot spots which in turn limit the uniformity of, for example, the surface temperature of the heater face.

The maximum operating temperature for the face of a heater was selected as approximately 930°F. Richmond and Harrison (11) found that below 930°F emittance values increased for Inconel and Types 321 and 430 stainless steel because of the removal of adsorbed films. The adsorbed films would probably exist below 930°F regardless of the material being heated. Even for these oxidation resistant materials, Richmond and Harrison (11) observed the formation of thin oxide films in an air atmosphere at a pressure of less than 4×10^{-5} torr. The oxide films which were found above 930°F tended to increase the emittance with an increase in temperature.

The description of the heater is limited to the three zones involved in the measurement of the net radiant flux at the heater surface. The object of the three heater zones is to create a thermal environment such that the electrical energy being dissipated in the center heater could be assumed to be transmitted perpendicularly to the heater face with a minimum of edge or back losses. This reduction of energy loss is accomplished with the back heater, which limits the energy loss to a negligible amount from the back of the center heater. The border heater in turn restricts the energy loss from the sides of the center heater.

Thermocouples T_9 and T_{10}, see Figure 15, were attached to the outside faces of the two stainless steel sheets, which were on either side of the 1/8 inch Pyrex sheet separating the back heater from the border and the center heater. Thermocouple T_2 was in the center of the hot plate with T_4 on the inside corner of the border heater. The two pairs of thermocouples determined if the electrical power regulation using the three variable auto transformers A, B, and C was adequate. A differential of not more than 10°F for thermocouples T_9 and T_{10}, and for thermocouples T_2 and T_1, was used as the guide in the voltage regulation of the heaters.

To prevent buckling on the face of the heater, a square piece of stainless steel smaller than the center heater was removed from the center of the heater face. Tabs formed from the edge of the hole on the heater face were bent in against the heating element on all four sides of the hole. Next, a stainless steel sheet with four edges bent inward on it to form a small open box was placed over the center heater. The tabs of the border and the center heater were next resistance welded together, as illustrated in Figure 15, giving added rigidity without interfering with the energy flow path

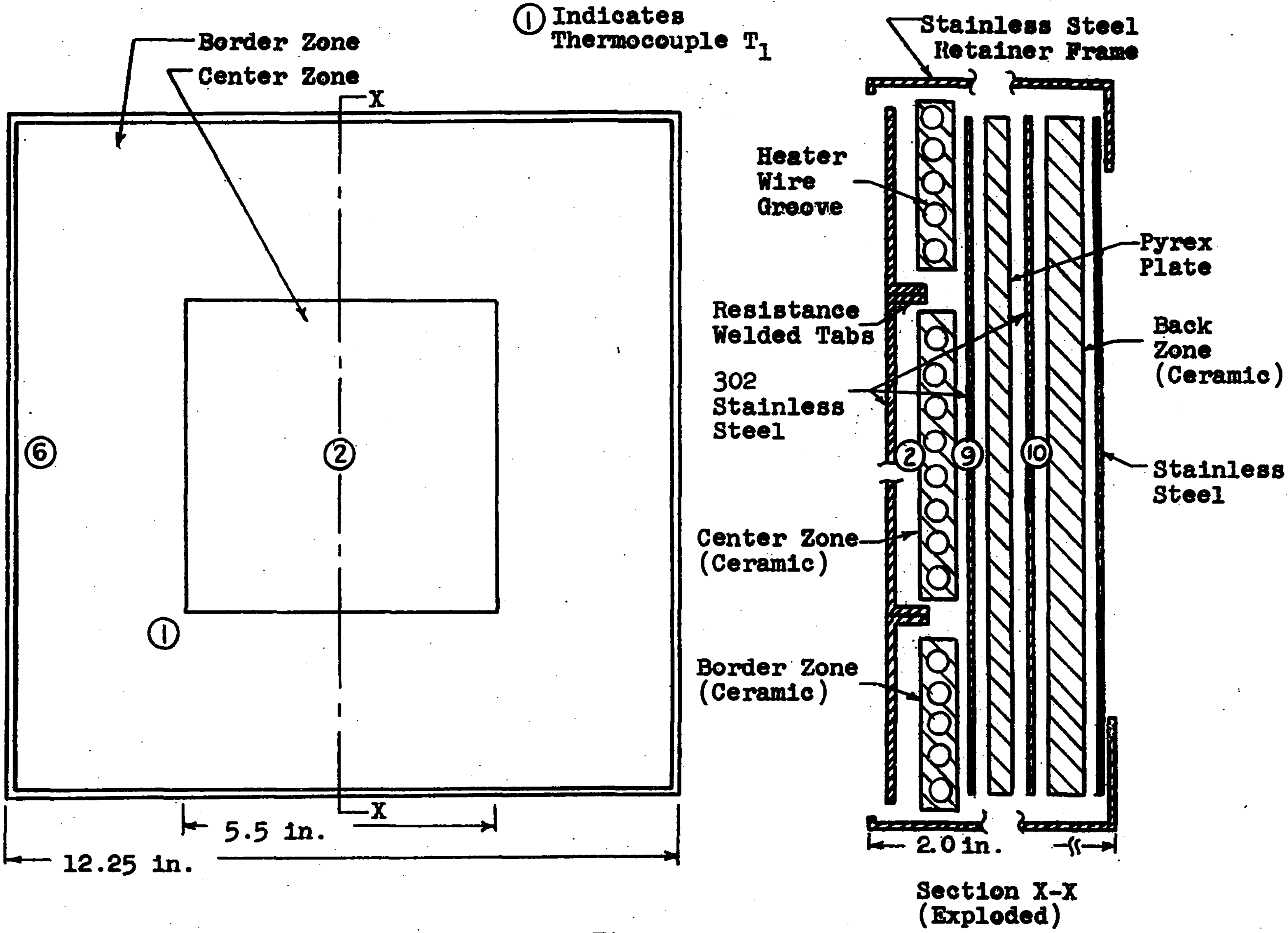

Figure 15

Heater Plate

of the center heater.

The technique which allowed for the shaping of the commercial ceramic heater elements, which contained grooves for coiled heater resistance wire, required first the removing of the wires. Second, a diamond saw was used to shape the elements, and then the wire was placed in the new configuration.

The power leads, 10-gauge copper wires insulated with fish-spine insulators, were connected to the feed throughs and then terminated at precisely the edge of the heater to which the connection was being made. According to Steinherz (21) both the heating element wire and ceramic backing were being used within an acceptable operating range of temperature and pressure.

In the wiring schematics, Figures 16, 17, and 18, the ohmmeter and voltmeter were never connected in the circuit at the same time with the wattmeter in order to eliminate power losses which they would cause. Because the electrodynamic wattmeter was the compensated type, power loss due to the wattmeter connections was corrected for in the instrument. The resistance of the three heaters, shown in Figures 16, 17, and 18, was a function of the diameter and length of the heater wire. Thus, with the resistances fixed, it was necessary to increase the line voltage in order to increase the current load which generated the thermal energy. The border heater at its peak voltage setting used 120 volts. Thus, with the electrical feed throughs rated at 115 volts,

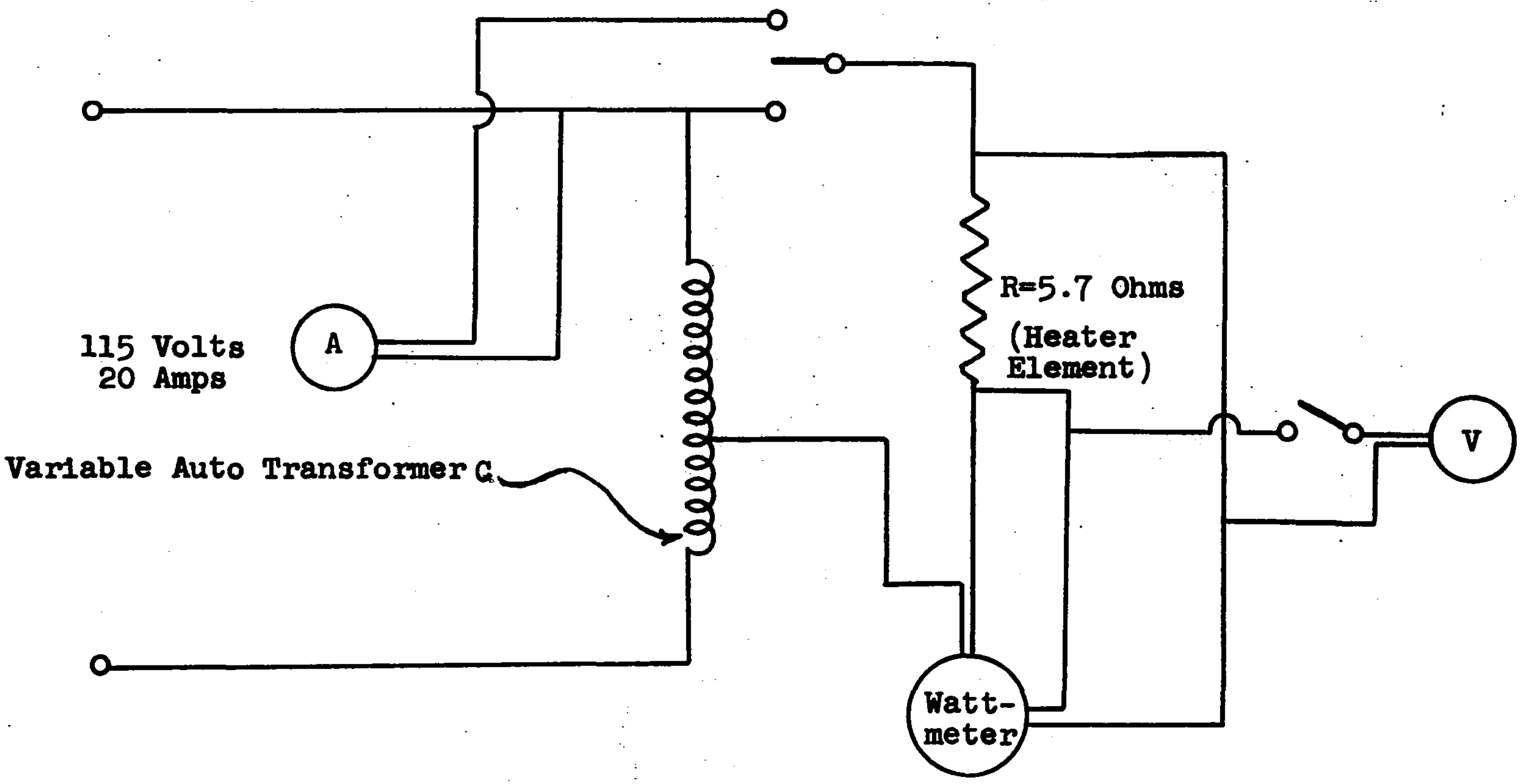

Figure 16

Center Heater and Control Circuit

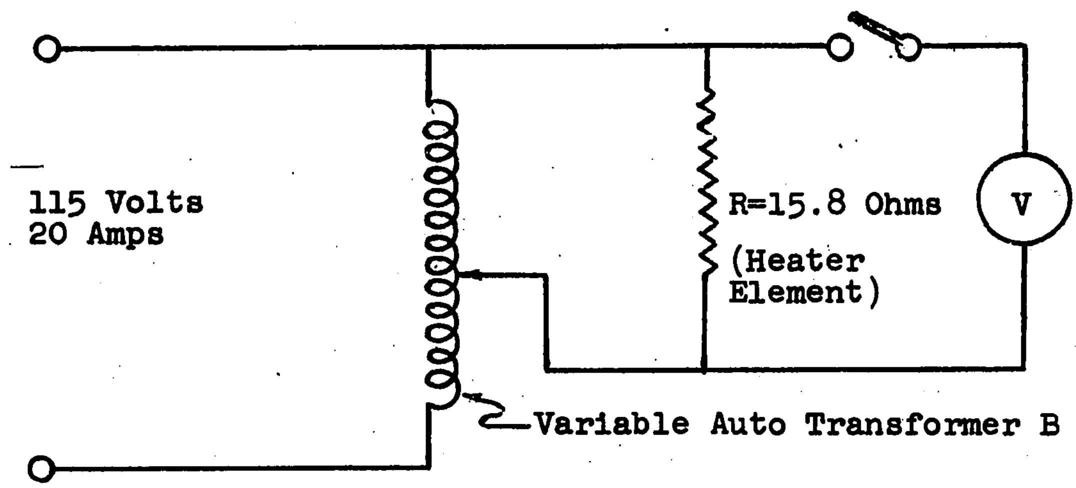

Figure 17

Back Heater and Control Circuit

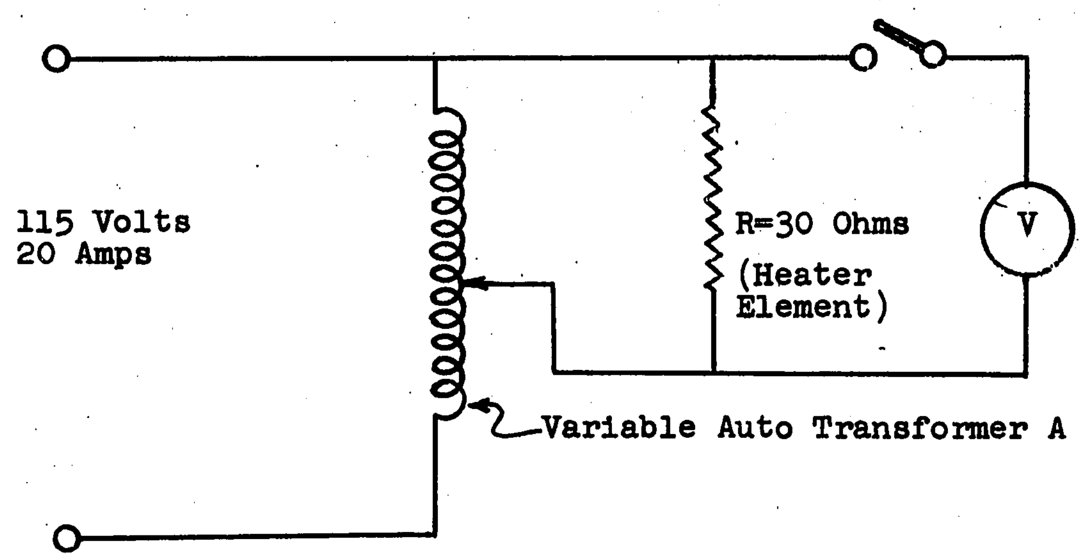

Figure 18

Border Heater and Control Circuit

the overall performance of the system was limited by both the line voltage capacity and the voltage rating of the feed throughs.

Thermocouple Circuit and Measurements

The temperature measuring system was designed with accuracy, stability, and cost being considered. Figure 19 gives the thermocouple circuit schematic with the function of the various thermocouples tabulated.

Chromel Alumel couples were used because of their resistance to oxidation even when subjected to oxidizing atmospheres for long periods of time at 2000°F. The Chromel and Alumel 24 gauge wires were twisted together through 2 or 3 complete turns, and then a thermocouple of the two wires was formed by passing an electrical current through the wires at their junction in such a manner that the region of contact of the dissimilar materials formed a point of high electrical resistance and thus welded the wires. Cold working of the wires was kept to a minimum as it produces appreciable inhomogeneity.

All of the thermocouples were attached to the outer face of the hot plate and the cold plate because of the thinness of the stainless steel cover sheets and the difficulty of placing the wires on the inside face of the two plates. They were attached to the surfaces with a capacitance discharge welder using approximately 40 watt-seconds of power. One of the difficulties in measuring the true surface

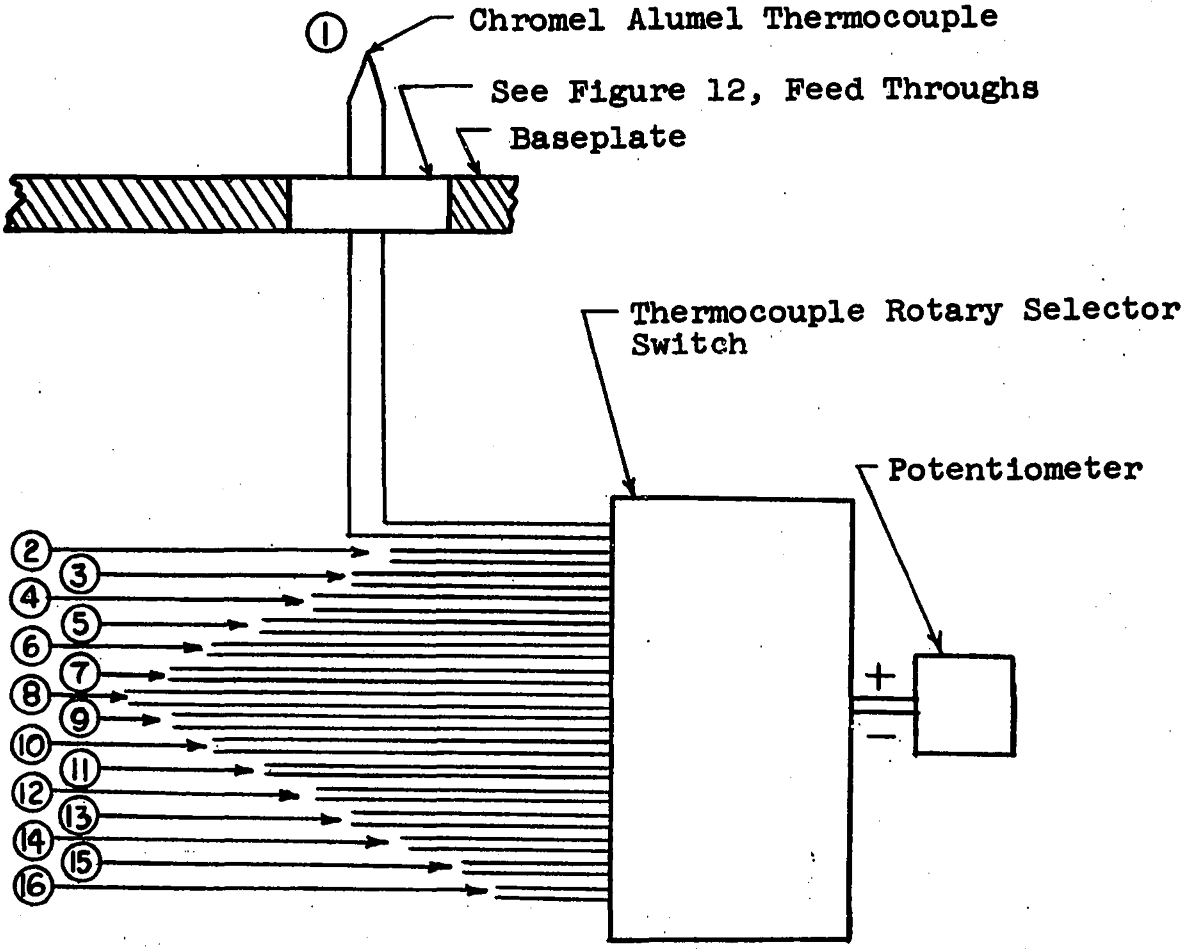

Figure 19

Thermocouple Selector Circuit

1. Hot Plate Border Corner
2. Hot Plate Center
3. Cold Plate Middle Border
4. Cold Plate Center
5. Bell Jar -- 5. Foil
6. Hot Plate Edge
7. Cold Plate Corner
8. Hot Plate Corner
9. Pyrex Front
10. Pyrex Back
11. Cold Plate Back
12. Hot Plate Border
13. Hot Plate Center Edge
14. Water Bath
15. Open

temperature in an environmental apparatus of this type was the possibility of radiation losses resulting in the thermocouples being cooled below the surface temperature.

Copper extension wires were used in connecting the thermocouples to the potentiometer, where a reference junction compensator was used in allowing for variation in room temperature. The rotary selector switch used solid silver contacts with durable silver alloy brushes to reduce error in the emf readings due to contact resistance.

Cold Plate and Ice Bath

The objective of the cold plate design was to provide the system with a heat sink fitted with interchangeable front surfaces. The composite view, Figure 20, and the sketch of the labyrinth water channel, Figure 21, give most of the details.

The cadmium plated labyrinth water channel was selected in preference to other water channels as it reduces temperature gradients across the plate and minimizes the danger of the water bypassing part of the plate as in the manifold type of cooler. The circulation of water from an ice bath to cool the cold plate was selected for simplicity. A submerged water pump circulated the cooled water through the feed throughs and through two ultra-high vacuum couplings. An aluminum gasket which was deformed to create a seal was used in the couplings. The front plate on the water channel was held in place by bolts around the outside of the

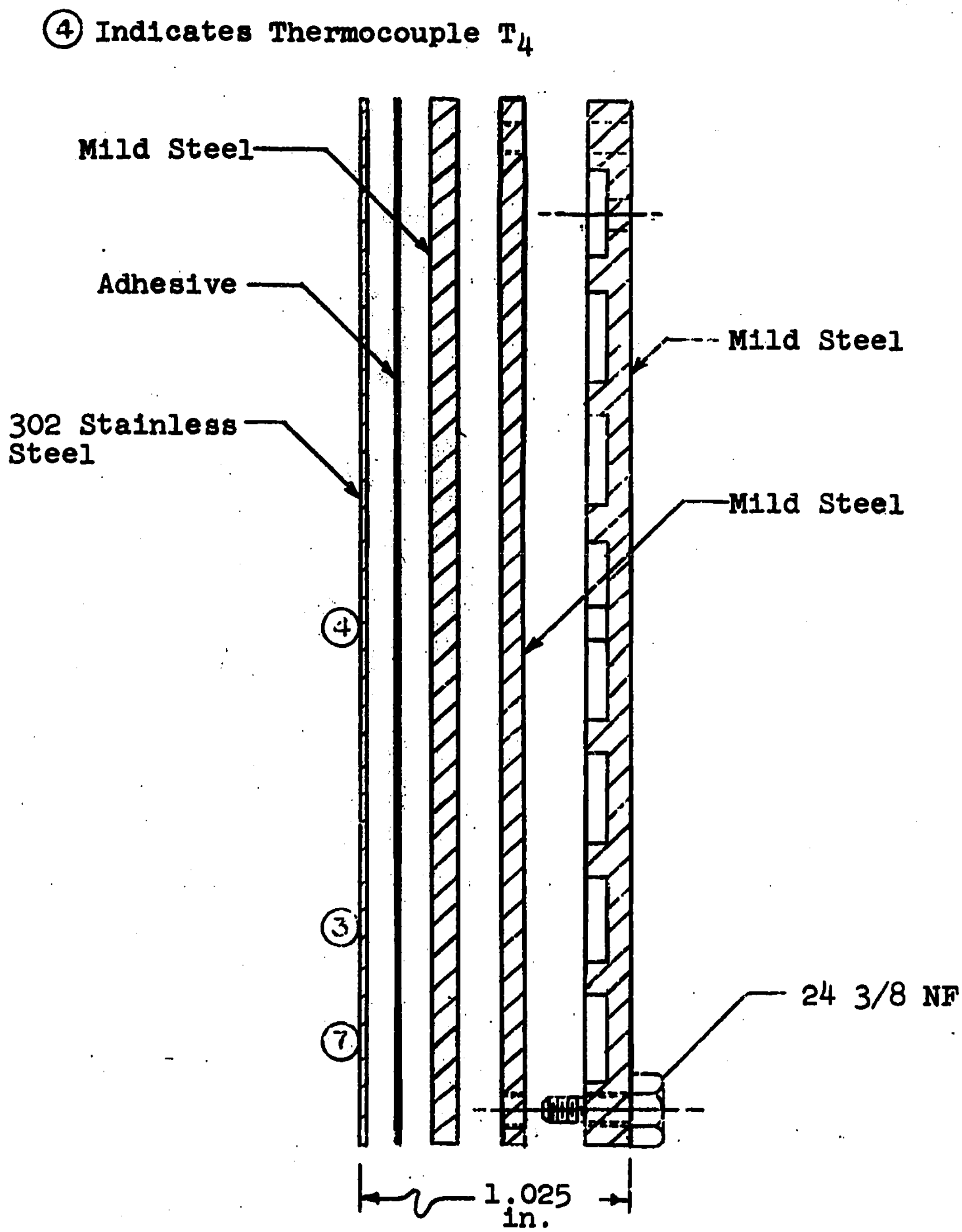

Figure 20

Exploded Section of Cold Plate

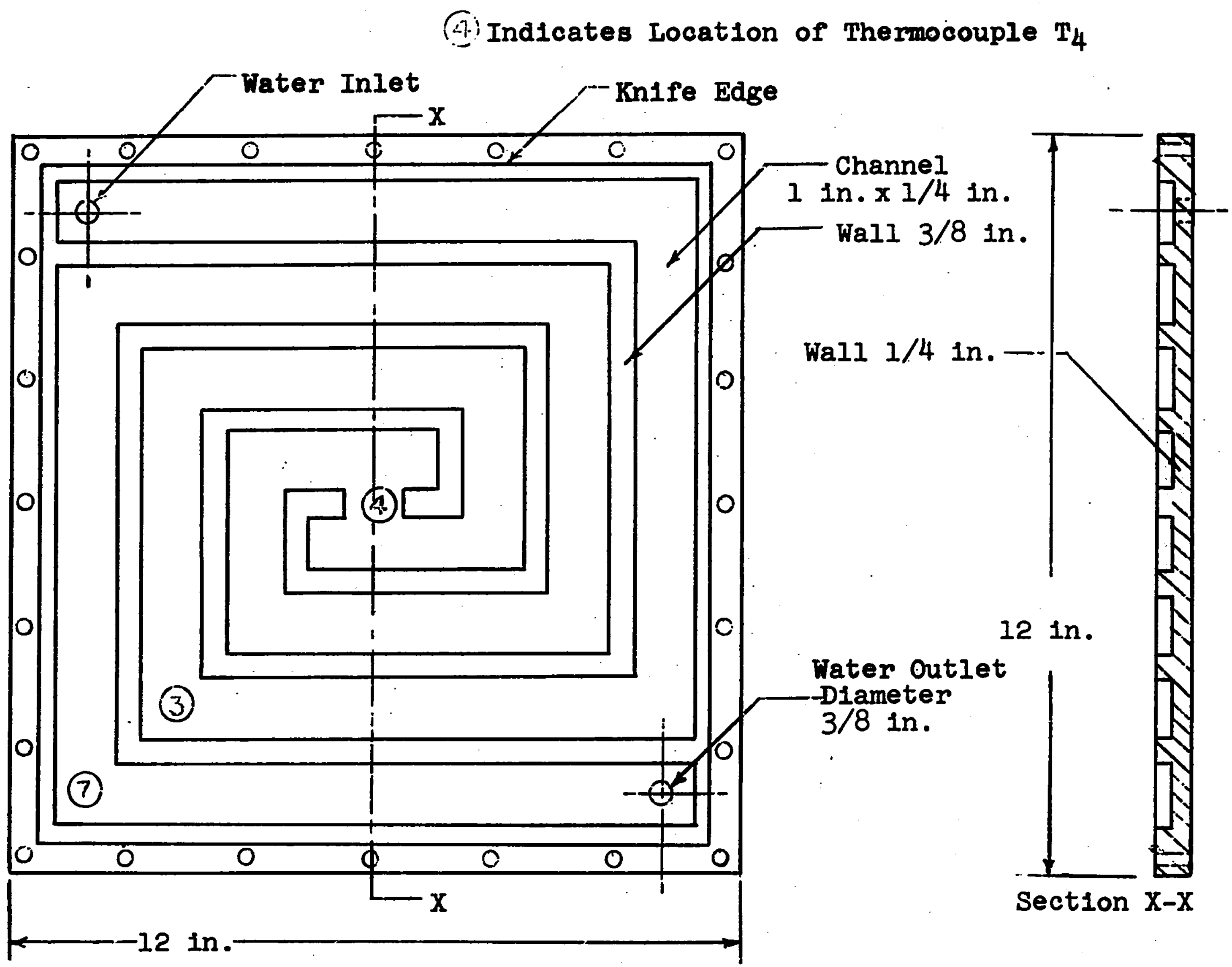

Figure 21

Sketch of Cold Plate Labyrinth Water Channel knife-edge seal, which was milled on the face of the back plate. It was not a true knife-edge seal in that it did not have an opposing knife-edge on the ground surface of the front plate. A neoprene gasket, 1/16 inch thick, was used as the material to seal between the knife-edge and the front plate. A second mild steel plate, on which was bonded the stainless steel face sheet, was clamped with eight "C" clamps to the front plate. Vacuum grease was used between these two plates to reduce thermal contact resistance.

Scotch-Weld, structural adhesive, AF-110, is a non-volatile, thermosetting film adhesive for the bonding of metals. This adhesive was used in bonding the stainless steel sheet to the second cover plate because of its high bond strength. Furthermore, as a result of its compression to only a few thousandths of an inch in thickness, its conductivity was high. The surface preparation of the two faces to be bonded consisted of sandblasting them with a 60 mesh fused aluminum oxide grit. Next, repeated flushings with acetone, being careful not to handle the surfaces, finished the treatment. The adhesive was kept in a freezer below 32°F before using. Contact pressure (approximately 10 pounds per square inch) from the heated aluminum platlets of a 100 ton press was applied to the mild steel plate and the stainless steel sheet. With the platlets at 350°F the bonding process was completed in 20 minutes.

A secondary consideration in cooling the cold plate to below room temperature was the reduction of the volatilization of the cadmium plating, the thermosetting film adhesive, and the silicone grease.

The ice bath consisted of a 60 gallon galvanized rectangular sheet metal tank insulated on all sides with a plastic-backed Fiberglas. The reservoir was electrically grounded to guard against pump failure due to breakdown of the electrical insulation on the pump's electrical cord.

The cold plate, like the hot plate had an aluminum foil shield near its back side to reduce the exchange of energy between the plate and the surroundings.

Shield

Using a Type 302 stainless steel sheet, suspended by nickel chrome wires which were attached to the four corners, the shield was positioned between the two plates. The shield, like the plate faces, was one foot square.

Surface Preparation Apparatus

As surface preparation is very important in the determination of the emittance of a surface, a sandblast booth was constructed to reclaim the abrasives and to prevent their becoming contaminated with foreign material. The booth consisted of a box approximately two feet on an edge with two openings for arms and a viewing port. An air supply of 75 pounds per square inch was attached to the portable sandblast gun with an air hose. The reservoir for the abrasive was a can attached to the gun. Heavy rubber gloves and goggles were always worn when the sandblast gun was being operated.

CHAPTER V

EXPERIMENTAL PROCEDURE AND DISCUSSION OF DATA

Nine preliminary runs were conducted which involved perfecting the data-taking procedures. One run, which was typical of these evaluation tests, was concerned with the determination of voltage inputs to the three heaters to obtain a uniform temperature on the surface of the heater together with minimum differential temperature across the back of the heater. Approximately 65 hours of continuous operation were required for this type of run to determine four data points at equilibrium conditions. To obtain steady state conditions as much as 17 hours were required for one of the points before voltage adjustments could be made for the next point. Once the experimental procedure was established, the tests, listed in Table 3, were conducted.

Experimental Procedure

The potentiometer was standardized and referenced to room temperature each time a reading was taken. All thermocouples were checked to determine if they read room temperature with the system at atmospheric pressure.

The vacuum system was started, and the necessary calibration of the thermocouple and the ionization gauges was

TABLE 3

TESTS CONDUCTED

Without Shield

Spacing Between Plates	Run No. No Foil (NF)	Run No. Foil (F)
0.5 inches	1 and 2	3
1.0 inches	4	5
3.0 inches	6	7

With Shield

Spacing of Shield From Hot Plate	Run No. With Foil	
	Hot Plate Side	Cold Plate Side
0.5 inches	8a	8b
1.5 inches	9a	9b
2.5 inches	10a	10b

made as discussed in the National Research Corporation Installation, Operating and Maintenance Manual for the Model 3307, Portable Pumping System.

When the vacuum was at least 1×10^{-5} torr the flow of ice water from the ice bath to the cold plate was started and the thermocouple readings were checked.

The auto transformers were adjusted to provide the proper voltage input to the border, back, and center heaters using the predetermined settings for Point A, see Figure 22. The first point in the test and the one requiring the longest time for steady state conditions (10.5 hours), was Point A. The voltage settings and the power input to the center heater were observed every 30 minutes, and minor adjustments were made when required to maintain the original voltage settings. The deviations were due to line voltage fluctuations.

Approximately 30 minutes after the electrical power was applied to the heater, the appropriate thermocouples were checked for response to the energy input before allowing the run to continue.

At one hour, and at one-half an hour before the final reading for a data point, preliminary readings were made and recorded to indicate how closely steady state was being approached. These last three readings were recorded and the differential temperatures between the readings were noted. A temperature difference of not more than $2\,^{\circ}F$ was desired, and in most cases a smaller differential temperature was obtained.

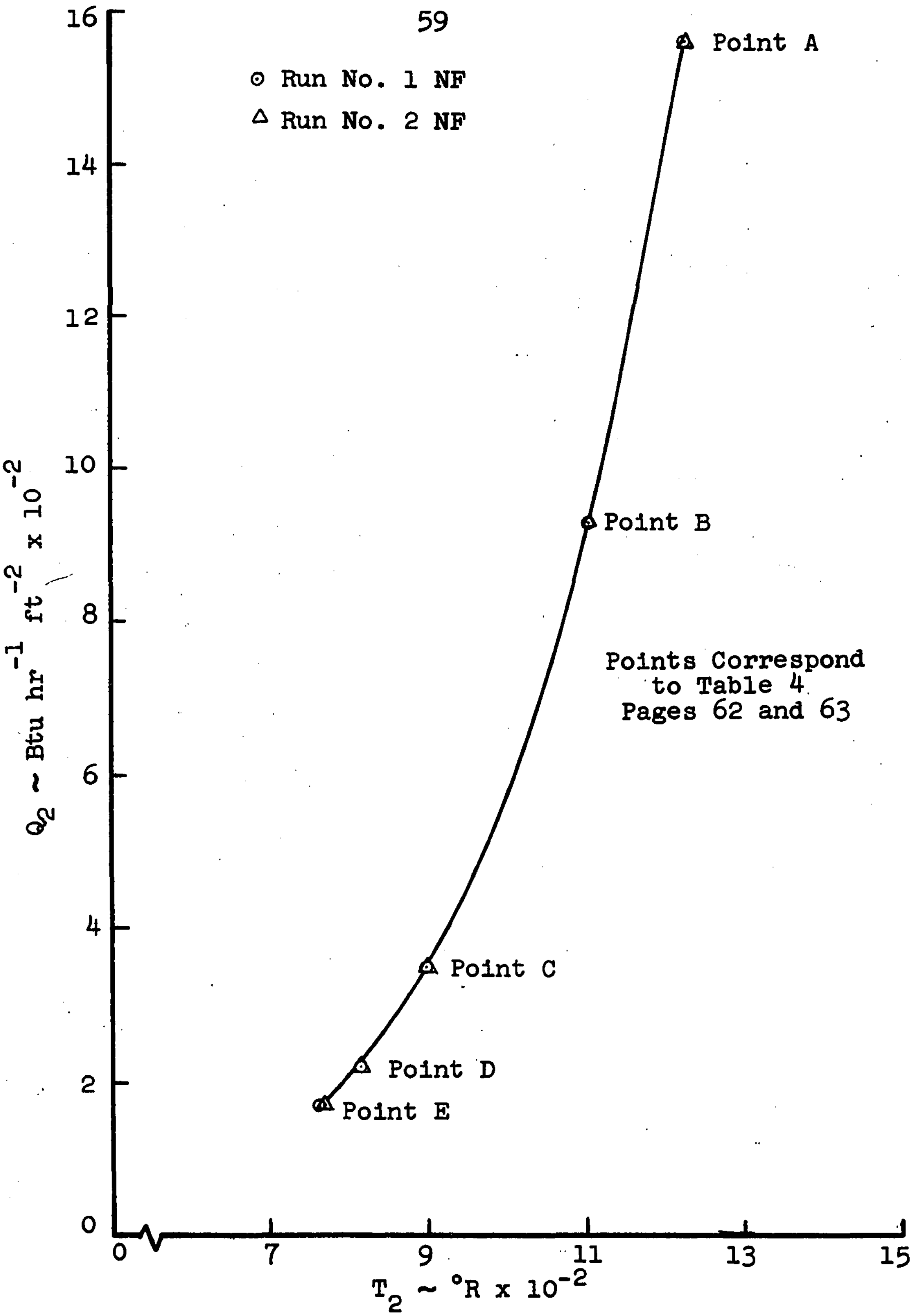

Figure 22

Reproducibility of Data At 0.5 Inch Spacing

The other arbitrary differential temperature requirement was that the temperature at the center of the hot plate and the temperature on the corner of the border of the hot plate must be within 10°F of each other, ($|T_2 - T_1| \leq 10°F$). This same requirement was also true of the differential temperature readings through the back of the heater ($|T_9 - T_{10}| \leq 10°F$).

Of the three variables, power input, time, and temperature, the first two were held constant for each data point of each run. Variations in data from one run to the next, due to such things as the changing of the spacing, were noted as a variation in the temperature of the surfaces.

As Point A was the point of maximum energy input to the heater, the vacuum system was required to remove large amounts of gases liberated by adsorption and volatilization because of the elevated temperatures reached by the bell jar and fixtures. With this procedure, the vacuum was 1×10^{-6} torr at Point A and improved to approximately 3×10^{-7} torr at Point E. Another advantage in this sequence was that at the conclusion of a run it was not necessary to cool the system for a long period of time before opening the bell jar to make adjustments for the next run.

At the completion of a run the experiment was terminated by turning off the heater and stopping the vacuum system in accordance with the procedures outlined in the Equipment Manual of the National Research Corporation. After the temperature of the heater was reduced to approximately 200°F, the circulation of the ice water was stopped, and the cold plate was allowed to increase to some value near room temperature. In this way, when the vacuum chamber was opened to the atmosphere, moisture from the air would not condense on the cold plate and create unnecessary pumping requirements for the vacuum system during the following run due to water vapor in the chamber.

Because all of the energy not being transferred to the water bath was dissipated to the room, any variation in room temperature could have possibly affected the equilibrium condition of the plates in a minor way.

Another background factor, which was observed, was that of line voltage fluctuation. The average change was 1 percent of the line voltage. Recommendations for correcting this variation are discussed in a later chapter.

Data Presentation

All data, both computed and measured, are plotted as net radiant flux at the center heater surface versus the temperature of the center of the hot plate. Also the plots of the net radiant flux versus the spacing parameter all have the same axes. Table 4 and Table 5 give data points A, B, C, D, and E for each run from which the experimental curves were plotted. Figure 22 locates the data points A, B, C, D, and E on a typical curve.

Accuracy of Measurement

With a properly constructed apparatus, the accuracy

TABLE 4

EXPERIMENTAL DATA WITHOUT SHIELD

Run No. 1

Point	T_1	T_2	T_3	T_4	T_5	T_6	T_7
A	1234	1231	515	525	612	1234.5	496.5
B	1113	1107.5	510	520	592	1100	499
C	893	899	503	510	564	887	500
D	810	817	502.5	509	554	807.5	501
E	759	766	501.5	506.5	548	758	501

Run No. 2

Point	T_1	T_2	T_3	T_4	T_5	T_6	T_7
A	1220	1230.5	519	535	612	1208	502
B	1104	1105	512	523	592	1093.5	501.5
C	893.5	899	503	511	564	889	499.5
D	808	815	499.5	505	554	808.5	498
E	766	772	501	506	548	766	500

Run No. 3

Point	T_1	T_2	T_3	T_4	T_5	T_6	T_7
A	1225	1236	518	545	618	1228	509
B	1108.5	1109	511	529.5	591	1110	507
C	895	903.5	504	515	569.5	893.5	504
D	812	819	502	508	563	811.5	503
E	767	775	500	506.5	555	769	500

Run No. 4

Point	T_1	T_2	T_3	T_4	T_5	T_6	T_7
A	1196.5	1218.5	495	509	627	1199	492
B	1089	1096	496	506	590	1089	493
C	877.5	890	495	502	562	877	492
D	798	809	495	500.5	563	800	494
E	757	767	496.5	501	551.5	760	495.5

Run No. 5

Point	T_1	T_2	T_3	T_4	T_5	T_6	T_7
A	1221.5	1232	520	551.5	718.5	1246	514.5
B	1110.5	1111	513	536	658	1126	510
C	897.5	902.5	502	515	585.5	904	502
D	814	819	501	510	568	829	501
E	767	774	501	508.5	553	772	500.5

Run No. 6

Point	T_1	T_2	T_3	T_4	T_5	T_6	T_7
A	1142	1167	495[1]	509[1]	639	1193	492
B	1046	1051	496	506	606	1082	493
C	857	864	495	502	567.5	877.5	492
D	783.5	790.5	495	500.5	559	800.5	494
E	745	752	496.5	501	556	760	495.5

TABLE 4 (continued)

EXPERIMENTAL DATA WITHOUT SHIELD

Run No. 7

Point	T_1	T_2	T_3	T_4	T_5	T_6	T_7
A	1195	1216	522	550	783	1259.5	538
B	1088	1095	513	533	724	1132.5	526
C	883	891	503	513	623	905	510
D	807	813	502.5	510	592	823.5	508
E	763	769	504	510	556	776.5	509

---

[1]The original temperatures were incorrect due to radiant energy from the hot plate reaching the thermocouple junctions at the feed through inside the vacuum chamber. This situation was a result of the wide spacing of the plates. New readings were selected from Run No. 4 as they are the most typical values available.

The Q measured values were the same for each run. They are as follows:

Point	Q measured
A	1559.66
B	926.05
C	349.30
D	219.33
E	170.59

TABLE 5

EXPERIMENTAL DATA WITH SHIELD

Run No. 8a

Point	T_1	T_2	T_3	T_4	$T_{5a} = T_{5b}$ (assumed)	Q measured
A	1341.5	1375	1185	1212	818.5	1559.66
B	1226	1243	1070	1090	762	926.05
C	986	1006	857	876.5	652	349.30
D	886	904	772	789	611	219.33
E	838	853	730.5	746	595	170.59

Run No. 8b

Point	T_1 (computed)	T_2	T_3	T_4	Q measured
A	1135.5	1162.5	508	529	1559.66
B	1029	1049	506	521.5	926.05
C	830.5	850	499	506	349.30
D	751	786	500	505	219.33
E	712.5	728	501	505	170.59

Run No. 9a

Point	T_1	T_2	T_3	T_4	$T_{5a} = T_{5b}$ (assumed)	Q measured
A	1325.5	1351	1158	1189	818	1559.66
B	1209	1222	1042	1068	754	926.05
C	969	983	832	852.5	635	349.30
D	876	889.5	757	775	600	219.33
E	833	845	720	736.5	585	170.59

Run No. 9b

Point	T_1 (computed)	T_2	T_3	T_4	Q measured
A	1110.5	1141.5	496.5	526	1559.66
B	1003	1029	494	514	926.05
C	807.5	828	495	505	349.30
D	736	754	498	505	219.33
E	702.5	719	497	502	170.59

TABLE 5 (continued)

EXPERIMENTAL DATA WITH SHIELD

Run No. 10a

Point	T_1	T_2	T_3	T_4	$T_{5a} = T_{5b}$ (assumed)	Q measured
A	1288	1328	1127.5	1161	728.5	1559.66
B	1175	1200	1014.5	1042	688	926.05
C	956	975	818.5	839	622.5	349.30
D	867	883	745	762	597	219.33
E	818.5	831.5	705.5	720.5	584	170.59

Run No. 10b

Point	T_1 (computed)	T_2	T_3	T_4	Q measured
A	1081.5	1115	494	520.5	1559.66
B	978	1005.5	497	515	926.05
C	796	816.5	497	505	349.30
D	727.5	744	497	502.5	502.5
E	687.5	704	498	502	170.59

of the measurements depends chiefly on:

1. The maintenance of steady state temperature conditions as illustrated by the invariance of the temperatures of the hot and cold plates with time.
2. The satisfactory balancing of the temperatures between the metering and the guard areas of the hot plate to assure minimal energy loss.
3. The accurate evaluation of measured quantities, such as temperatures, power input to metering area, and dimensions of the metering area.

Analyzing the measurement of the data for Point A of Run No. 1 and of Run No. 3 and all the data for Run No. 1 and Run No. 2 yields the following results:

1. From Appendix H the variation of each of the temperature readings on the hot and cold plates was from 0.0°F to 2.0°F during a 30 minute period ending half an hour before the final data point reading. During the final 30 minute time period, the maximum temperature fluctuation was 1.0°F. Of the ten temperature readings listed, four of the thermocouples indicated no change during the final time period. Based on these measurements, which are typical of the other data runs, it was concluded that the requirement of steady state conditions was met.
2. An estimate of the net energy exchange between the center heater and the border and back heaters was made in Appendix H using the measured temperature

readings as being absolute. Due to the physical configuration of the materials forming the heaters, the analysis was limited to estimating the difference between the computed and the measured output of the center heater due to conduction losses. For Point A of Run No. 1, the computed heater output was approximately 3 percent above the measured value. For Point A of Run No. 3, the difference in fluxes was less than 1 percent. The assumption of energy transfer by radiation gave only negligible energy exchange between the center heater and the border and back heaters. Because of the small estimated net energy exchange between the center heater and the guard heaters, the requirement of a minimal energy loss for the center heater was satisfied. Hence, the energy output of the heater was assumed as equal to the energy input to the heater.

3. An evaluation of the accuracy of the measured results is exhibited by Figure 22, where the capacity of the experimental apparatus to generate reproducible data was established. The maximum variation in any of the temperatures recorded for Run No. 1 and Run No. 2 was 26.5°R or 2.15 percent. The procedure for both runs was identical. Thus a reasonably accurate evaluation of the measured quantities was made.

Discussion of Measured Results

In Table 4 for the tests conducted without aluminum foil around the border zone of the plates, T_5 was measured on the vertical outside surface of the bell jar directly opposite the border region between the two walls. For the case where aluminum foil was used around the border zone of the plates, the thermocouple measuring T_5 was mechanically held against the inside surface of the aluminum foil forming the border area. The cases just discussed are referred to as the no foil and the foil cases respectively.

In Figures 23, 24, and 25 the no foil and the foil cases were considered for the three spacings of 0.5, 1.0, and 3.0 inches. Run No. 2 was considered only once and that was in Figure 22.

The measured net radiant flux was the same for each run as the energy input was constant for a fixed time period. In Figure 23 the no foil and the foil curves were nearly identical. As the spacing increased, the temperature of the surface of the heater decreased. The increased loss of energy from the border zone of the plates resulted in the decrease of the temperature of the surface. If the surface temperature could be maintained constant as the spacing increased, then an increase in the net energy flux at the heater surface would result.

As the instrumentation for the experiment was designed for the metering of energy at the heater surface, only the data for the hot plate side of the shield was plotted.

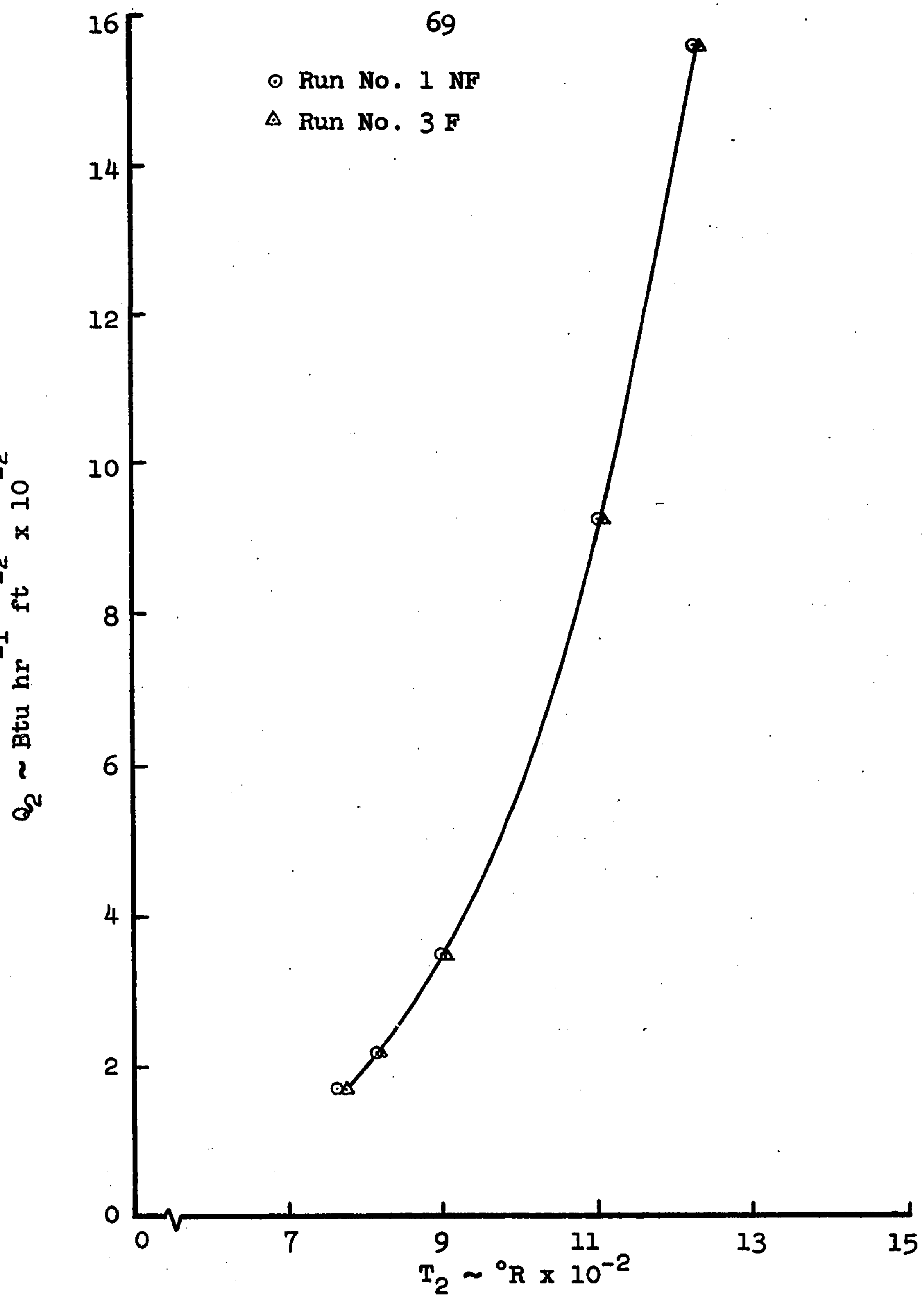

Figure 23
Experimental Data At 0.5 Inch Spacing

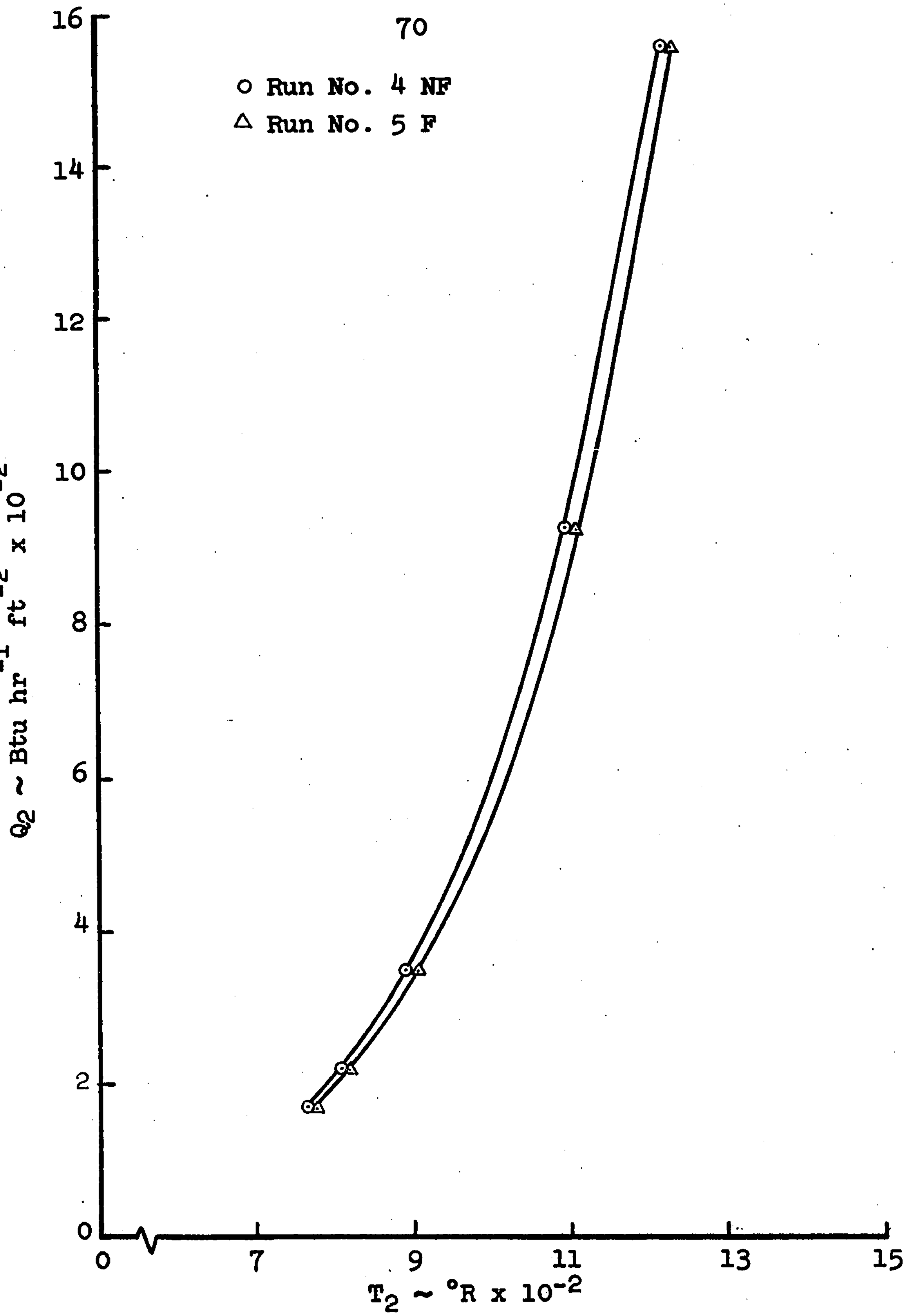

Figure 24

Experimental Data At 1.0 Inch Spacing

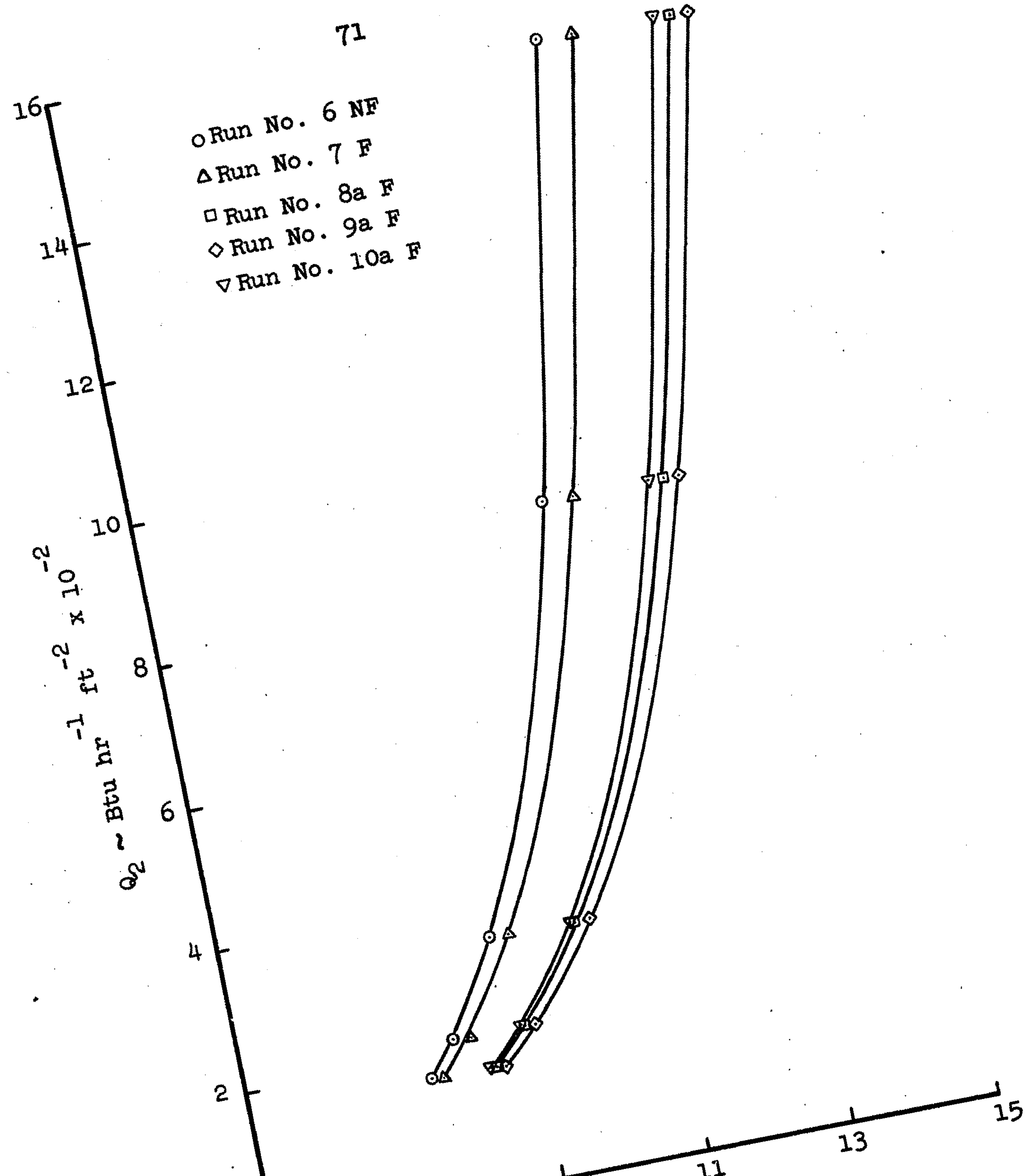

Figure 25

Experimental Data At 3.0 Inch Spacing

Considering the no foil and the foil cases separately with respect to spacing gives the expected decrease in temperature at the center of the heater with spacing as shown in Figure 26. However, in Figure 27 the spacing has almost no effect on the energy transfer rate except in the 3.0 inch case where a maximum temperature difference of 20°F occurs at Point A. The effect of spacing was again illustrated in Figure 28 and Figure 29. Plots of the spacing parameter h/a allowed the application of the experimental results to square plates of various sizes and spacings.

Possible Sources of Error

(1) By measuring the temperatures individually and computing the temperature differential, the importance of obtaining accurate absolute temperatures was increased.

(2) Absolute temperature measurement considerations were:

a. The creation of a region of uniform temperature from the measuring junction and along a specific length of the wires with no sharp temperature gradients after the wires leave the uniform temperature zone.

b. The placing of the junction on the surface such that it does not appreciably alter the surface temperature by its presence.

c. The undesired creation of a thermoelectric junction at the feed throughs where the extension wires were connected to the thermocouple wires.

d. The loss of energy by the junction on the heater face

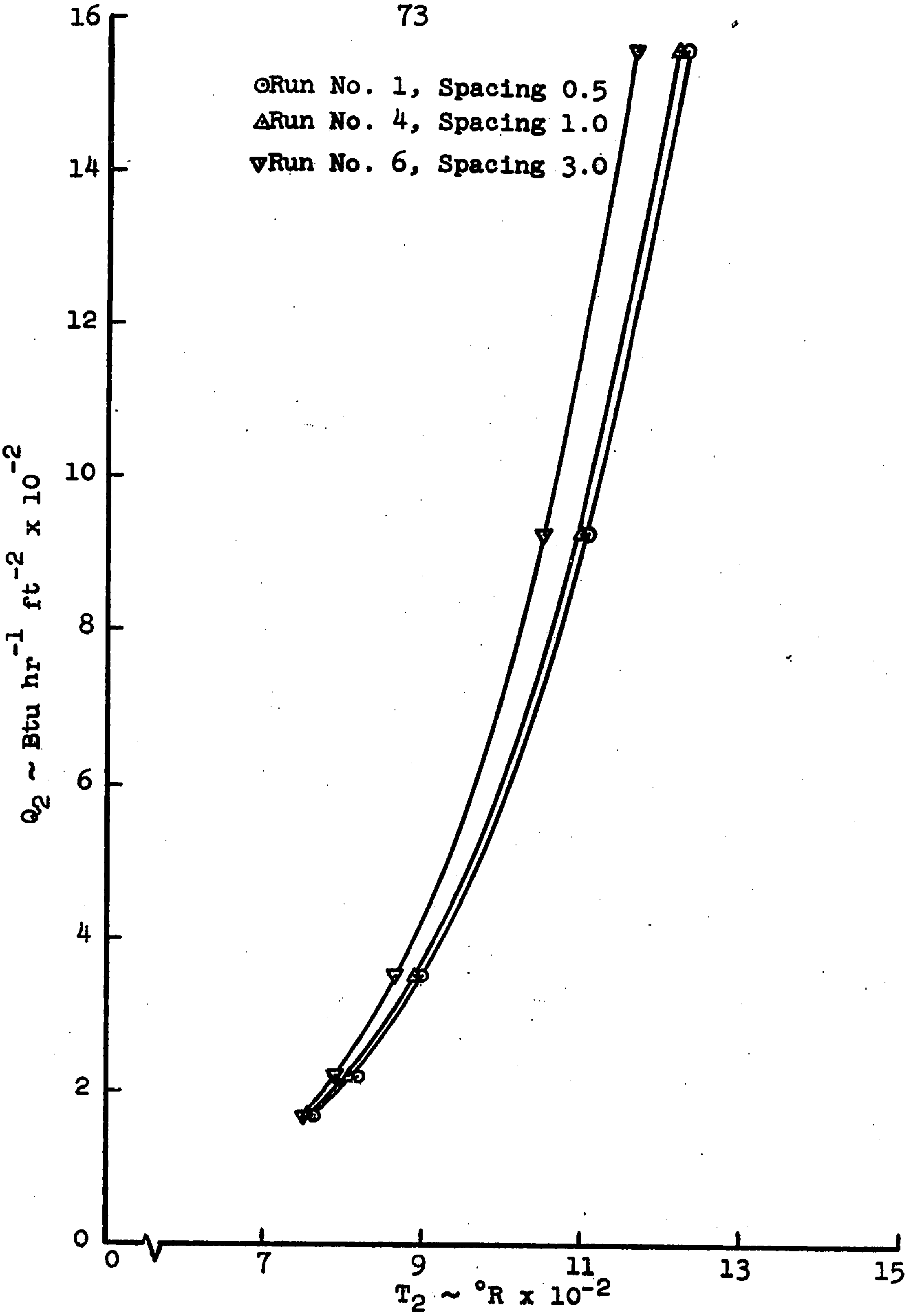

Figure 26
Experimental Data for No Foil Case

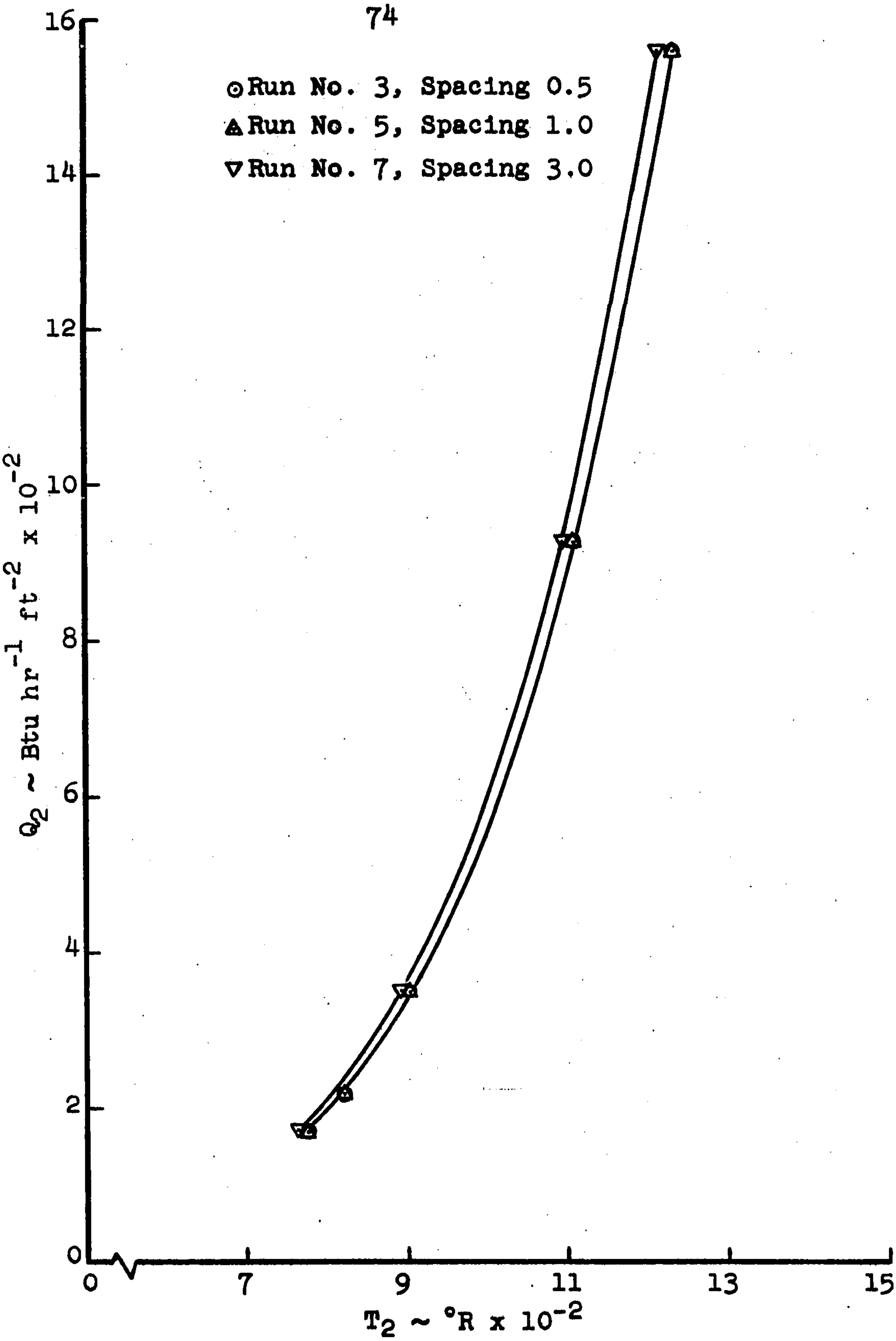

Figure 27
Experimental Data for Foil Case

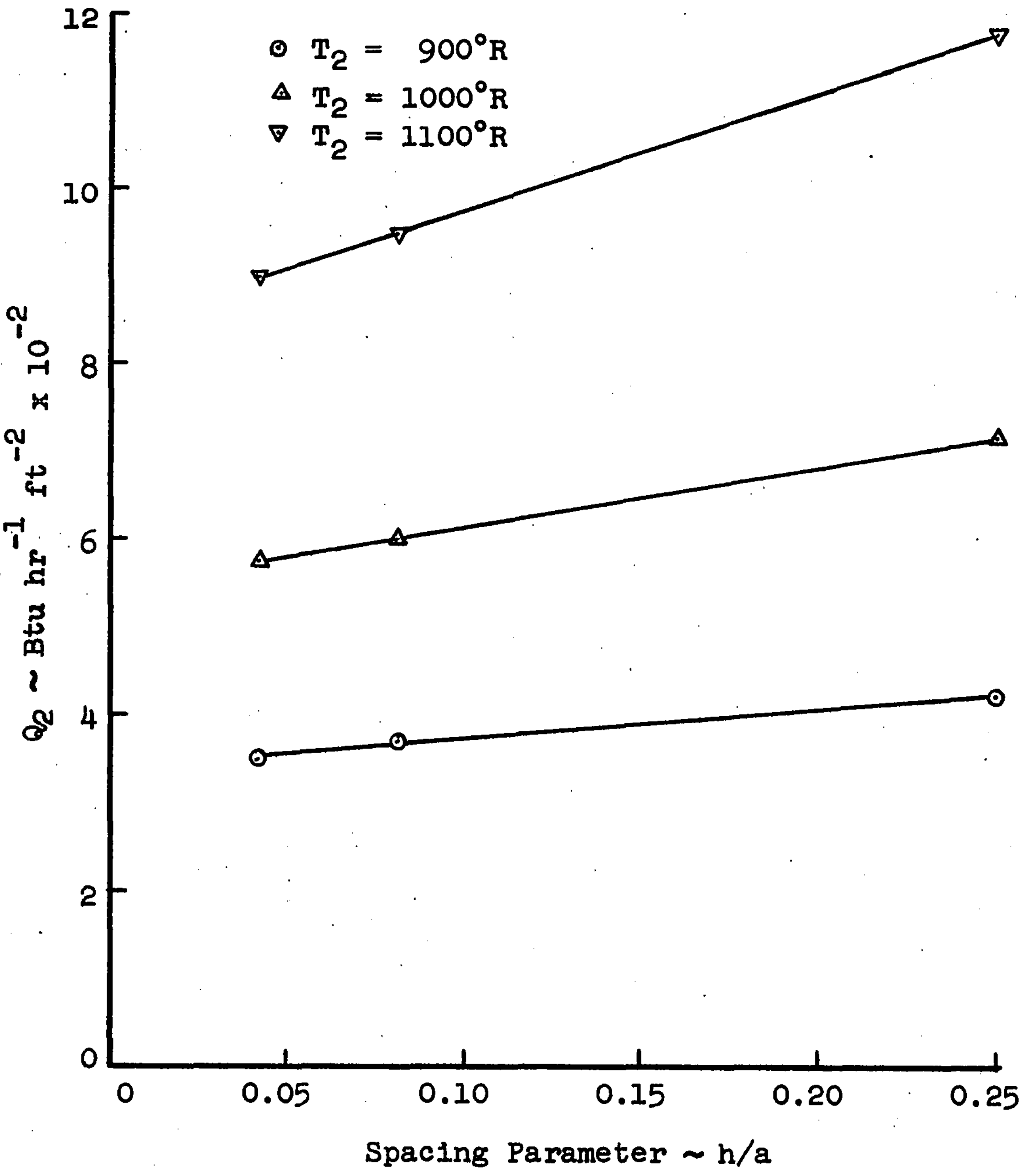

Figure 28

Effect of Plate Spacing for No Foil Case

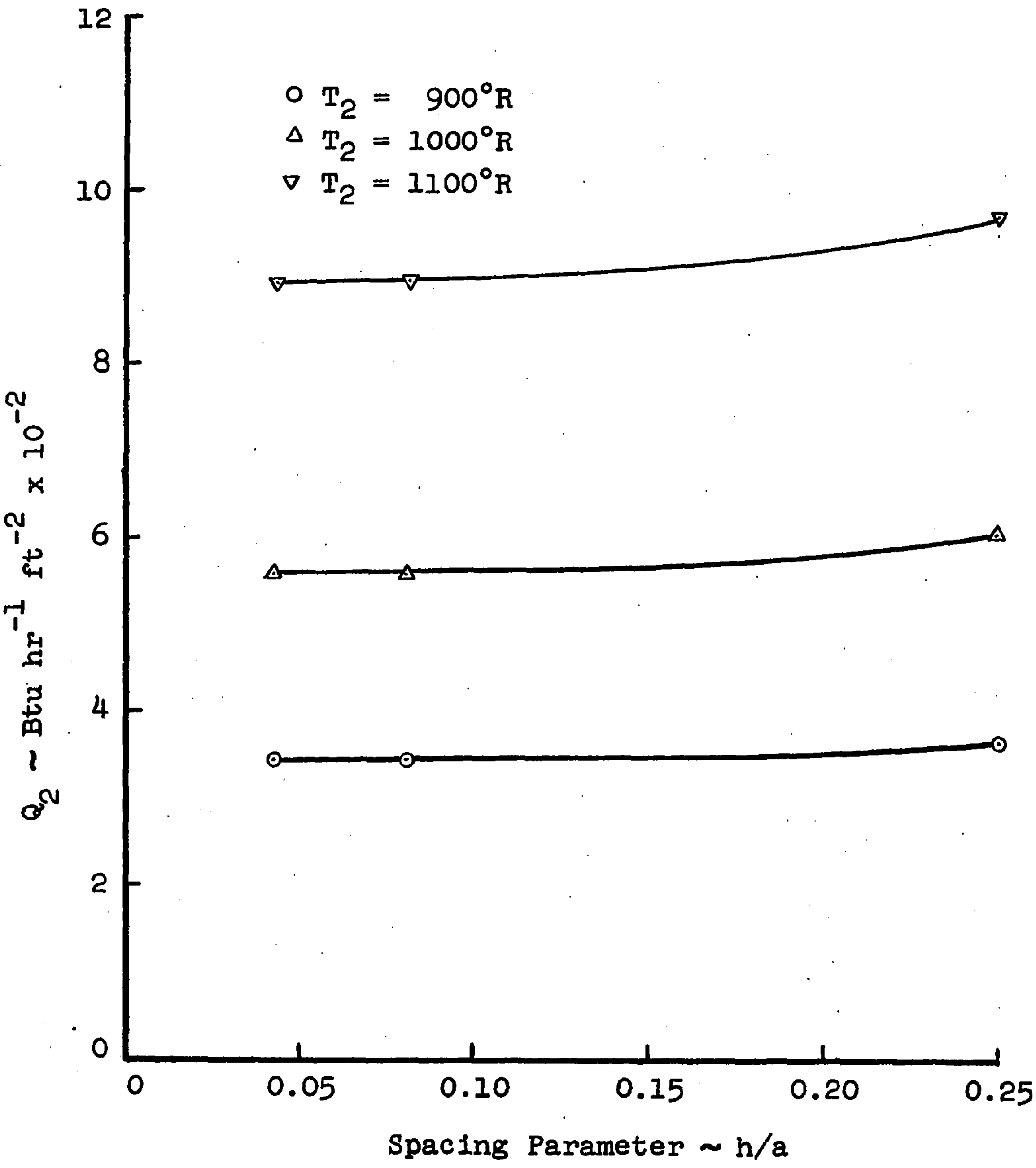

Figure 29

Effect of Plate Spacing for Foil Case

due to radiant losses in excess of the losses of the hot plate surface.

(3) As this vacuum system was only partially baked-out, two potential problems existed:

a. The directional pressure effect due to the release of adsorbed gases between the plates and throughout the system causing a net movement of molecules from a region of higher density to one of lower density.

b. The pressure measurement error introduced by the release of adsorbed gases in the ionization gauge could be large according to Santeler (22). After liberating much of the adsorbed gas in the gauge by resistance heating of the grid in the gauge, the liberated gas was removed from the system. The tubulation connecting the gauge and the vacuum system would not be affected by this technique; hence, it might act as a continual source of gas resulting in erroneous vacuum readings.

CHAPTER VI

CALCULATED RESULTS

Parallel Plane Method

By using the infinite, parallel plane method, the sample calculation in Appendix I illustrates how net radiant fluxes are calculated using the measured temperatures of the surfaces. The results are given in Table 6 and plotted in Figure 30.

As the computed values for the infinite, parallel plane method were not affected by the spacing of the plates or the presence of aluminum foil, only one representative curve was plotted. The only variation noted in a plot of the infinite, parallel plane computations is in the upper and lower limit of the curve. In Figure 30 the effect of different surface emittances is noted.

Lumped Parameter Method

In the lumped parameter method of computation the surface temperature, reflectance and radiosity were assumed constant over each area. The tabulated values in Tables 7 and 8 were determined as shown in Appendix J. The basic assumption in this calculation is that one is dealing with an enclosure. The foil case represents $\rho_5 = 1$ while the no

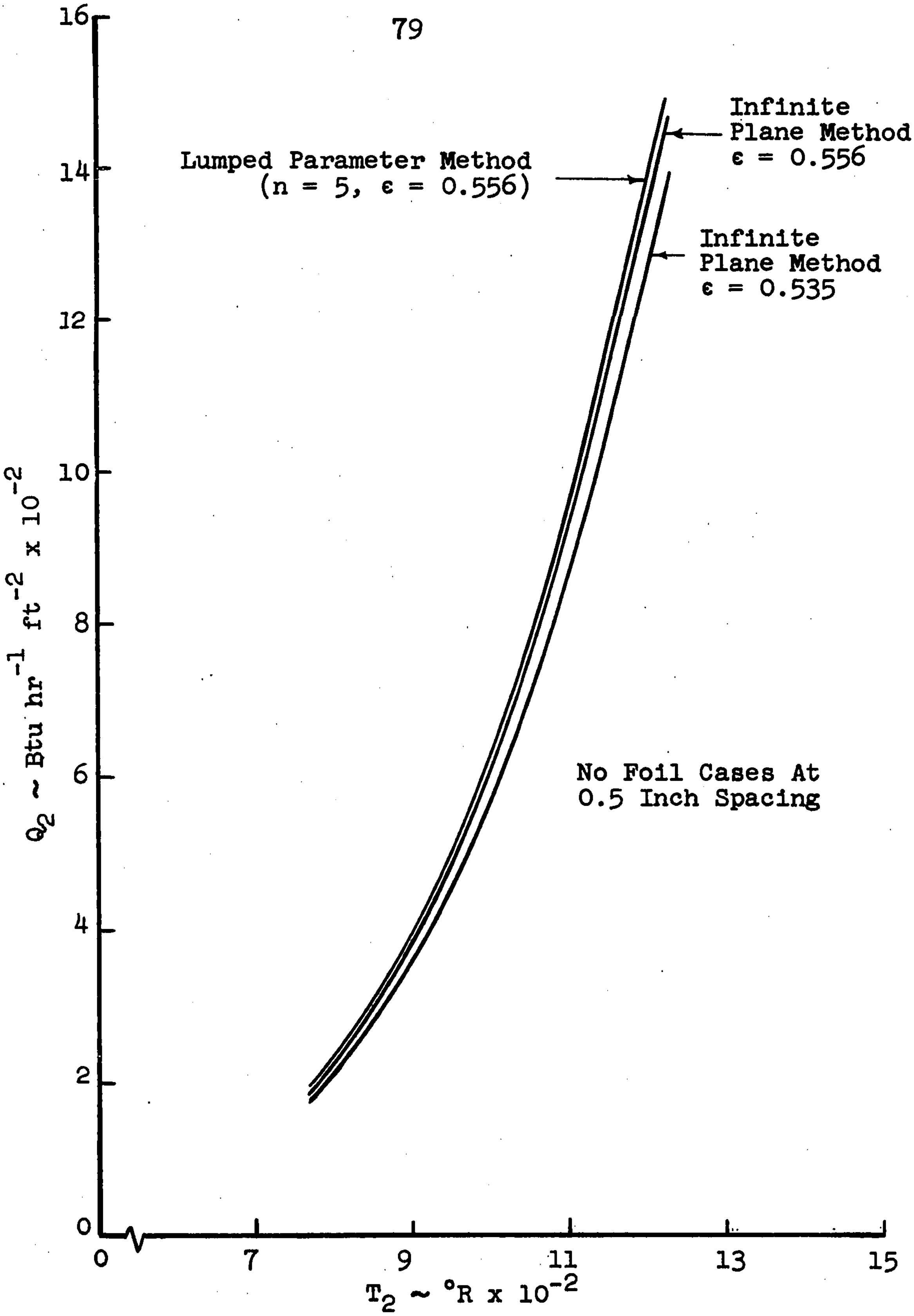

Figure 30

Comparison of Computed Values

TABLE 6

INFINITE PARALLEL PLANE METHOD

Point	T_2 measured	T_4 measured	Q computed ($\epsilon = 0.556$)	Q computed ($\epsilon = 0.535$)
Run No. 1				
A	1231.0	525.0	1463.89	1388.41
B	1107.5	520.0	943.68	895.02
C	899.0	510.0	386.05	366.14
D	817.0	509.0	249.49	236.63
E	766.0	506.5	183.60	174.13
Run No. 2				
A	1230.5	535.0	1457.51	1382.35
B	1105.0	523.0	933.63	885.50
C	899.0	511.0	385.70	365.81
D	815.0	505.0	248.00	235.22
E	772.0	506.0	190.96	181.12
Run No. 3				
A	1236.0	545.0	1480.56	1404.22
B	1109.0	529.5	945.45	896.70
C	903.5	515.0	392.96	372.70
D	819.0	508.0	252.73	239.70
E	775.0	506.5	194.45	184.43
Run No. 4				
A	1218.5	509.0	1409.16	1336.50
B	1096.0	506.0	908.11	861.28
C	890.0	502.0	371.79	352.62
D	809.0	500.5	241.04	228.61
E	767.0	501.0	186.64	177.01
Run No. 5				
A	1232.0	551.5	1457.91	1382.74
B	1111.0	536.0	950.07	901.08
C	902.5	515.0	391.02	370.86
D	819.0	510.0	252.03	239.04
E	774.0	508.5	192.54	182.61
Run No. 6				
A	1167.0	509.0	1178.59	1117.82
B	1051.0	506.0	761.23	721.98
C	864.0	502.0	325.53	308.75
D	790.5	500.5	216.08	204.94
E	752.0	501.0	169.31	160.58

TABLE 6 (continued)

INFINITE PARALLEL PLANE METHOD

Run No. 7			ε = 0.556	ε = 0.535
Point	T_2 measured	T_4 measured	Q computed	Q computed
A	1216.0	550.0	1381.19	1309.97
B	1095.0	533.0	894.65	848.52
C	891.0	513.0	369.86	350.79
D	813.0	510.0	243.43	230.88
E	769.0	510.0	185.96	176.37
Run No. 8a				
A	1375.0	1212.0	934.01	885.86
B	1243.0	1090.0	643.22	610.05
C	1006.0	876.0	286.14	271.39
D	904.0	789.0	184.81	175.28
E	853.0	746.0	144.85	137.38
Run No. 8b				
A	1162.5	529.0	1152.46	1093.04
B	1049.0	521.0	749.58	710.93
C	850.0	506.0	300.94	285.42
D	768.0	505.0	186.49	176.87
E	728.0	505.0	142.31	134.97
Run No. 9a				
A	1351.0	1189.0	878.69	833.38
B	1222.0	1068.0	612.41	580.84
C	983.0	852.5	267.38	253.59
D	889.5	775.0	174.89	165.87
E	845.0	736.5	142.15	134.82
Run No. 9b				
A	1141.5	526.0	1068.95	1013.83
B	1029.0	514.0	693.16	657.42
C	828.0	505.0	267.01	253.24
D	754.0	505.0	170.21	161.44
E	719.0	502.0	134.33	127.40
Run No. 10a				
A	1328.0	1161.0	852.71	808.74
B	1200.0	1042.0	589.89	559.48
C	975.0	839.0	269.12	255.24
D	883.0	762.0	178.52	169.31
E	831.5	720.5	137.49	130.40

TABLE 6 (continued)

INFINITE PARALLEL PLANE METHOD

Run No. 10b			$\epsilon = 0.556$	$\epsilon = 0.535$
Point	T_2 measured	T_4 measured	Q computed	Q computed
A	1115.0	520.5	970.64	920.59
B	1005.5	515.0	627.55	595.19
C	816.0	505.0	250.15	237.25
D	744.0	502.5	159.98	151.73
E	704.0	502.0	120.08	113.87

TABLE 7

LUMPED PARAMETER METHOD

($n = 5$ case for $\epsilon = 0.556$)

Run No. 1 $\epsilon_5 = 1$ $\rho_5 = 0$

Point	Q_1	Q_2	Q_3	Q_4	Q_5
A	1611.73	1490.40	-1295.37	-1437.00	-1559.00
B	1050.36	959.48	-846.06	-928.38	-1002.34
C	406.48	394.20	-333.20	-376.32	-368.22
D	259.52	255.45	-214.79	-242.78	-226.29
E	189.38	187.98	-158.08	-178.60	-158.81

Run No. 2 $\epsilon_5 = 1$ $\rho_5 = 0$

Point	Q_1	Q_2	Q_3	Q_4	Q_5
A	1533.35	1492.81	-1238.04	-1417.78	-1487.32
B	1013.57	952.31	-818.45	-913.99	-967.98
C	407.52	394.39	-333.98	-376.10	-369.25
D	257.35	253.70	-213.44	-241.44	-222.02
E	198.51	195.36	-165.31	-186.01	-167.77

Run No. 3 $\epsilon_5 = 0$ $\rho_5 = 1$

Point	Q_1	Q_2	Q_3	Q_4	Q_5
A	1407.50	1490.03	-1412.00	-1466.72	0.0
B	932.20	946.74	-931.95	-943.47	0.0
C	372.53	395.98	-373.94	-388.73	0.0
D	239.69	254.51	-240.48	-250.16	0.0
E	183.00	196.24	-183.83	-191.98	0.0

Run No. 4 $\epsilon_5 = 1$ $\rho_5 = 0$

Point	Q_1	Q_2	Q_3	Q_4	Q_5
A	1491.33	1505.68	-1037.59	-1293.59	-1208.60
B	1011.77	963.33	-697.62	-845.39	-818.38
C	395.84	395.75	-281.34	-343.35	-304.02
D	252.80	255.28	-186.25	-223.65	-177.46
E	195.70	197.86	-144.38	-173.18	-136.86

Run No. 5 $\epsilon_5 = 0$ $\rho_5 = 1$

Point	Q_1	Q_2	Q_3	Q_4	Q_5
A	1363.29	1470.26	-1371.55	-1432.95	0.0
B	921.06	951.06	-921.62	-944.63	0.0
C	370.81	393.78	-372.50	-385.49	0.0
D	238.01	254.04	-239.22	-248.12	0.0
E	179.09	194.86	-180.50	-188.45	0.0

TABLE 7 (continued)

LUMPED PARAMETER METHOD

Run No. 6 $\epsilon_5 = 1$ $\rho_5 = 0$

Point	Q_1	Q_2	Q_3	Q_4	Q_5
A	1347.64	1429.70	-619.92	-827.88	-701.27
B	935.32	914.74	-424.13	-555.33	-479.30
C	387.80	388.61	-185.87	-239.02	-190.93
D	251.66	255.39	-127.51	-160.99	-117.90
E	193.57	198.43	-102.43	-127.67	-86.86

Run No. 7 $\epsilon_5 = 0$ $\rho_5 = 1$

A	1163.36	1378.20	-1191.07	-1274.02	0.0
B	785.85	881.19	-795.65	-844.36	0.0
C	323.13	365.23	-327.78	-347.75	0.0
D	214.18	240.09	-216.98	-229.54	0.0
E	163.00	183.72	-165.34	-174.90	0.0

Run No. 8a $\epsilon_5 = 0$ $\rho_5 = 1$

A	805.54	991.84	-834.25	-868.86	0.0
B	607.51	669.33	-619.23	-615.27	0.0
C	258.99	300.71	-266.01	-270.08	0.0
D	166.61	194.21	-171.14	-174.40	0.0
E	133.17	151.76	-136.42	-137.31	0.0

Run No. 8b $\epsilon_5 = 0$ $\rho_5 = 1$

A	955.51	1167.91	-983.38	-1063.10	0.0
B	633.09	756.12	-648.64	-697.53	0.0
C	247.44	305.95	-255.35	-276.20	0.0
D	152.76	189.97	-157.89	-170.67	0.0
E	116.33	145.10	-120.33	-130.05	0.0

Run No. 9a $\epsilon_5 = 0$ $\rho_5 = 1$

A	776.38	976.25	-833.40	-763.75	0.0
B	583.38	661.00	-611.09	-558.08	0.0
C	244.74	289.42	-257.71	-241.15	0.0
D	158.17	189.97	-167.09	-156.77	0.0
E	129.35	153.83	-136.27	-128.11	0.0

TABLE 7 (continued)

LUMPED PARAMETER METHOD

Run No. 9b $\epsilon_5 = 0$ $\rho_5 = 1$

Point	Q_1	Q_2	Q_3	Q_4	Q_5
A	901.16	1098.66	-925.83	-1006.50	0.0
B	588.22	711.37	-603.49	-654.37	0.0
C	225.26	274.86	-231.64	-251.05	0.0
D	142.98	175.54	-147.25	-159.63	0.0
E	112.54	138.48	-115.90	-125.97	0.0

Run No. 10a $\epsilon_5 = 0$ $\rho_5 = 1$

Point	Q_1	Q_2	Q_3	Q_4	Q_5
A	646.68	988.94	-735.40	-655.30	0.0
B	491.02	658.85	-536.59	-487.48	0.0
C	225.34	295.84	-243.61	-227.14	0.0
D	150.19	194.99	-161.62	-152.02	0.0
E	117.89	149.07	-125.97	-118.65	0.0

Run No. 10b $\epsilon_5 = 0$ $\rho_5 = 1$

Point	Q_1	Q_2	Q_3	Q_4	Q_5
A	841.50	989.18	-852.36	-944.13	0.0
B	549.33	638.87	-555.87	-611.41	0.0
C	219.04	254.73	-221.63	-243.65	0.0
D	141.01	162.82	-142.57	-155.97	0.0
E	104.14	122.45	-105.44	-116.73	0.0

TABLE 8

LUMPED PARAMETER METHOD

(n = 5 case for ϵ = 0.535)

Run No. 1 $\epsilon_5 = 1$ $\rho_5 = 0$

Point	Q_1	Q_2	Q_3	Q_4	Q_5
A	1536.89	1416.06	-1223.06	-1360.50	-1549.76
B	1001.54	911.54	-798.89	-879.01	-996.38
C	387.46	375.16	-314.76	-356.26	-366.07
D	247.34	242.75	-202.83	-229.83	-224.98
E	180.46	178.63	-149.40	-160.09	-157.89

Run No. 2 $\epsilon_5 = 1$ $\rho_5 = 0$

Point	Q_1	Q_2	Q_3	Q_4	Q_5
A	1462.19	1418.80	-1169.02	-1342.00	-1478.66
B	966.42	904.88	-772.85	-865.29	-962.27
C	388.46	374.78	-315.50	-356.04	-367.09
D	245.26	241.17	-201.69	-228.57	-220.73
E	189.17	186.64	-156.22	-176.10	-166.80

Run No. 3 $\epsilon_5 = 0$ $\rho_5 = 1$

Point	Q_1	Q_2	Q_3	Q_4	Q_5
A	1486.48	1442.39	-1190.25	-1362.20	-1497.26
B	983.15	916.69	-786.63	-876.14	-977.39
C	390.29	382.71	-318.38	-361.51	-365.05
D	249.60	245.69	-206.26	-233.01	-219.71
E	189.87	189.30	-158.38	-178.94	-160.95

Run No. 4 $\epsilon_5 = 1$ $\rho_5 = 0$

Point	Q_1	Q_2	Q_3	Q_4	Q_5
A	1425.55	1435.19	-977.37	-1220.61	-1196.78
B	967.25	917.94	-657.05	-798.04	-810.26
C	378.27	377.12	-265.78	-324.15	-301.04
D	241.45	243.41	-175.41	-211.23	-175.72
E	186.92	188.48	-136.23	-163.56	-135.52

Run No. 5 $\epsilon_5 = 0$ $\rho_5 = 1$

Point	Q_1	Q_2	Q_3	Q_4	Q_5
A	1295.30	1395.49	-1303.37	-1358.89	0.0
B	875.22	902.33	-875.76	-896.02	0.0
C	352.33	373.71	-353.78	-365.58	0.0
D	226.15	241.10	-227.33	-235.30	0.0
E	170.17	184.98	-171.53	-178.69	0.0

TABLE 8 (continued)

LUMPED PARAMETER METHOD

Point	Q_1	Q_2	Q_3	Q_4	Q_5
Run No. 6		$\epsilon_5 = 1$		$\rho_5 = 0$	
A	1293.35	1370.72	-581.34	-775.70	-687.44
B	896.31	875.89	-399.11	-521.36	-467.23
C	372.07	372.37	-199.93	-224.20	-187.15
D	241.37	244.63	-174.56	-151.63	-115.56
E	185.61	190.01	-96.45	-119.97	-85.14
Run No. 7		$\epsilon_5 = 0$		$\rho_5 = 1$	
A	1108.28	1311.12	-1135.10	-1210.27	0.0
B	755.25	835.48	-763.06	-806.12	0.0
C	307.87	347.31	-312.37	-330.40	0.0
D	204.07	228.30	-206.78	-218.09	0.0
E	155.30	174.70	-157.57	-166.17	0.0
Run No. 8a		$\epsilon_5 = 0$		$\rho_5 = 1$	
A	764.18	943.34	-792.51	-821.81	0.0
B	576.54	635.96	-588.09	-582.52	0.0
C	245.74	285.85	-252.66	-255.59	0.0
D	158.08	184.62	-162.55	-105.04	0.0
E	126.36	144.24	-129.57	-129.96	0.0
Run No. 8b		$\epsilon_5 = 0$		$\rho_5 = 1$	
A	909.61	1110.82	-936.64	-1009.19	0.0
B	602.71	719.02	-617.82	-662.20	0.0
C	235.54	291.02	-243.21	-262.18	0.0
D	145.41	180.71	-150.39	-161.99	0.0
E	110.74	138.03	-114.62	-123.44	0.0
Run No. 9a		$\epsilon_5 = 0$		$\rho_5 = 1$	
A	737.61	929.36	-793.25	-722.04	0.0
B	554.47	628.57	-581.52	-528.17	0.0
C	232.58	275.30	-245.25	-228.21	0.0
D	150.31	180.73	-159.02	-148.34	0.0
E	122.93	146.32	-129.68	-121.24	0.0
Run No. 9b		$\epsilon_5 = 0$		$\rho_5 = 1$	
A	856.60	1044.18	-880.67	-954.31	0.0
B	559.14	676.05	-574.05	-620.44	0.0
C	214.12	261.24	-220.35	-236.01	0.0
D	135.91	166.85	-140.07	-151.33	0.0
E	106.97	131.63	-110.25	-119.42	0.0

TABLE 8 (continued)

LUMPED PARAMETER METHOD

Run No. 10a $\epsilon_5 = 0$ $\rho_5 = 1$

Point	Q_1	Q_2	Q_3	Q_4	Q_5
A	614.97	943.11	-701.01	-619.55	0.0
B	467.19	627.65	-511.38	-461.46	0.0
C	214.42	281.75	-232.14	-215.13	0.0
D	142.92	185.68	-154.00	-144.01	0.0
E	112.19	141.92	-120.03	-112.42	0.0

Run No. 10b $\epsilon_5 = 0$ $\rho_5 = 1$

A	798.65	939.29	-809.37	-894.77	0.0
B	521.37	606.61	-527.83	-579.47	0.0
C	207.90	241.87	-210.45	-230.92	0.0
D	133.83	154.59	-135.38	-147.82	0.0
E	98.83	116.27	-100.12	-110.62	0.0

foil case is $\epsilon_5 = 1$.

This type of calculation lends itself to an energy balance such as for Run No. 1, Point A, where if Q_1 and Q_2 are added as a function of their areas and Q_3, Q_4, and Q_5 are also added as a function of their areas, the two sums must be equal. A calculation found that the two sums differed by only 1.3 Btu/hr ft^2.

The variation in the upper limit of the net flux in Figure 31 is a function of the ability of the apparatus to measure temperatures accurately. The expected trend would be a decrease in surface temperatures resulting in a reduced computed value for the radiant heat transfer rate between plates. The only change in the three curves in Figure 32 is the reduction of the upper magnitude of flux. The plot of the (n = 5 case) for the lumped parameter method in Figure 30 is parallel to the infinite, parallel plane method for ϵ = 0.556. If the (n = 7 case) were also plotted in Figure 30 it would be exactly between the curves with emittance values of 0.556. Values for the (n = 7 case) are in Table 9.

Determination of the configuration factors necessary for these calculations is discussed next.

Configuration Factors

The configuration factor for the infinite, parallel plane method of computation is unity. For the quadrature method the kernel of the integral equation is a function of the geometry of the enclosure. The configuration factor, the

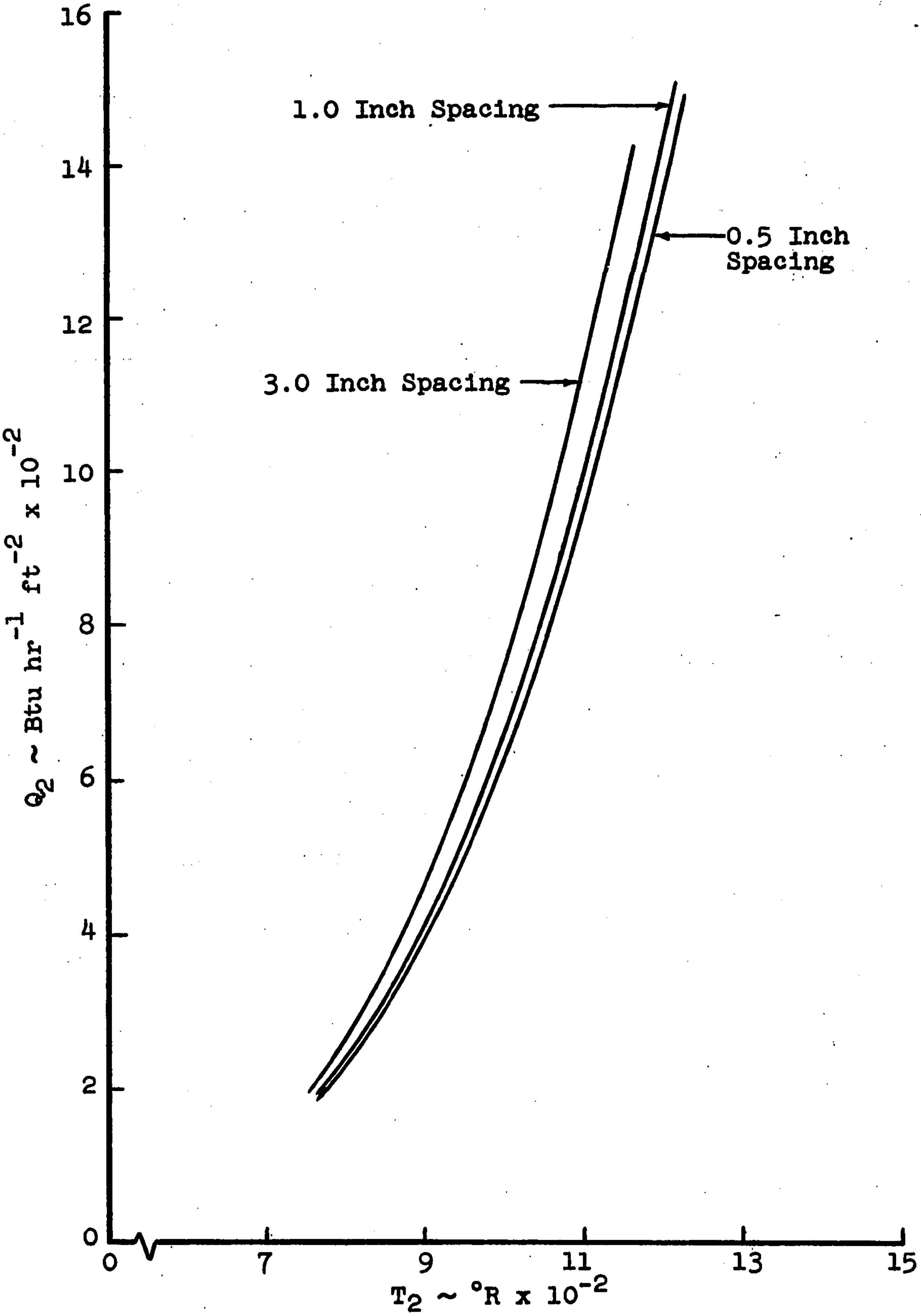

Figure 31
Lumped Parameter Method for No Foil Case

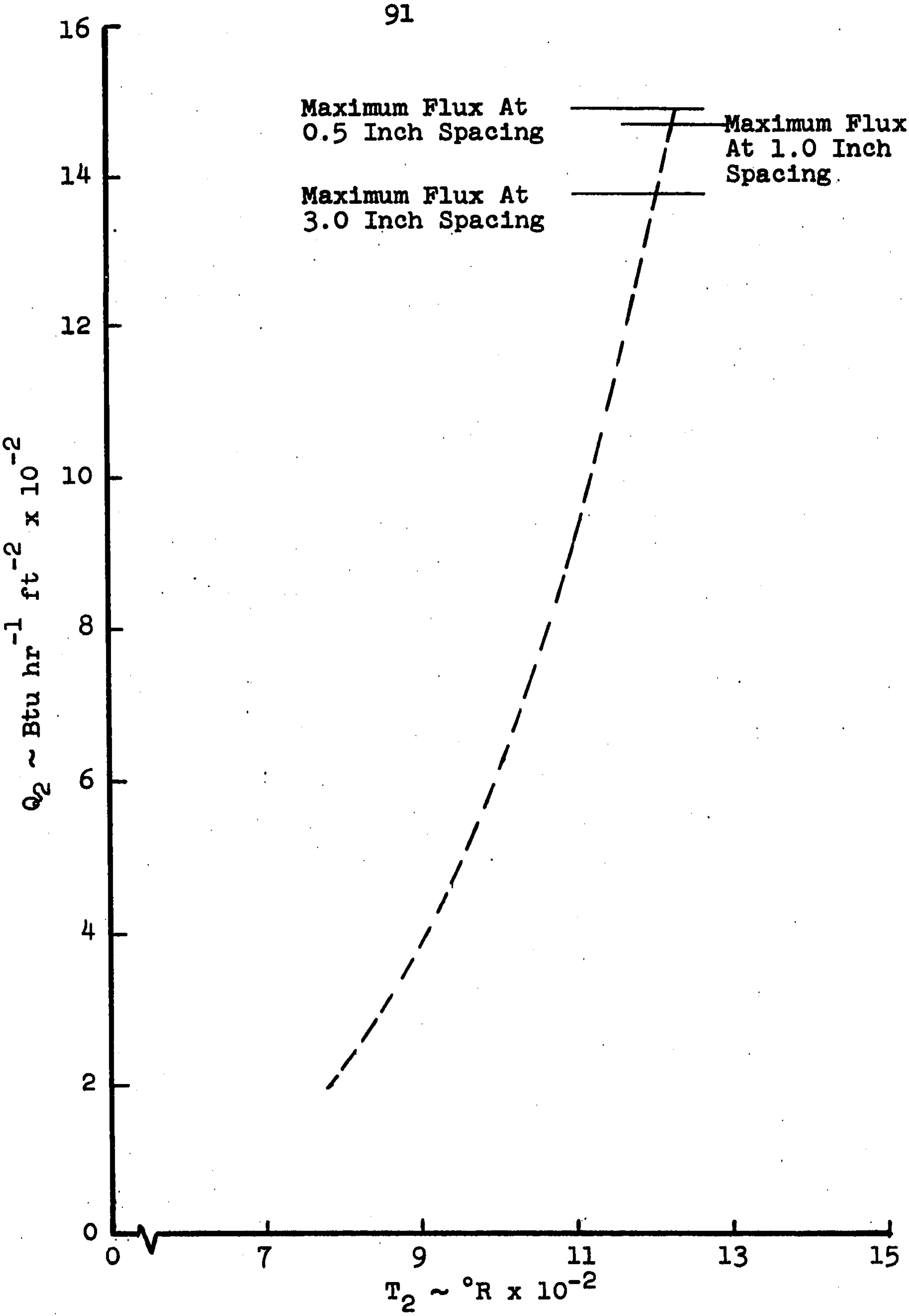

Figure 32
Lumped Parameter Method for Foil Case

TABLE 9

LUMPED PARAMETER METHOD

($n = 7$ case for $\epsilon = 0.556$)

Point	Q_1	Q_2	Q_3	Q_4	Q_5	Q_6	Q_7
Run No. 1		$\epsilon_5 = 1$		$\rho_5 = 0$			
A	1514.07	1476.00	-1455.62	-1448.57	-1259.03	1709.00	-1133.92
B	991.69	950.97	-942.58	-935.07	-773.39	1049.88	-716.94
C	384.55	391.50	-370.46	-378.89	-289.01	413.57	-287.04
D	245.90	253.35	-238.47	-244.41	-180.41	267.99	-187.61
E	179.81	186.47	-175.09	-179.77	-127.86	196.73	-139.18
Run No. 2		$\epsilon_5 = 1$		$\rho_5 = 0$			
A	1443.99	1479.85	-1384.38	-1428.04	-1155.58	1551.13	-1051.06
B	955.95	943.91	-913.35	-920.62	-752.85	1024.09	-697.13
C	385.34	391.05	-371.69	-378.71	-291.82	418.82	-289.37
D	243.73	251.66	-237.30	-243.10	-180.15	270.92	-188.83
E	188.32	193.76	-183.36	-187.25	-135.86	207.95	-146.27
Run No. 3		$\epsilon_5 = 0$		$\rho_5 = 1$			
A	1434.97	1488.10	-1446.41	-1465.88	0.0	1387.08	-1385.47
B	951.11	945.61	-953.32	-942.77	0.0	912.66	-911.97
C	380.23	395.60	-382.19	-388.37	0.0	359.04	-361.28
D	244.48	254.23	-245.99	-249.97	0.0	231.97	-232.77
E	186.36	195.95	-188.53	-191.90	0.0	180.61	-180.18

TABLE 9 (continued)

LUMPED PARAMETER METHOD

Run No. 4 $\epsilon_5 = 1$ $\rho_5 = 0$

Point	Q_1	Q_2	Q_3	Q_4	Q_5	Q_6	Q_7
A	1423.80	1489.17	-1169.42	-1305.27	-1167.95	1592.31	-853.20
B	967.21	952.55	-784.32	-853.15	-786.88	1069.06	-572.57
C	379.69	391.69	-314.37	-346.20	-291.54	415.49	-233.95
D	243.59	253.01	-206.62	-225.38	-172.29	267.64	-158.54
E	188.53	195.88	-160.32	-174.56	-133.68	209.00	-123.61

Run No. 5 $\epsilon_5 = 0$ $\rho_5 = 1$

Point	Q_1	Q_2	Q_3	Q_4	Q_5	Q_6	Q_7
A	1378.40	1460.36	-1433.22	-1438.32	0.0	1450.49	-1385.98
B	934.92	945.90	-957.03	-946.72	0.0	949.92	-919.21
C	377.56	392.24	-384.92	-385.74	0.0	369.94	-364.90
D	240.46	252.24	-250.17	-249.13	0.0	253.86	-242.16
E	182.30	194.11	-186.63	-188.59	0.0	178.70	-176.89

Run No. 6 $\epsilon_5 = 1$ $\rho_5 = 0$

Point	Q_1	Q_2	Q_3	Q_4	Q_5	Q_6	Q_7
A	1317.58	1413.90	-721.34	-847.83	-667.83	1679.28	-541.43
B	916.33	905.33	-487.86	-566.33	-448.96	1116.34	-367.83
C	381.02	385.23	-210.49	-242.59	-176.55	444.55	-161.85
D	247.71	253.24	-143.15	-163.22	-109.20	287.02	-111.80
E	190.86	190.81	-114.25	-129.33	-80.54	219.94	-90.67

Run No. 7 $\epsilon_5 = 0$ $\rho_5 = 1$

Point	Q_1	Q_2	Q_3	Q_4	Q_5	Q_6	Q_7
A	1142.10	1335.56	-1301.61	-1323.30	0.0	1510.15	-1228.08
B	786.42	856.49	-861.37	-873.28	0.0	961.43	-810.39
C	324.08	359.10	-346.89	-354.13	0.0	361.45	-323.67
D	215.25	236.35	-228.75	-233.22	0.0	234.48	-212.33
E	164.06	181.07	-173.91	-177.43	0.0	176.29	-161.22

fraction of energy leaving one surface and striking another surface, was calculated for the lumped parameter case.

With or without aluminum foil the border between the two plates is considered as zone 5 or area 5. Thus the system is considered as an enclosure made up of areas A_1, A_2, A_3, A_4, and A_5 such that

$$\begin{array}{ccccccccccc} F_{1-1} & + & F_{1-2} & + & F_{1-3} & + & \cdots & + & F_{1-n} & = & 1 \\ F_{2-1} & + & F_{2-2} & + & F_{2-3} & + & \cdots & + & F_{2-n} & = & 1 \\ \vdots & & \vdots & & \vdots & & \vdots & & \vdots & & \\ F_{n-1} & + & F_{n-2} & + & F_{n-3} & + & \cdots & + & F_{n-n} & = & 1 \end{array} \tag{6.1}$$

To solve this system of equations for all of the configuration factors, the reciprocity relation

$$F_{ij}A_i = F_{ji}A_j \tag{6.2}$$

is used together with other expressions developed by the decomposition of one or more surfaces into subdivisions which relate various configuration factors. The determination of additional relations among shape factors, using the decomposition of surfaces, is illustrated by

$$A_2F_{2-3} + A_2F_{2-4} + A_2F_{2-7} = A_2F_{2-347}$$

or

$$F_{2-3} + F_{2-4} + F_{2-7} = F_{2-347} \tag{6.3}$$

which is typical of the many different expressions used. An important expression using the decomposition of surfaces is illustrated in Figure 33.

$$A_2F_{2-34} = A_{2abc}F_{2abc-4def} + A_cF_{c-f} - A_{ac}F_{ac-df} - A_{bc}F_{bc-ef} \tag{6.4}$$

To determine the configuration factors for substitution into equation 6.4 the shape factor for finite, parallel, opposed rectangles is used.

$$F_{12-34} = \frac{1}{\pi}\Bigg[\frac{1}{R_1R_2} \ln \frac{(1+R_1^2)(1+R_2^2)}{(1+R_1^2+R_2^2)} - \frac{2}{R_1}\tan^{-1} R_2 - \frac{2}{R_2}\tan^{-1} R_1 + 2\sqrt{1+\frac{1}{R_1^2}}\tan^{-1}\frac{R_2}{\sqrt{1+R_1^2}} + 2\sqrt{1+\frac{1}{R_2^2}}\tan^{-1}\frac{R_1}{\sqrt{1+R_2^2}} \Bigg] \tag{6.5}$$

where

$$R_1 = \frac{L}{h}, \qquad R_2 = \frac{W}{h} \tag{6.6}$$

with L = length of rectangle and W = width of rectangle.

These results are tabulated in Table 10. The matrices formed by the configuration factors from equation 6.1 are given in Table 11 for the various spacings of the planes. A check was made to determine if the left and right sides of equation 6.1 were equal, and agreement was found in every case.

Quadrature Method

The quadrature method considered the variation of

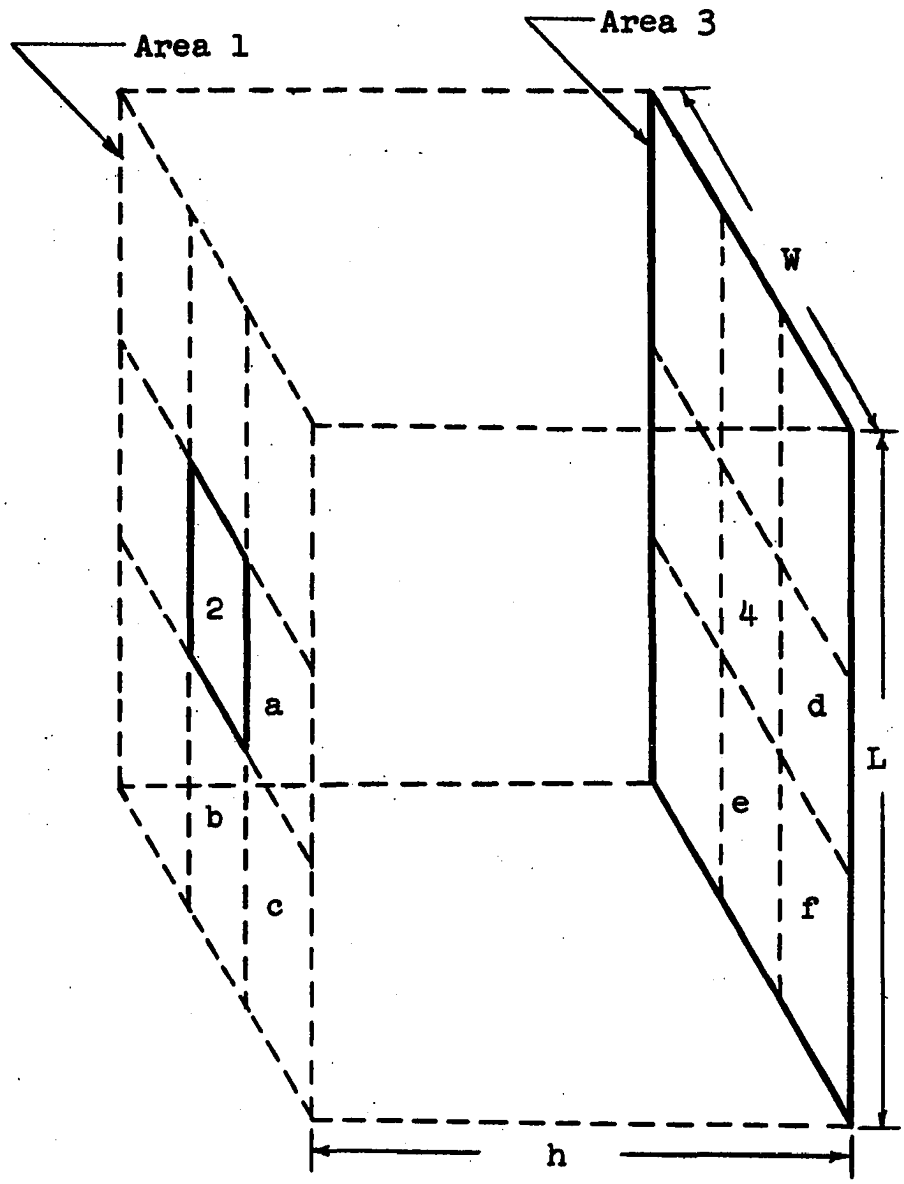

Area 1 = L x W - Area 2
Area 3 = L x W - Area 4

Figure 33

Configuration Factor Geometry For Finite, Parallel Opposed Rectangles

TABLE 10

CONFIGURATION FACTORS

h inches	L inches	W inches		
0.5	5.50	5.50	0.840993	F_{2-4}
0.5	12.00	12.00	0.922322	$F_{126-347}$
0.5	8.75	8.75	0.895694	$F_{2abc-4def}$
0.5	3.25	3.25	0.749686	F_{c-f}
0.5	8.75	3.25	0.816997	F_{ac-df}
0.5	3.25	8.75	0.816997	F_{bc-ef}
1.0	5.50	5.50	0.712967	F_{2-4}
1.0	12.00	12.00	0.852887	$F_{126-347}$
1.0	8.75	8.75	0.805573	$F_{2abc-4def}$
1.0	3.25	3.25	0.571917	F_{c-f}
1.0	8.75	3.25	0.673909	F_{ac-df}
1.0	3.25	8.75	0.673909	F_{bc-ef}
1.5	5.50	5.50	0.607503	F_{2-4}
1.5	12.00	12.00	0.789953	$F_{126-347}$
1.5	8.75	8.75	0.726350	$F_{2abc-4def}$
1.5	3.25	3.25	0.441981	F_{c-f}
1.5	8.75	3.25	0.560526	F_{ac-df}
1.5	3.25	8.75	0.560526	F_{bc-ef}
2.0	5.50	5.50	0.519976	F_{2-4}
2.0	12.00	12.00	0.732583	$F_{126-347}$
2.0	8.75	8.75	0.656243	$F_{2abc-4def}$
2.0	3.25	3.25	0.346149	F_{c-f}
2.0	8.75	3.25	0.470321	F_{ac-df}
2.0	3.25	8.75	0.470321	F_{bc-ef}
2.5	5.50	5.50	0.447063	F_{2-4}
2.5	12.00	12.00	0.680116	$F_{126-347}$
2.5	8.75	8.75	0.593988	$F_{2abc-4def}$
2.5	3.25	3.25	0.274920	F_{c-f}
2.5	8.75	3.25	0.398209	F_{ac-df}
2.5	3.25	8.75	0.398209	F_{bc-ef}
3.0	5.50	5.50	0.386162	F_{2-4}
3.0	12.00	12.00	0.632036	$F_{126-347}$
3.0	8.75	8.75	0.538587	$F_{2abc-4def}$
3.0	3.25	3.25	0.221471	F_{c-f}
3.0	8.75	3.25	0.340168	F_{ac-df}
3.0	3.25	8.75	0.340168	F_{bc-ef}

TABLE 10 (continued)

CONFIGURATION FACTORS

h inches	L inches	W inches		
0.5	5.50	5.50	0.840993	$F_2 - 4$
0.5	10.00	10.00	0.907853	$F_{12} - 34$
0.5	7.75	7.75	0.883366	$F_{2abc} - 4def$
0.5	2.25	2.25	0.663625	$F_c - f$
0.5	7.75	2.25	0.760711	$F_{ac} - df$
0.5	2.25	7.75	0.760711	$F_{bc} - ef$
1.0	5.50	5.50	0.712967	$F_2 - 4$
1.0	10.00	10.00	0.826994	$F_{12} - 34$
1.0	7.75	7.75	0.784170	$F_{2abc} - 4def$
1.0	2.25	2.25	0.454529	$F_c - f$
1.0	7.75	2.25	0.588595	$F_{ac} - df$
1.0	2.25	7.75	0.588595	$F_{bc} - ef$
1.5	5.50	5.50	0.607503	$F_2 - 4$
1.5	10.00	10.00	0.754910	$F_{12} - 34$
1.5	7.75	7.75	0.698208	$F_{2abc} - 4def$
1.5	2.25	2.25	0.320056	$F_c - f$
1.5	7.75	2.25	0.463616	$F_{ac} - df$
1.5	2.25	7.75	0.463616	$F_{bc} - ef$
2.0	5.50	5.50	0.519976	$F_2 - 4$
2.0	10.00	10.00	0.690244	$F_{12} - 34$
2.0	7.75	7.75	0.623199	$F_{2abc} - 4def$
2.0	2.25	2.25	0.232087	$F_c - f$
2.0	7.75	2.25	0.372055	$F_{ac} - df$
2.0	2.25	7.75	0.372055	$F_{bc} - ef$
2.5	5.50	5.50	0.447063	$F_2 - 4$
2.5	10.00	10.00	0.632036	$F_{12} - 34$
2.5	7.75	7.75	0.557516	$F_{2abc} - 4def$
2.5	2.25	2.25	0.173270	$F_c - f$
2.5	7.75	2.25	0.303932	$F_{ac} - df$
2.5	2.25	7.75	0.303932	$F_{bc} - ef$
3.0	5.50	5.50	0.386162	$F_2 - 4$
3.0	10.00	10.00	0.579530	$F_{12} - 34$
3.0	7.75	7.75	0.499875	$F_{2abc} - 4def$
3.0	2.25	2.25	0.132910	$F_c - f$
3.0	7.75	2.25	0.252282	$F_{ac} - df$
3.0	2.25	7.75	0.252282	$F_{bc} - ef$

TABLE 10 (continued)

CONFIGURATION FACTORS

h inches	L inches	W inches		
0.5	10.00	10.00	0.907853	$F_{12} - 34$
0.5	12.00	12.00	0.922322	$F_{126} - 347$
0.5	11.00	11.00	0.915706	$F_{12abc} - 34def$
0.5	1.00	1.00	0.415242	$F_{c} - f$
0.5	11.00	1.00	0.597658	$F_{ac} - df$
0.5	1.00	11.00	0.597658	$F_{bc} - ef$
1.0	10.00	10.00	0.826994	$F_{12} - 34$
1.0	12.00	12.00	0.852887	$F_{126} - 347$
1.0	11.00	11.00	0.840993	$F_{12abc} - 34def$
1.0	1.00	1.00	0.199824	$F_{c} - f$
1.0	11.00	1.00	0.388895	$F_{ac} - df$
1.0	1.00	11.00	0.388895	$F_{bc} - ef$
1.5	10.00	10.00	0.754910	$F_{12} - 34$
1.5	12.00	12.00	0.789953	$F_{126} - 347$
1.5	11.00	11.00	0.773786	$F_{12abc} - 34def$
1.5	1.00	1.00	0.110706	$F_{c} - f$
1.5	11.00	1.00	0.275849	$F_{ac} - df$
1.5	1.00	11.00	0.275849	$F_{bc} - ef$
2.0	10.00	10.00	0.690244	$F_{12} - 34$
2.0	12.00	12.00	0.732583	$F_{126} - 347$
2.0	11.00	11.00	0.712967	$F_{12abc} - 34def$
2.0	1.00	1.00	0.068589	$F_{c} - f$
2.0	11.00	1.00	0.208541	$F_{ac} - df$
2.0	1.00	11.00	0.208541	$F_{bc} - ef$
2.5	10.00	10.00	0.632036	$F_{12} - 34$
2.5	12.00	12.00	0.680116	$F_{126} - 347$
2.5	11.00	11.00	0.657746	$F_{12abc} - 34def$
2.5	1.00	1.00	0.046138	$F_{c} - f$
2.5	11.00	1.00	0.164854	$F_{ac} - df$
2.5	1.00	11.00	0.164854	$F_{bc} - ef$
3.0	10.00	10.00	0.579530	$F_{12} - 34$
3.0	12.00	12.00	0.632036	$F_{126} - 347$
3.0	11.00	11.00	0.607503	$F_{12abc} - 34def$
3.0	1.00	1.00	0.032971	$F_{c} - f$
3.0	11.00	1.00	0.134540	$F_{ac} - df$
3.0	1.00	11.00	0.134540	$F_{bc} - ef$

TABLE 12

CONFIGURATION FACTOR MATRICES

(n = 5 case)

h = 0.5 inches

0.0	0.0	0.863275	0.040337	0.096367
0.0	0.0	0.151682	0.840993	0.007325
0.863275	0.040337	0.0	0.0	0.096387
0.151682	0.840993	0.0	0.0	0.007325
0.456835	0.007325	0.456835	0.007325	0.067875

h = 1.0 inches

0.0	0.0	0.752571	0.068762	0.178665
0.0	0.0	0.258567	0.712967	0.028464
0.752571	0.068762	0.0	0.0	0.178665
0.258569	0.712967	0.0	0.0	0.028464
0.423400	0.017938	0.423400	0.017938	0.115322

h = 1.5 inches

0.0	0.0	0.662249	0.088111	0.249700
0.0	0.0	0.331329	0.607503	0.061168
0.662249	0.088111	0.0	0.0	0.249700
0.331328	0.607503	0.0	0.0	0.061168
0.394395	0.025699	0.394395	0.025699	0.159812

h = 2.5 inches

0.0	0.0	0.527425	0.107333	0.365241
0.0	0.0	0.403611	0.447063	0.149326
0.527425	0.107333	0.0	0.0	0.365241
0.403611	0.447063	0.0	0.0	0.149326
0.346218	0.037642	0.346218	0.037642	0.232279

h = 3.0 inches

0.0	0.0	0.476826	0.110298	0.412875
0.0	0.0	0.414757	0.386162	0.119081
0.476826	0.110298	0.0	0.0	0.412875
0.414756	0.386162	0.0	0.0	0.119081
0.326142	0.041820	0.326142	0.041820	0.264073

TABLE 11 (continued)

CONFIGURATION FACTOR MATRICES

(n = 7 case)

h = 0.5 inches

0.0	0.0	0.809338	0.063755	0.001457	0.0	0.125450
0.0	0.0	0.147006	0.840993	0.007325	0.0	0.004676
0.809338	0.063755	0.0	0.0	0.001457	0.125450	0.0
0.147006	0.840993	0.0	0.0	0.007325	0.004676	0.0
0.004234	0.009232	0.004234	0.009232	0.201995	0.385535	0.385535
0.0	0.0	0.198866	0.003214	0.210292	0.0	0.587627
0.198866	0.003214	0.0	0.0	0.210292	0.587627	0.0

h = 1.0 inches

0.0	0.0	0.666837	0.104866	0.082218	0.0	0.146077
0.0	0.0	0.241512	0.712967	0.028464	0.0	0.017057
0.666837	0.104866	0.0	0.0	0.082218	0.146077	0.0
0.241512	0.017938	0.0	0.0	0.028464	0.017057	0.0
0.119473	0.017938	0.119473	0.017938	0.116952	0.304112	0.304112
0.0	0.0	0.231566	0.011726	0.331759	0.0	0.426675
0.231566	0.011726	0.0	0.0	0.331759	0.426675	0.0

h = 3.0 inches

0.0	0.0	0.362952	0.153961	0.335440	0.0	0.147647
0.0	0.0	0.337747	0.386162	0.199081	0.0	0.077010
0.362952	0.153961	0.0	0.0	0.335440	0.147647	0.0
0.337747	0.386162	0.0	0.0	0.199081	0.077010	0.0
0.162478	0.041820	0.162478	0.041820	0.348995	0.121203	0.121203
0.0	0.0	0.234053	0.052944	0.535580	0.0	0.177422
0.235053	0.052944	0.0	0.0	0.535580	0.177422	0.0

radiosity over a surface. In all cases ($n = 1, 2, 3$, and 4) the net flux at the heater surface, and the net flux at the cold plate surface, were computed for plate spacings up to 24 inches in increments of 0.5 inches. At an average spacing of 18 inches, all of the flux values were approaching their final value. From Table 12 the net fluxes at the heater surface for the ($n = 1$ case and $n = 2$ case) approached each other at 24 inches, with values of 2179.56 Btu hr^{-1} ft^{-2} and 2180.90 Btu hr^{-1} ft^{-2} respectively. The ($n = 3$ case and $n = 4$ case) yielded slightly lower values of 2093.68 Btu hr^{-1} ft^{-2} and 2095.75 Btu hr^{-1} ft^{-2} for a 24 inch spacing. The fluxes computed in all of the cases were for Point A of Run No. 1.

TABLE 12

QUADRATURE METHOD

Run No. 1, Point A, $T_1 = 1231°R$, $T_2 = 525°R$

(n = 1 case)

h	Q_1	Q_2
0.5	4925.37	196.54
1.0	4934.93	297.96
1.5	4967.85	470.43
2.0	5052.36	726.22
2.5	5239.62	1100.61
3.0	5639.16	1689.89
3.5	6564.71	2798.40
4.0	9540.62	5944.78
4.5	289520.24	282479.54
5.0	-3411.25	-6712.99
5.5	-189.01	-3367.51
6.0	825.04	-2244.82
6.5	1302.23	-1672.19
7.0	1570.01	-1320.66
7.5	1736.13	-1081.01
8.0	1846.17	-906.36
8.5	1922.53	-773.09
9.0	1977.42	-667.98
9.5	2017.99	-582.95
10.0	2048.67	-512.82
10.5	2072.30	-454.06
11.0	2090.81	-404.18
11.5	2105.51	-361.38
12.0	2117.33	-324.32
12.5	2126.94	-291.97
13.0	2134.83	-263.54
13.5	2141.37	-238.39
14.0	2146.84	-216.02
14.5	2151.44	-196.04
15.0	2155.34	-178.09
15.5	2158.67	-161.91
16.0	2161.53	-147.27
16.5	2163.99	-133.98
17.0	2166.13	-121.88
17.5	2168.00	-110.81
18.0	2169.29	-100.68
18.5	2171.07	-91.37
19.0	2172.33	-82.80
19.5	2173.46	-74.88
20.0	2174.46	-67.56
20.5	2175.35	-60.78
21.0	2176.15	-54.48
21.5	2176.87	-48.62
22.0	2177.52	-43.15
22.5	2178.10	-38.06
23.0	2178.64	-33.29
23.5	2179.12	-28.82
24.0	2179.56	-24.64

TABLE 12 (continued)

QUADRATURE METHOD

Run No. 1, Point A, $T_1 = 1231°R$, $T_2 = 525°R$

(n = 2 case)

h	Q_1	Q_2	h	Q_1	Q_2
0.5	4934.92	297.95	21.5	2179.19	-28.18
1.0	5052.13	725.65	22.0	2179.59	-24.37
1.5	5631.39	1679.57	22.5	2179.96	-20.75
2.0	9237.61	5633.07	23.0	2180.30	-17.32
2.5	-4563.94	-7885.25	23.5	2180.61	-14.08
3.0	580.65	-2623.45	24.0	2180.90	-10.99
3.5	1419.49	-1522.15			
4.0	1729.40	-1091.20			
4.5	1878.97	-850.62			
5.0	1962.55	-697.44			
5.5	2014.10	-591.46			
6.0	2048.34	-513.59			
6.5	2072.46	-453.62			
7.0	2090.28	-405.66			
7.5	2103.95	-366.07			
8.0	2114.77	-332.56			
8.5	2123.56	-303.61			
9.0	2130.83	-278.20			
9.5	2136.95	-255.59			
10.0	2142.16	-235.27			
10.5	2146.64	-216.87			
11.0	2150.52	-200.11			
11.5	2153.92	-184.75			
12.0	2156.90	-170.62			
12.5	2159.53	-157.58			
13.0	2161.86	-145.51			
13.5	2163.93	-134.32			
14.0	2165.78	-123.92			
14.5	2167.43	-114.24			
15.0	2168.91	-105.21			
15.5	2170.24	-96.78			
16.0	2171.44	-88.90			
16.5	2172.52	-81.52			
17.0	2173.50	-74.60			
17.5	2174.39	-68.11			
18.0	2175.19	-62.01			
18.5	2175.93	-56.28			
19.0	2176.60	-50.88			
19.5	2177.21	-45.82			
20.0	2177.77	-41.01			
20.5	2178.28	-36.49			
21.0	2178.75	-32.22			

TABLE 12 (continued)

QUADRATURE METHOD

Run No. 1, Point A, T_1 = 1231°R, T_2 = 525°R

(n = 3 case)

h	Q_1	Q_2	h	Q_1	Q_2
0.5	5105.31	168.90	21.5	2072.19	68.55
1.0	5820.72	192.57	22.0	2077.04	68.71
1.5	7749.30	256.37	22.5	2081.58	68.87
2.0	300275.76	9934.03	23.0	2085.86	69.01
2.5	-3931.69	-130.07	23.5	2089.88	69.14
3.0	-826.35	-27.34	24.0	2093.68	69.27
3.5	138.85	4.59			
4.0	598.19	19.79			
4.5	868.31	28.73			
5.0	1050.65	34.76			
5.5	1186.06	39.24			
6.0	1293.38	42.79			
6.5	1382.14	45.73			
7.0	1457.61	48.22			
7.5	1522.92	50.38			
8.0	1580.11	52.27			
8.5	1630.60	53.94			
9.0	1675.41	55.43			
9.5	1715.38	56.75			
10.0	1751.16	57.93			
10.5	1783.29	59.00			
11.0	1812.21	59.95			
11.5	1838.33	60.82			
12.0	1861.97	61.60			
12.5	1883.42	62.31			
13.0	1902.92	62.95			
13.5	1920.70	63.54			
14.0	1936.79	64.08			
14.5	1951.79	64.57			
15.0	1965.41	65.02			
15.5	1977.93	65.44			
16.0	1989.46	65.82			
16.5	2000.08	66.17			
17.0	2009.90	66.49			
17.5	2018.99	66.79			
18.0	2027.41	67.07			
18.5	2035.24	67.33			
19.0	2042.51	67.57			
19.5	2049.28	67.80			
20.0	2055.60	68.01			
20.5	2061.50	68.20			
21.0	2067.02	68.38			

TABLE 12 (continued)

QUADRATURE METHOD

Run No. 1, Point A, $T_1 = 1231°R$, $T_2 = 525°R$

(n = 4 case)

h	Q_1	Q_2	h	Q_1	Q_2
0.5	4923.98	162.90	21.5	2046.41	67.70
1.0	4925.96	162.97	22.0	2058.60	68.10
1.5	4933.43	163.21	22.5	2069.48	68.46
2.0	4948.53	163.71	23.0	2079.20	68.79
2.5	4970.67	164.44	23.5	2087.92	69.07
3.0	5003.64	165.54	24.0	2095.75	69.33
3.5	5110.28	169.06			
4.0	4045.93	133.85			
4.5	4014.60	132.82			
5.0	-3702.59	-122.49			
5.5	8883.72	293.90			
6.0	7902.11	261.43			
6.5	8126.97	268.86			
7.0	8909.62	294.76			
7.5	10498.31	347.32			
8.0	14089.51	466.12			
8.5	27314.26	903.64			
9.0	-75930.81	-2512.02			
9.5	-11244.96	-372.02			
10.0	-4665.32	-154.34			
10.5	-2196.44	-72.66			
11.0	-918.92	-30.40			
11.5	-147.14	-4.87			
12.0	363.97	12.04			
12.5	723.68	23.94			
13.0	988.06	32.67			
13.5	1188.77	39.33			
14.0	1345.03	44.50			
14.5	1469.17	48.60			
15.0	1569.42	51.92			
15.5	1651.52	54.64			
16.0	1719.54	56.89			
16.5	1776.47	58.77			
17.0	1824.53	60.36			
17.5	1865.43	61.71			
18.0	1900.47	62.87			
18.5	1930.67	63.87			
19.0	1956.86	64.74			
19.5	1979.67	65.49			
20.0	1999.64	66.15			
20.5	2017.20	66.73			
21.0	2032.69	67.25			

CHAPTER VII

DISCUSSION OF RESULTS AND RECOMMENDATIONS

The equipment for this experimental investigation was designed and built to measure the exchange of radiant energy between parallel walls. Once the equipment was built and data were obtained, a comparison with computed values was made. The ability to generate reproducible data at a 0.5 inch spacing of the walls without aluminum foil around the edges of the plates was established. Net radiant flux measurements were made at spacings of 0.5, 1.0, and 3.0 inches. The two cases considered at each spacing were that of an open zone between the plates and that in which aluminum foil was placed around the edge of the plates, forming an enclosure.

Figures 34, 35, and 36 compare the infinite, parallel plate computation with the measured data at three plate spacings. The lumped parameter case was compared in Figures 37, 38, and 39. Figures 40 and 41 are cross plots of the experimental data compared with the lumped parameter method computations and infinite parallel plate computations. From Figure 40 the infinite plate method reasonably approximates the experimental data for the 0.5 inch and 1.0 inch spacings.

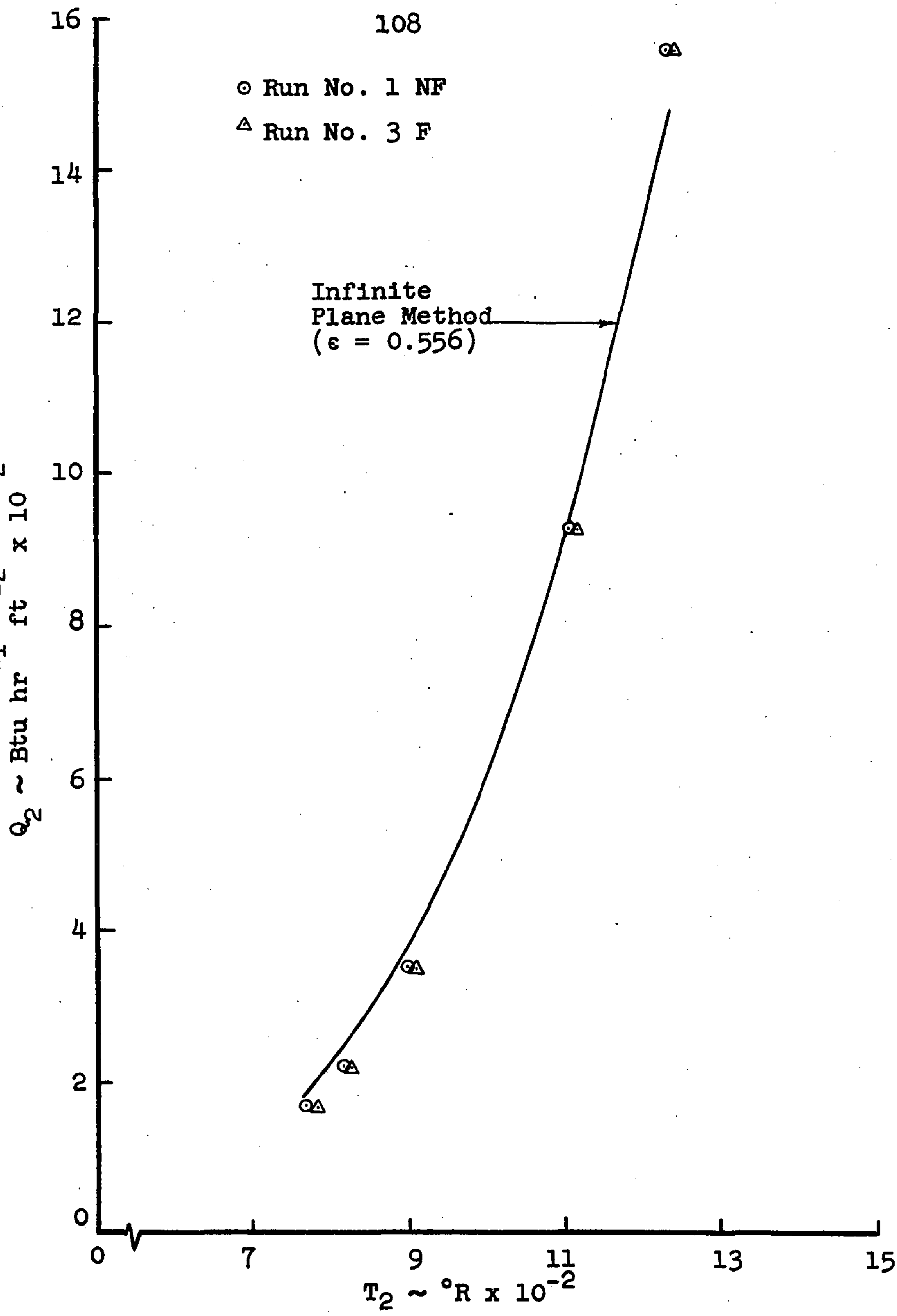

Figure 34
Comparison of Infinite Plane Method With Experimental Data At 0.5 Inch Spacing

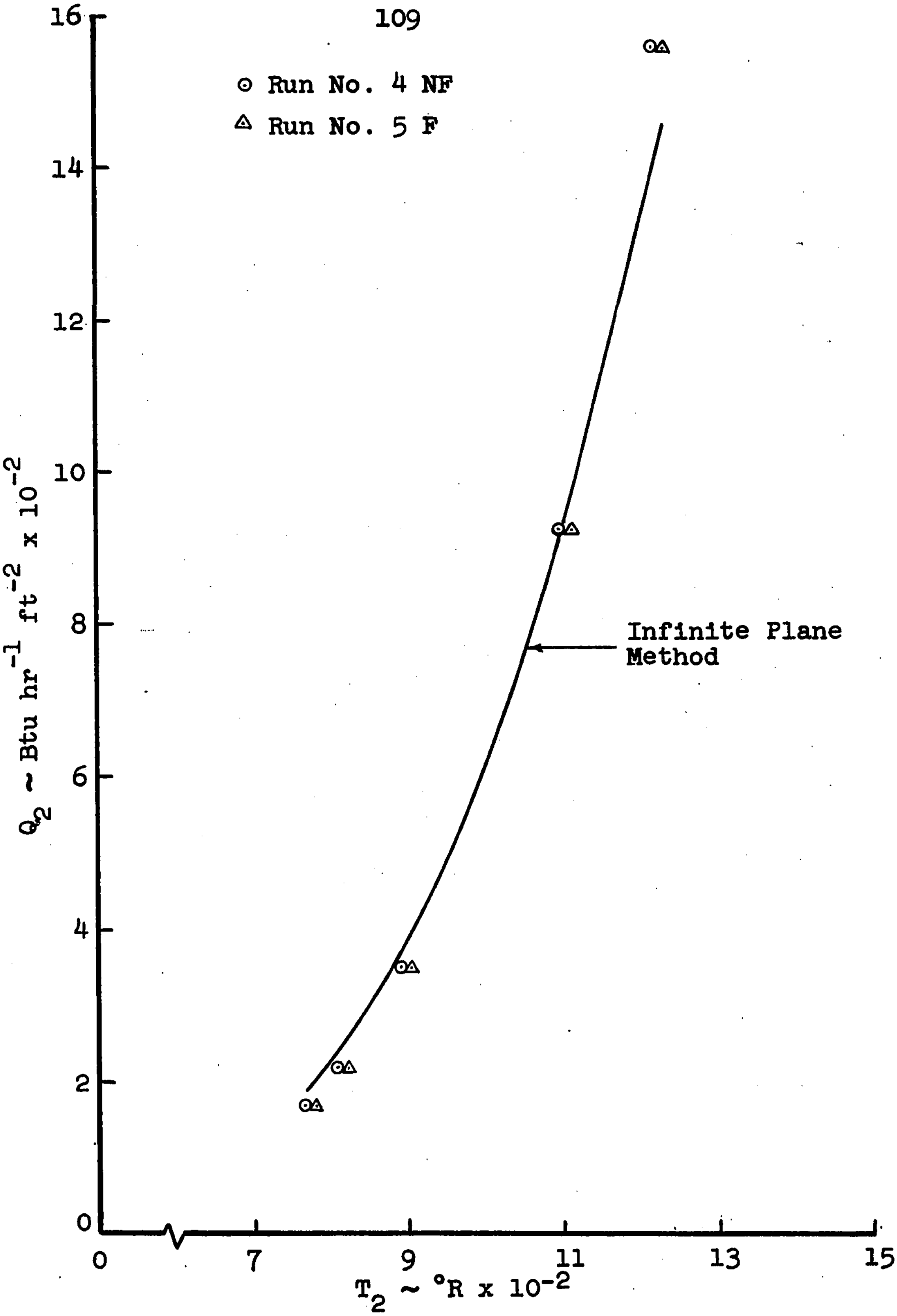

Figure 35
Comparison of Infinite Plane Method With Experimental Data At 1.0 Inch Spacing

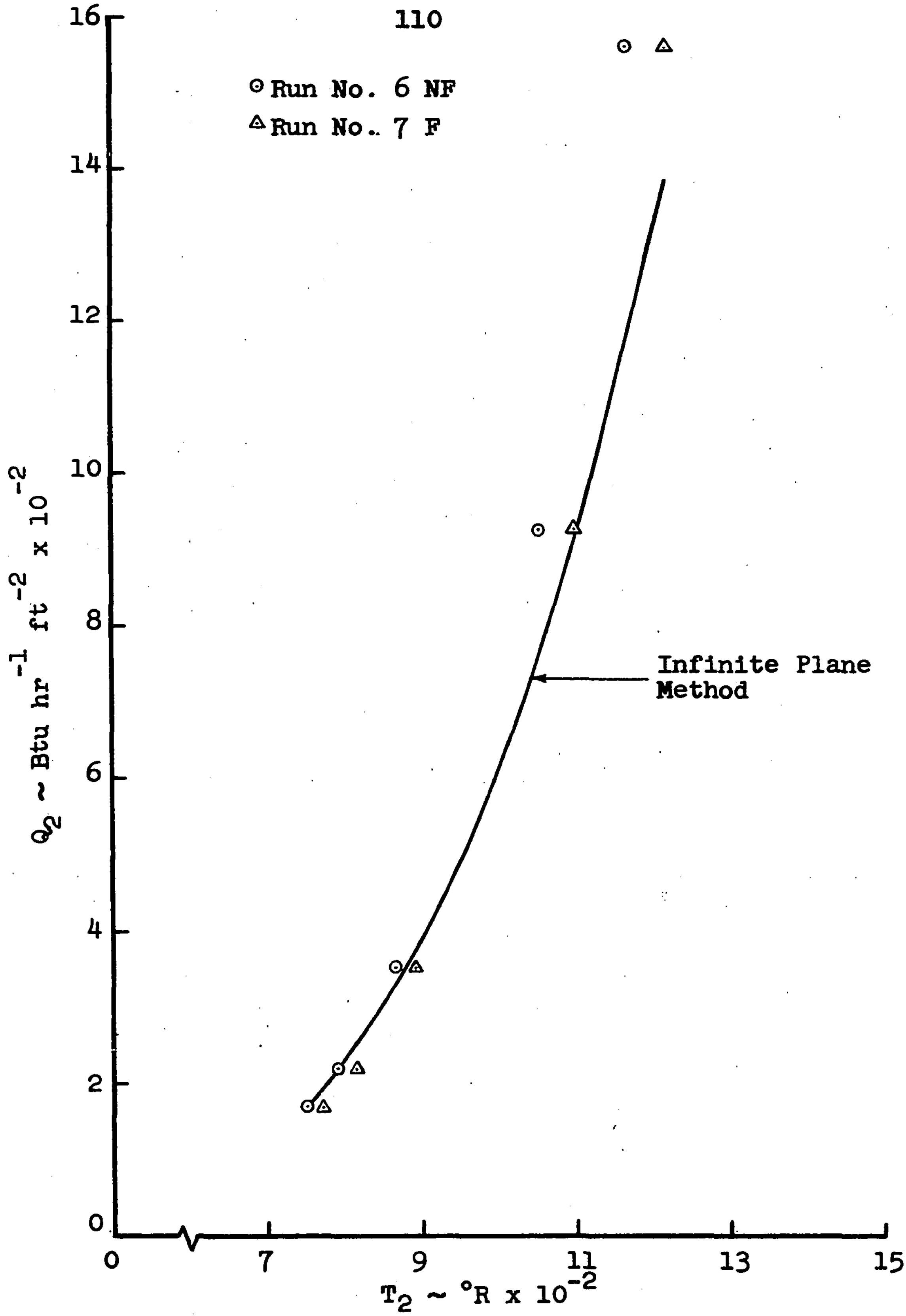

Figure 36
Comparison of Infinite Plane Method With Experimental Data At 3.0 Inch Spacing

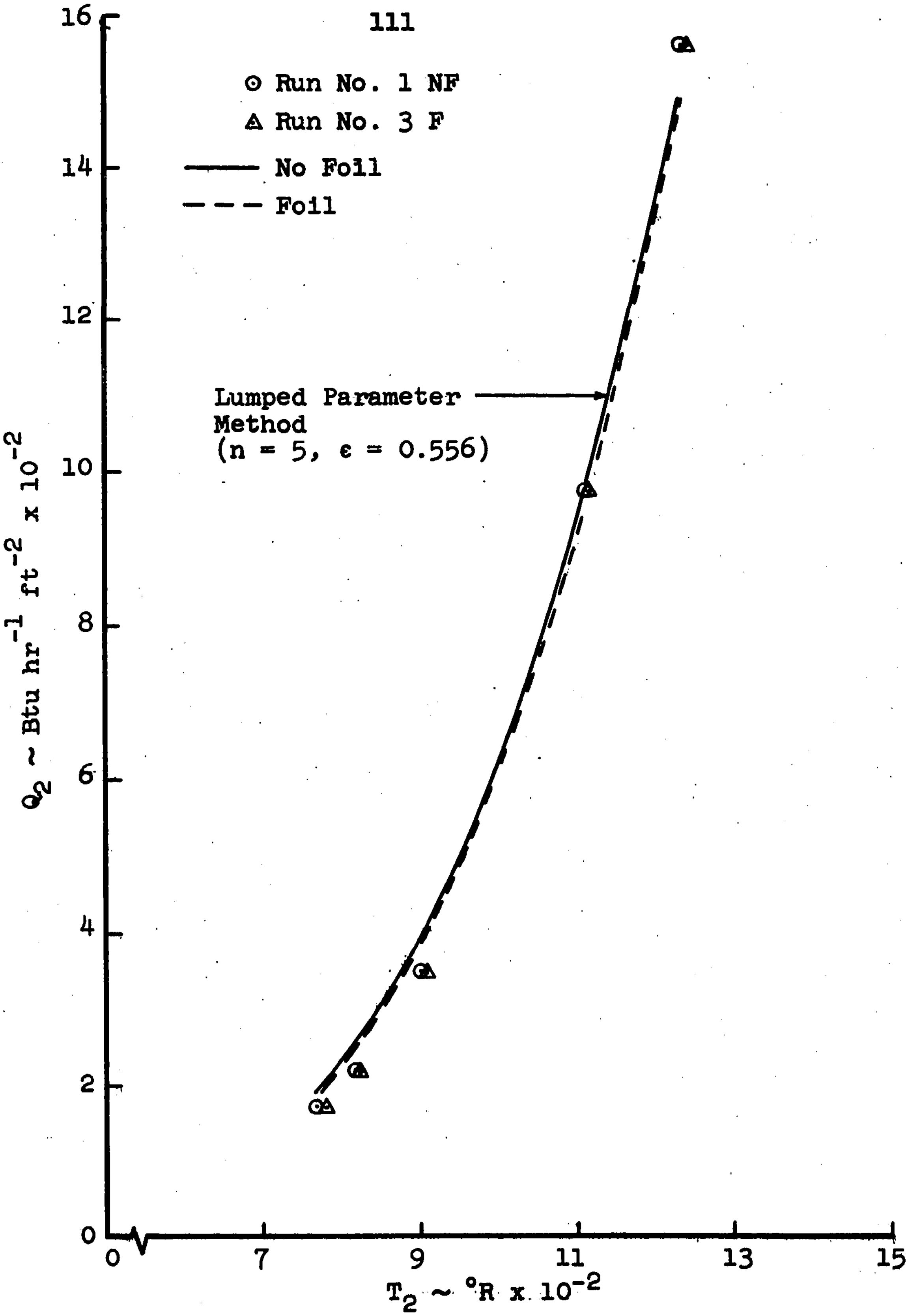

Figure 37
Comparison of Lumped Parameter Method With Experimental Data At 0.5 Inch Spacing

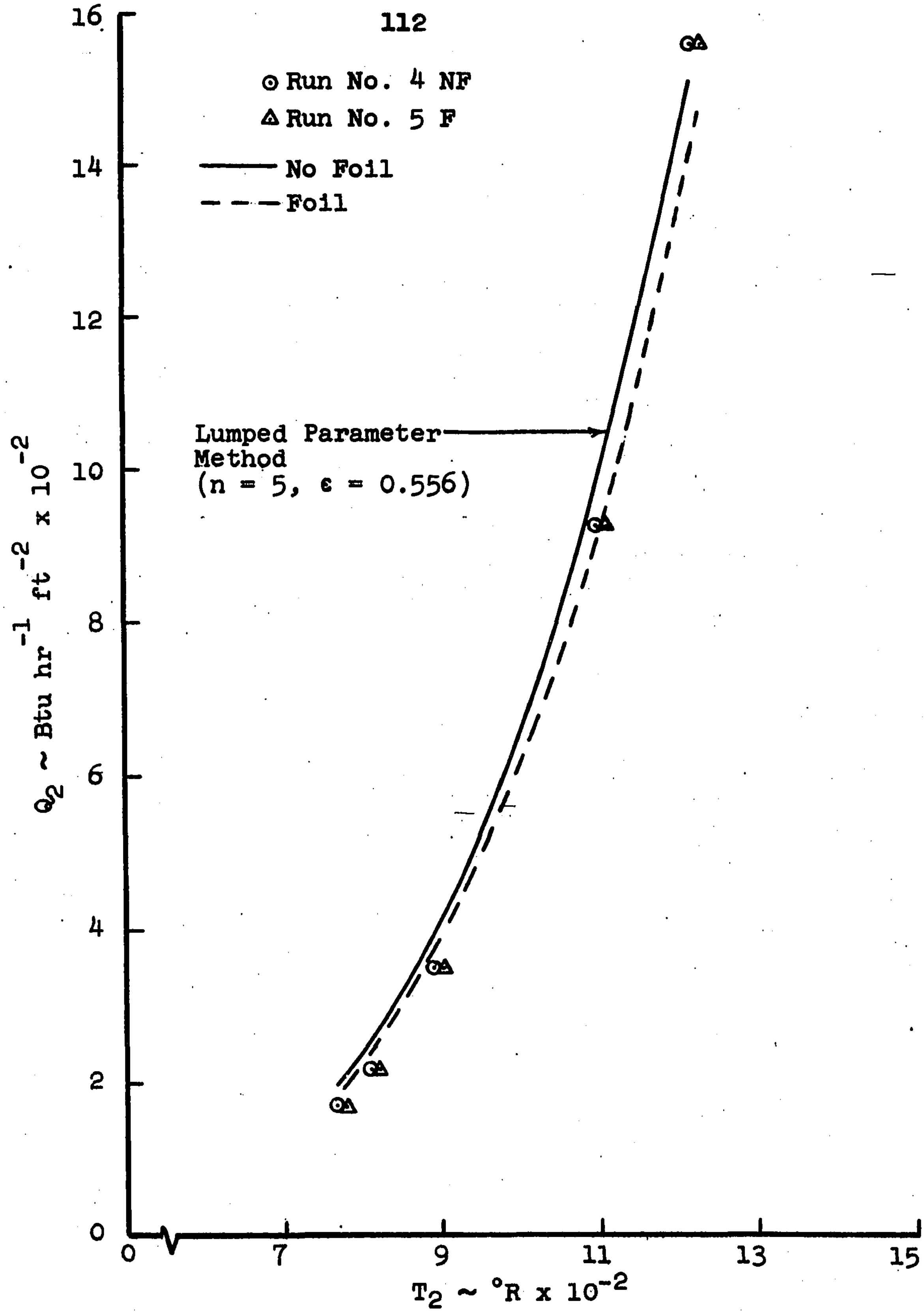

Figure 38
Comparison of Lumped Parameter Method With Experimental Data At 1.0 Inch Spacing

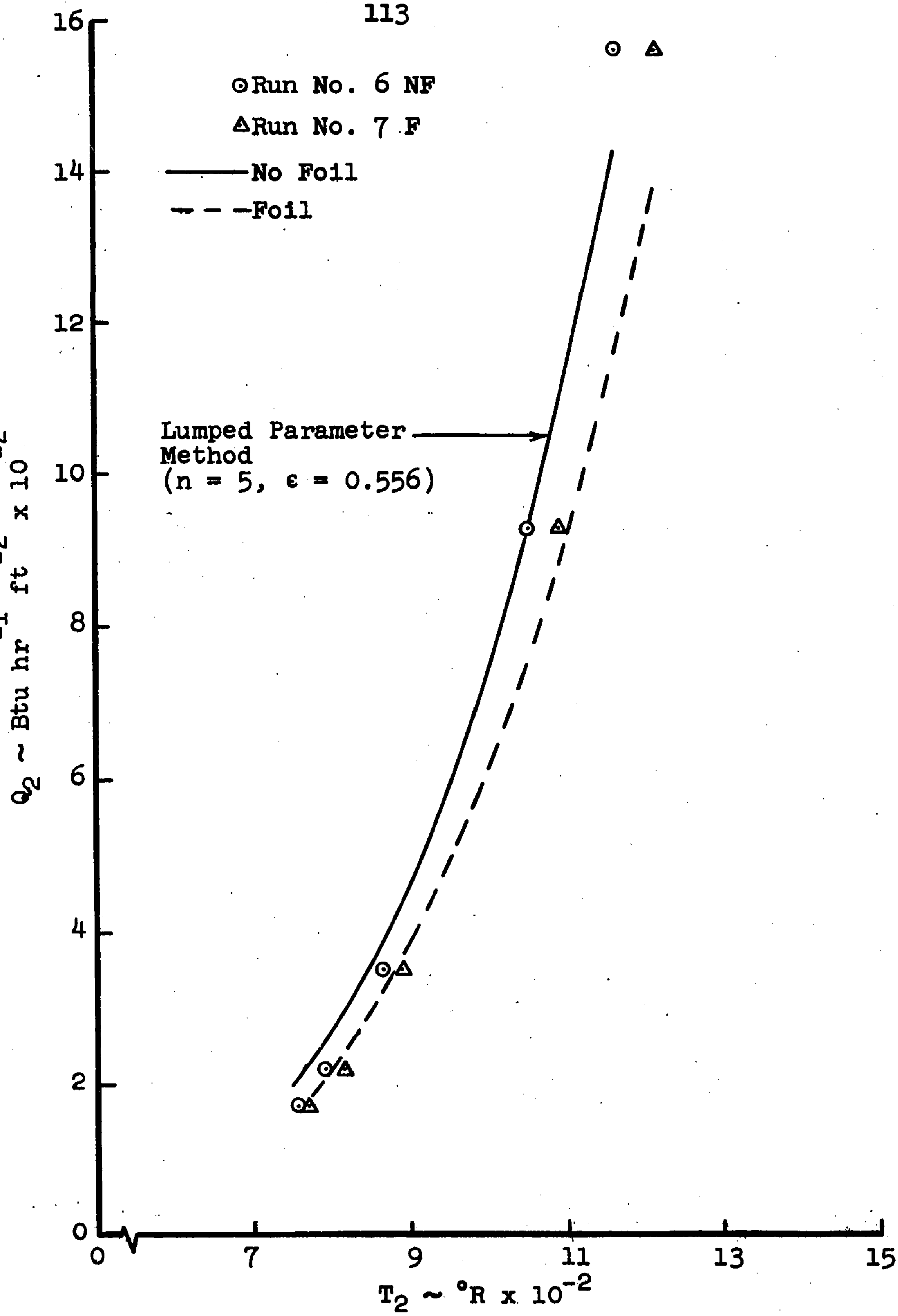

Figure 39
Comparison of Lumped Parameter Method With Experimental Data At 3.0 Inch Spacing

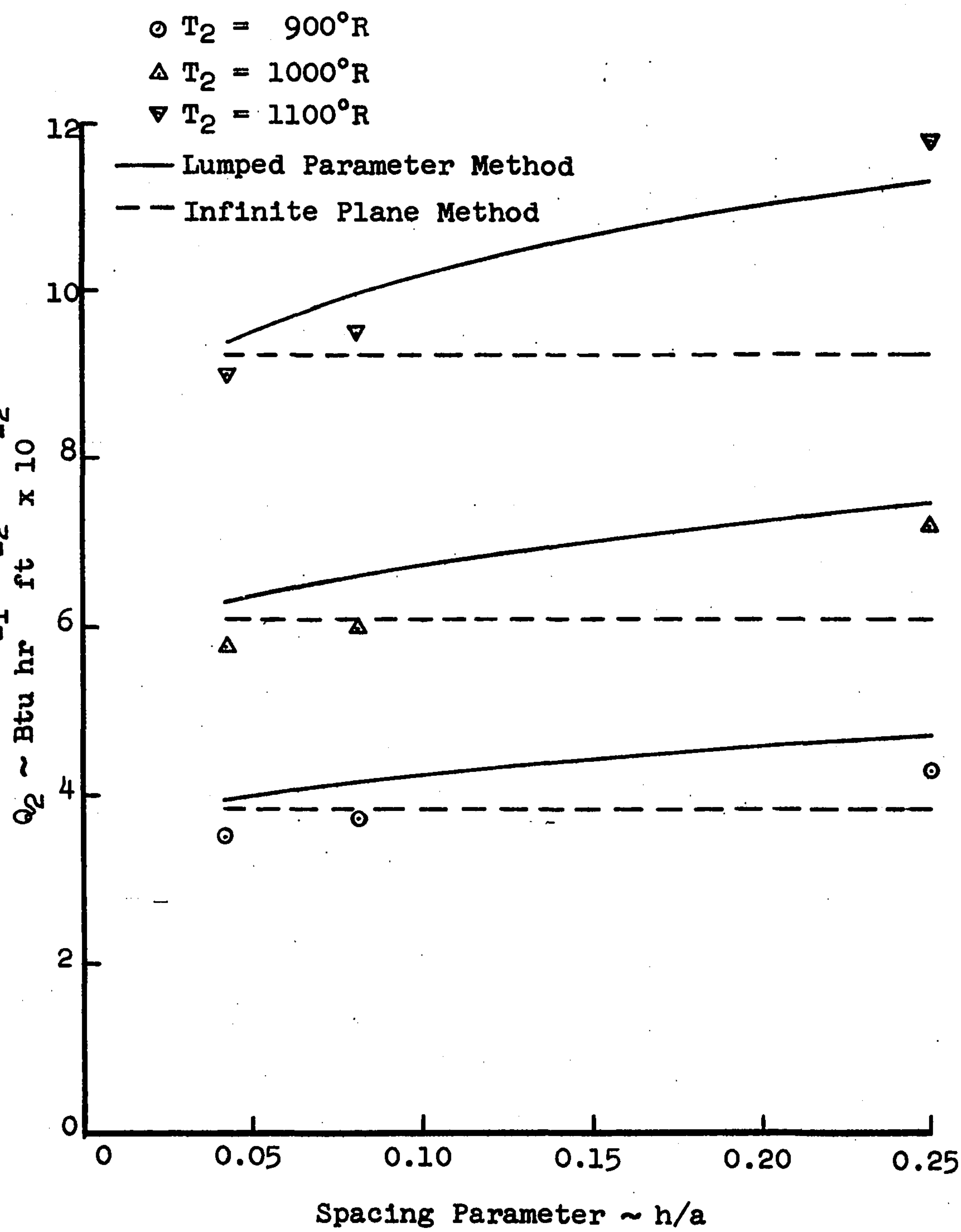

Figure 40

Comparison of Lumped Parameter Method And Infinite Plane Method With Experimental Data for No Foil Case

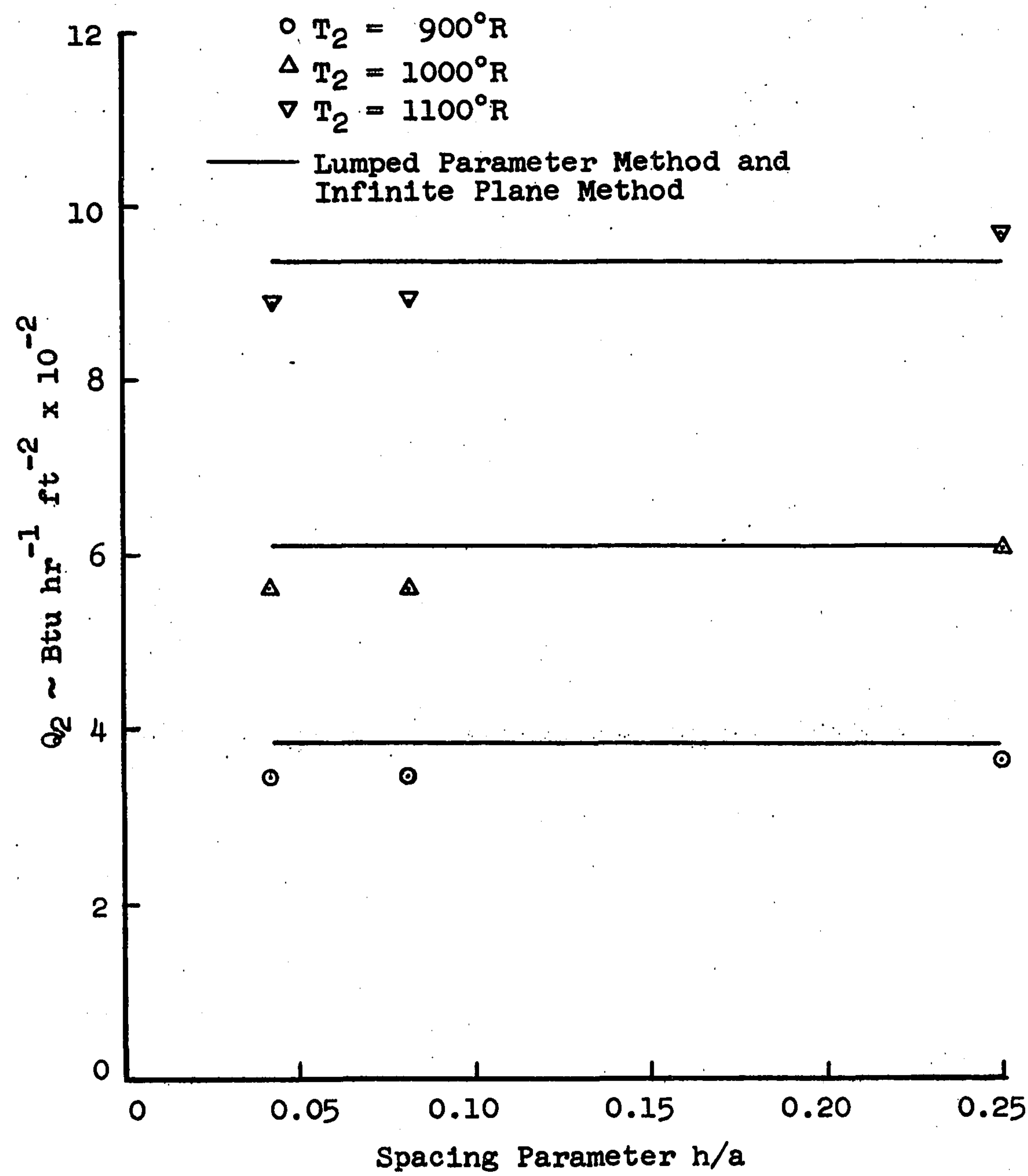

Figure 41

Comparison of Lumped Parameter Method And Infinite Plane Method With Experimental Data for Foil Case

However, the trend of the experimental data is away from the computed values. The lumped parameter method in Figure 40 was found to be a more descriptive model of the experimental apparatus for the no foil case than was the infinite plane method. This condition can be observed from the six different comparison plots of net flux versus temperature in this chapter. The lumped parameter method for the no foil case is within 3.46 percent of the measured value and 5.73 percent for the foil case with a spacing of 1.0 inch. These results are based on the assumption of $\rho_5 = 1$ for the foil case. Figure 41 illustrates that over the portion of the curves from which the cross plots were made, the two computational methods are almost identical for the foil case. In Figure 42 the experimental data for three runs were plotted. The curves are for both the foil and the no foil case at a spacing of 0.5 inch and the foil case at a spacing of 1.0 inch. In summary, for both the foil and the no foil cases, the infinite parallel method compares closely with the measured values for a 0.5 inch spacing. The same reasonable comparison occurs between the foil case experimental values and the infinite parallel plate computations. Hence, the objective of this study was accomplished.

The choice of the border zone values of emittance is difficult to evaluate. The selection of the emittance values of the surfaces for the above computational method and for the infinite parallel method is only approximate. Therefore, any discussion of the curves cannot extend beyond comparisons

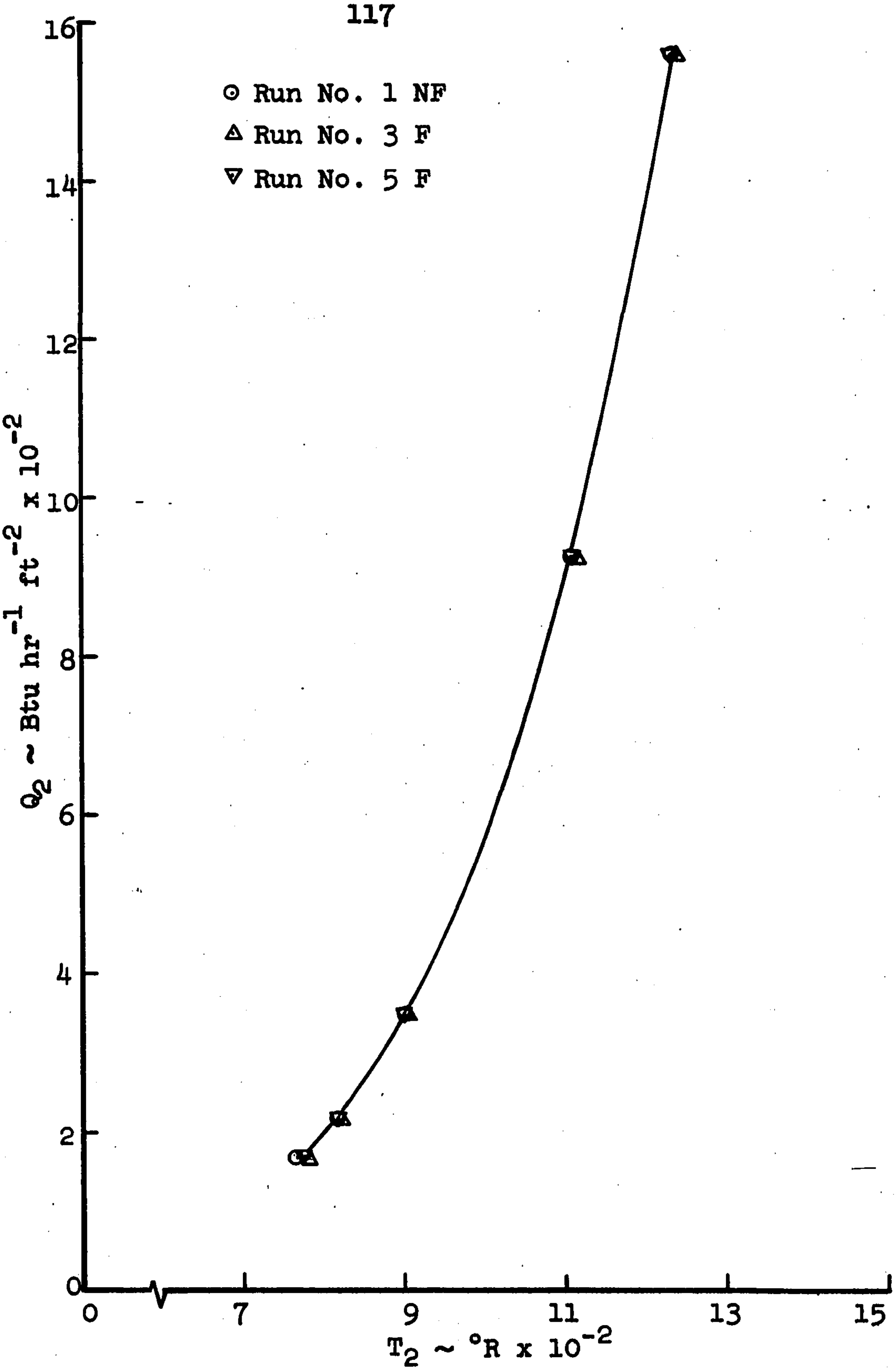

Figure 42

Similarity of Experimental Data

of the trends of the curves. In all the cases considered, the trends were reasonable. Comparison with other experimental results was not possible as none were available.

The quadrature method may provide a good comparison if the number of points approximating the surfaces are increased. The development of a criteria is recommended to determine the limits of the double summation for reasonable engineering solutions at different spacings of the plates.

For a better analysis of the results of this experiment, a recommendation is made that hemispherical spectral emittance measurements of the surfaces used be made for several temperatures. The net radiant energy flux between two infinite, parallel plates would then be computed by summing the monochromatic energy exchange. The computed results would then be greater than the results of a gray body computation based on the same emissivity data.

Recommended Improvements

(1) To allow the system to operate unattended for long periods of time and thus improve the vacuum capabilities of the system, safety devices are required to guard against possible failures. For example, if the mechanical pump stopped due to an electrical power failure, a gravity value would prevent air from carrying oil back into the vacuum chamber. Second, a failure of the cooling water supply to the diffusion pump, which would damage the pump, could be prevented by adding a relay operated by a selected differential pressure.

(2) If the apparatus is required to be raised to atmospheric pressure periodically, it is preferable to admit dry nitrogen rather than room air, thus avoiding the adsorption of water vapor on internal surfaces. If the nitrogen is not available, then a filter connected to the air release valve and containing a drying agent, such as silica gel, could be used to reduce the water content of the air.

(3) To provide a larger operating temperature range and because of the vast amount of information available on the emittance of tungsten surfaces and other pertinent properties that it possesses in a vacuum environment, the stainless steel faces could be replaced by a tungsten sheet.

(4) Operating the heaters with higher energy fluxes would require a water-cooled stainless steel bell jar and gasket. An additional improvement would be a cryogenic shroud on the inside of the vacuum chamber.

(5) Correct the line voltage fluctuations by using a motor generator set or by using a voltmeter switch to control motors for mechanically adjusting each variable auto transformer.

(6) Use thermocouple feed throughs which provide for connecting the thermocouples directly to the potentiometer without introducing dissimilar materials in the circuit.

(7) Record the important temperatures which allow for determination of steady state conditions. A multi-channel strip recorder would provide this data record.

(8) Replace the entire electrical power system, including the heaters in the hot plate and the feed throughs in the

baseplate, with components for use with a 220 volt power supply. These changes would allow for taking advantage of the high operating temperature range of tungsten heater faces.

CHAPTER VIII

CONCLUSIONS

An experimental apparatus was developed for the measurement of the exchange of radiant energy between two congruent, parallel and directly opposed plane areas.

The testing procedure and the equipment design were such that reproducible data could be obtained. As the spacing of the walls increased, the temperature of the heater wall decreased during a constant energy input. An equivalent situation exists if the net flux increases to maintain a constant temperature on the high temperature surface as the spacing is widened.

Infinite parallel walls can be simulated by plates which are one foot square at a spacing of 1.0 inch by placing aluminum foil around the border zone between the edges of the plates.

Provision for taking more temperature readings must be made before the shield case can be completely analyzed.

Application of the infinite parallel plane computation is acceptable for spacings up to 0.5 inch for plates which are one foot square.

The lumped parameter method, where parameters such as surface temperature are assumed constant, approximates the experimental apparatus for the no foil case by assuming the border zone has an emittance value of unity.

The quadrature method required lengthy computations and yielded limited results. A technique for determining the number of terms in the quadrature equations necessary to yield engineering answers, deserves investigation.

The significance of this study is that by considering the spacing parameter, one can determine when square, parallel plates of various sizes and spacings can be considered as infinite. Being able to simulate infinite parallel plates enables one to carry out experiments which assumed no edge effects.

BIBLIOGRAPHY

1. Love, Tom J., Jr., An Investigation of Radiant Heat Transfer in Absorbing, Emitting, and Scattering Media, Norman, Oklahoma: University of Oklahoma Research Institute, 1963. (Contract AF 33(657)-(8859) (ARL63-3).

2. Worthing, A. G., "Temperature Radiation Emissivities and Emittances", Journal of Applied Physics, Vol. 11, June, 1940.

3. Chapman, A. J., Heat Transfer, New York: The MacMillan Company, 1960.

4. Love, T. J., Jr., (Radiative heat transfer text to be published in 1965 by Charles E. Merrill Books, Inc., Columbus, Ohio).

5. Sparrow, E. M., J. L. Gregg, J. V. Szel, and P. Manos, "Analysis, Results, and Interpretation for Radiation Between Some Simply-Arranged Gray Surfaces", Journal of Heat Transfer, May, 1961.

6. Branstetter, J. Robert, "Radiant Heat Transfer Between Nongray Parallel Plates of Tungsten", Technical Note D-1088, National Aeronautics and Space Administration, Lewis Research Center, Cleveland, Ohio, August, 1961.

7. Goodman, Stanley, "Radiant-Heat Transfer Between Nongray Parallel Plates", Journal of Research of the National Bureau of Standards, Vol. 58, No. 1, Research Paper 2732, January, 1957.

8. Gubareff, G. G., J. E. Janssen, and R. H. Torborg, Thermal Radiation Properties Survey, Honeywell Research Center, Minneapolis-Honeywell Regulator Company, Minneapolis, Minnesota, 1960.

9. Wood, W. D., H. W. Deem, and C. F. Lucks, "The Emittance of Stainless Steels", EMIC Memorandum 111, Defense Metals Information Center, Batelle Memorial Institute, Columbus, Ohio, June, 1961.

10. Richmond, Joseph C. and William H. Harrison, "Total Hemispherical Emittance of Coated and Uncoated Inconel and Types 321 and 430 Stainless Steel", Journal of Research of the National Bureau of Standards-C Engineering and Instrumentation, Vol. 66C, No. 3, July-September, 1962.

11. Richmond, J. C. and W. N. Harrison, "Equipment and Procedures for Evaluation of Total Hemispherical Emittance", American Ceramic Society Bulletin, Vol. 39, No. 11, pp. 668-673.

12. O'Sullivan, Wm. J., Jr., Wm. R. Wade, "Theory and Apparatus for Measurement of Emissivity for Radiative Cooling of Hypersonic Aircraft with Data for Inconel and Inconel X", Technical Note 4121, Langley Aeronautical Laboratory, Langley Field, Va., October, 1957.

13. Snyder, N. W., J. T. Gier, and R. V. Dunkle, "Total Normal Emissivity Measurement on Aircraft Materials Between 100 and 800 F", Transactions of the ASME, Vol. 77, No. 7, October, 1955.

14. Bevans, J. T., J. T. Gier, and R. V. Dunkle, "Comparison of Total Emittances With Values Computed From Spectral Measurements", Transactions of the ASME, Vol. 80, No. 7, October, 1958.

15. Fletcher, L. S. and George Leppert, "Experimental Determination of Emissivity: A Teaching Experiment", Journal of Engineering Education, Vol. 55, No. 9, pp. 272-274.

16. Ewbank, W. J., George Townsend, and Eugene Keutzer, private communication with W. J. Ewbank who supervised experiment performed by George Townsend and Eugene Keutzer at the University of Oklahoma, May 30, 1965.

17. Clauss, Francis J., Editor, Surface Effects on Spacecraft Materials, Symposium: Palo Alto, California, John Wiley & Sons, 1960.

18. Maki, Arthur G., E. K. Plyler, "Method of Measuring Emissivities of Metal in the Infrared", Journal of Research of the National Bureau of Standards, Vol. 66C, No. 3, July-September, 1962.

19. Maki, Arthur G., Ralph Stair, and Russell G. Johnston, "Apparatus for the Measurement of the Normal Spectral Emissivity in the Infrared", Journal of Research of the National Bureau of Standards, Vol. 64C, No. 2, April-June, 1960.

20. Rohsenow, W. M. and Choi, H. Y., Heat, Mass and Momentum Transfer, Englewood Cliffs, New Jersey: Prentice-Hall, Incorporated, 1961.

21. Steinherz, H. A., Handbook of High Vacuum Engineering, New York: Reinhold Publishing Corporation, 1963.

22. Santeler, D. J., "Pressure Measurement in Nonbaked Ultra-High Vacuum Systems", The Review of Scientific Instruments, XXXIII, March, 1962, pp. 283-287.

23. Kohl, Walter H., Materials Technology For Electron Tubes, New York: Reinhold Publishing Corporation, 1951.

24. Wheasler, Robert, Measurement of the Angular Distribution of Scattered Monochromatic Intensity From an Aerosol Containing Particles of Irregular Size and Shape--For Wave Lengths in the Infrared, Ph.D. Thesis; University of Oklahoma, 1964.

25. Smith, John C., private communication, Contract Project Officer, U.S. Army Chemical Research and Development Laboratories, Edgewood Arsenal, Maryland.

26. American Society for Testing and Materials, 1961 Standards, Part 4, Philadelphia, Pa.

27. Aaron, R. L. and H. A. Blum, "Heat Transfer Across Surfaces In Contact: Effect of Ambient Pressure Changes", Aerospace Group, Hughes Aircraft Company, May, 1963.

28. Fenech, H. and W. M. Rohsenow, "Thermal Conductance of Metallic Surfaces in Contact", M.I.T. Heat Transfer Laboratory, U.S.A.E.C. NYO-2136, May, 1959.

APPENDIX A

RESEARCH ON THE FEASIBILITY OF EQUIPMENT

The purpose of this section is to guide future researchers around problems which were encountered and thus enable them to use greater sophistication in their experimental approach.

Heaters and Controls

Some of the original requirements of a heater were to have one of low thermal inertia, a cross section of less than 0.100 inch, and a temperature range of from room temperature to 2000°F. The small cross section was to reduce the thermal inertia and at the same time eliminate the requirement for a guard heater.

The first type heater considered was a Corning Pyrex panel heater. It was 0.250 inch in cross section and it had an upper temperature limit of 660°F in ambient air at 70°F. The Pyrex panel heater was a tempered borosilicate glass panel. One surface of the glass had an electrical conductive tin oxide film that served as an electrical resistance element to heat the glass panel. It was necessary for the electrical input to have bus bars on the back edges. The oxide film was a very poor emitter, so it actually served as a reflector to direct approximately 2/3 of the radiant energy to the cold wall. Problems with this type heater were the low maximum temperature together with the effect of a vacuum on the conductive film at the elevated temperature. If a Corning glass known as Vycor could be used in place of the Pyrex, then the upper temperature limit would be 1000°F. The bonding of various light gauge metal sheets and foils were considered for bonding to the front of the glass panel with Emerson and Cuming, Inc., Eccobond 104 ultra high temperature epoxy adhesive. Naturally, due to the difference in the coefficient of expansion, the bond failed as the adhesive hardened and resisted the movement of the glass and the metal sheet. If the foil was thin enough to allow the bonding, then the foil would retain air pockets in the adhesive and defeat the goal of a uniform energy flow path. Corning markets a Micro-Sheet glass in 6.00 inch squares and in thicknesses that range from 0.002 to 0.0138 inch. Even though the thin glass was desired to reduce the energy loss through the edges, the handling problem for such thin glass was too great.

The next type of heater considered was a high strength graphite cloth (grade GS GC-2) produced by Basic Carbon Corporation. Its composition of 99.9% carbon and 0.05% ash would allow vacuum applications according to Kohl (23). Its cost at approximately $40.00 per square yard was an attractive feature. Also its thickness of 0.018 inch with a weight of 7.5 ounces per square yard gave the desired low thermal inertia characteristic. This flexible graphite fabric has been used as filler material in ablative design for aerospace use because of its high strength of 60 pounds per square inch cut strip tensile, good wetting characteristics, and a neutral pH of approximately 7. This material possesses a very uniform resistance of 0.5 ohm per square inch and accommodates operating temperatures to 5700°F in inert atmospheres. The high temperature feature was checked in a nitrogen atmosphere to 2,500°F which was the temperature limit of the Chromel Alumel thermocouple being used. It is unaffected by the action of practically all corrosives and features outstanding thermal stability, even under conditions of severe thermal shock. The major problem was that of shaping the cloth for use on a flat surface and of providing for an electrical path with a resistance of 12 ohms which was desired for use with an alternating current supply of 110 volts. The fabric could be cut with scissors, but it frayed on the edges. At each corner a point of low resistance occurs, thus a point of high current concentration. These points became white hot while the rest of the material was at a much lower temperature. Electrical contact was made to the cloth by clamping it between two copper strips with small bolts. By using Sauereisen No. 78 electrical refractory cement, the cloth was with moderate success bonded to and insulated from a stainless steel Type 301 sheet 0.050 inch in thickness. The configuration consisted of three heaters similar to the final design now being used. The electrical resistor cement acted as an electrical insulator which radiated energy and withstood temperatures up to 3000°F.

The most straightforward type of heater is one where a metal sheet, which serves as the heater surfaces, is suspended in a vertical position by insulators, and sufficient electrical current is passed through the heater to obtain the temperature required. This method was not used because of the high current loads required together with the related problems of controlling the electrical energy input. The possibility of Nichrome or Nichrome V ribbon was considered, but to obtain heating elements of the size desired, it was necessary to fold the ribbon at the corners which was not acceptable. The ribbon also could have been wrapped around a thin ceramic plate, but such a piece of ceramic which is thin and possesses moderate strength with low thermal inertia is difficult to fabricate.

The last type of heater which was built and which gave reasonable results consisted of three 0.050 inch stainless steel Type 301 sheets with three commercial heaters of the Hevi-Duty Heating Equipment Corporation. These were rectangular ceramic heaters approximately 1/2 inch in thickness with coils of resistance wire placed in grooves in a "S" pattern in the ceramic. The wires were not embedded; therefore, a maximum temperature of 1832°F was suggested by the supplier to provide protection for the wires. These heaters proved satisfactory in a vacuum environment as any adsorbed gases were driven off at the elevated temperatures. The configuration of the heaters was similar to the final working version except that the back heater did not cover the back, but instead was equal in size to the center heater. The border and the center heaters were between the front sheet and the middle sheet. The back heater was thus placed between the middle sheet and the back sheet. The sandwich construction was held together by 12 stainless steel bolts which were sandblasted on their heads to present a surface similar to the one of the front sheet. Problems with a heater of this type were that of holding it in place without permitting warpage due to the elevated temperatures. Also, the fact that the back heater did not cover the entire back created an extended fin effect with the middle and back sheets partly exposed.

The main consideration in the heater controller and metering device was one of cost. If funds had been available, a magnetic amplifier and saturable reactor to allow for continuous regulation of electric input to each of the furnace heaters would have been purchased. For a period of three months a Marshall Temperature Control Console built by the Marshall Products Company was available. Its rating was 2 KVA, 120 V, 60 cycle, single phase. This unit used one thermocouple for regulation with manual adjustment of the power input to each zone by three variable voltage regulators. It was not available long enough to determine if this type of controller was adequate. Both the carbon cloth and the ceramic element heaters were used with this controller. When power was applied to the carbon cloth elements using the

Marshall controller, an approximate steady state temperature, corresponding to the particular power input, was achieved in less than thirty seconds.

A portable temperature controller, model JEP of the West Instrument Corporation, was purchased as there were already two other controllers available on a loan basis. With this type of control, close temperature tolerances were held. After the temperature rises to within narrow limits of the control index, called the proportioning band, the instrument will automatically set a ratio of "on time" and "off time" to keep the temperature, which is being controlled, constant. Three independent thermocouples were placed in meaningful positions in the ceramic heater. Three variable transformers were added to the heater circuit to decrease the number of cycles between "on time" and "off time".

Power measurements were not made with the console controller; however, with the West controller, induction watt-hour meters were used. These are rated at 5 amperes for average usage; however, they will operate with reasonable accuracy with a load of 15 amperes. Oklahoma Gas and Electric Company in Oklahoma City, Oklahoma calibrated the watt-hour meters within 1/10% accuracy. To read the watt-hour meters, it was necessary to count the number of revolutions and fractions of a revolution per unit time to arrive at a reasonably accurate value for the power consumed. With this type of meter 0.6 watt per revolution was measured.

Due to the difficulty of metering the power consumed and the undesirable situation of having the power being switched off and on, manual power control was selected.

Water Bath

With the original concept of having the heated wall reach very high temperatures, and thus a large differential temperature being created between the hot wall and the cold wall, a water bath which operated above room temperature was selected. The cost of this type of bath was nominal as a refrigeration system was not needed but instead four electrical immersion heaters, two mixers, and an electronic relay controller using a mercury to wire contact regulator. Two or three of the heaters were to be operated continuously with the remaining heaters being switched off and on by the electronic relay controller to balance the energy dissipation load with the room. Because the upper limit of the heater was reduced and the problems connected with building a heat flow meter to operate at several hundred degrees Fahrenheit in a vacuum, the warm water bath was replaced with an ice bath in the final stage.

Particle Cloud Generator

The generation of a cloud of particles in a vacuum environment proved to be one of the most interesting features of the experiment attempted. This was done by building a light aluminum, rectangular box with a sieve cloth bottom. The sieve sizes used were American Society For Testing and Materials No. 8, 14, 20, and 50. The particles as described in reference (24) had a size range of from 1 to 20 microns with 90 percent in the 5 micron range. Reynolds Aluminum Company supplied the particles which were 40 x D aluminum powder with an average particle size of 6 microns. Stearic acid was present according to Smith (25) to prevent the particles from collecting in large groups. Because of the vacuum there was not sufficient air to support a cloud. Thus, the box or hopper was filled with from 15 to 100 grams of the powder and vibrated in a horizontal plane in the direction parallel to the top and bottom edge of the hot and cold plates. The two electrical and mechanical vibrators were operated on 24 volts. By using an electrical feed through, the vibrator can be energized and thus the particle feed can be started and stopped for each run. Optical depths of the cloud were recorded from 0.1 to over 2.0 which varied with the time duration of a run from 2 minutes to 30 minutes. A typical particle run was monitored using a Raytheon Em 1502 CdSe fast switching photocell in one leg of an electrical Wheatstone bridge. The output was amplified with a Hewlett-Packard 413 A DC Null Voltmeter. A visual display of the optical depth versus time was made with a Honeywell 906 C Visicorder oscillograph using a M 1650 fluid damped sub-miniature galvanometer rated at 0.223 volt per inch. The optical depth varied from 1.7 initially to 0.037 after 3 minutes with the variation between 1 and 2 minutes being the smallest. The particles were collected in an aluminum foil tray between the hot and cold plates and below their bottom edge. The collection tray had been weighed previous to the run and could be folded up with the particles in it to allow for weighing on a sensitive balance after a run. Knowing the total weight of the particles falling past the face of the plates, together with the assumption that the particles were in a free fall, allowed for the determination of the optical depth. A problem encountered was the removal of the gas load imposed on the vacuum system by trapped air in the system being liberated. One source of gas in the system was acid which vaporized due to the energy picked up by the particles from the hot plate. The hopper was mounted several inches above the hot plate and had reflector shields below it to reflect radiant energy off of the hopper. Liquid nitrogen was used in the cryogenic baffle of the vacuum system to trap the additional air molecules on the cryogenic surface and thus created an improvement in the vacuum of from 1×10^{-5} torr to at least 5×10^{-6} torr. With a maximum load of particles in the hopper the total surface area represented by the particles was 724 square feet, even if the fisure and other surface characteristics were not considered. In addition to the outgassing problem, the difficulty of separating the particles is illustrated by the fact that the smallest standard sieve size is an American Society For Testing and Materials sieve No. 400 which will not allow a particle larger than 37 microns in diameter to pass. This means that probably the average size particle was much larger than the 5 to 6 microns specified by the manufacturer.

Reference (26) gives all of the construction details for micro-precision sieves. A check was made of all possible suppliers for these type of sieves and none were found who could supply them. A problem with using a finer and finer sieve to break up the particles is that all sieves have a choke flow rate. Even by mechanical means, such as brushing the particles through, the author was not able to force a significant amount of material through the No. 400 sieve. If one attempts to drop particles on a vibrating sieve, there is always a vertical component of motion of the sieve, plus the very low mass of the particle, which causes the particles to bounce on the sieve and actually regroup rather than pass on through. A problem which occurs in air, according to Smith (25), and which was probably solved by using a vacuum, is the fact that because the particles are platlets which have a large area in comparison to their thickness, they fall with their large area parallel with the surface on which they collect. Thus the extinction of radiant energy is greatly reduced from what might be expected.

Even with the limitation mentioned, the method recommended for dispersing a particle cloud in a vacuum would be similar to the one just discussed. All techniques found in the literature varied greatly and none consider the problem of dispersion without a vehicle to support and separate the particles.

Vacuum Design

Before the vacuum system was selected, the feasibility of taking certain experimental measurements in a vacuum was experimentally investigated. The baseplate, feed throughs, bell jar and bell jar guard were purchased, and a vacuum system was obtained on a loan basis. This system consisted of a Cenco Hypervac 23 mechanical vacuum pump rated at 5×10^{-3} torr. To the mechanical pump was attached a Consolidated Vacuum Corporation Type MCF 300 metal fractionating pump rated at 1×10^{-5} torr using Silicone DC-704 pump oil with a pumping capacity of 265 liters per second. Two cast iron flanges were ground and threaded onto the ends of an expanding pipe nipple, 4 inches to 6 inches in size. The pipe fitting allowed for a quick attachment of the diffusion pump using an O-ring seal in the pump and a Consolidated Vacuum Corporation Con-O-Ring between the baseplate and the top flange. A Consolidated Vacuum Corporation type GP 110 Pirani gauge was attached to the pipe nipple. This instrument provided for readings down to 1×10^{-3} torr. Glyptal paint was used to seal the threaded joints.

When only the mechanical pump was used and particles were dispersed in the system with the heater on and cooling water circulating in the cold plate, a blanket of particles up to 1/8 of an inch in thickness covered the cold plate at the end of a run. Also particles were found on the baseplate and fixtures on only the half of the system with the cold plate. It was concluded that sufficient air remained to carry the particles around in the bell jar and thus defeat the object of the experiment. Next the diffusion pump was activated and this eliminated the above problem except as the heater surface reached approximately 1000°F particles once again appeared on the face of the cold plate. The results of the experimental feasibility study were not conclusive because the vacuum gauge was limited to vacuum readings to 1×10^{-3} torr. Thus the amount of convective heating between the plates was not determined. If the gas load, due to the particles was not too great, the particles could probably be dispersed between the two plates successfully.

Detection Devices And Cold Plate

Two approaches can be taken in experimentally recording the effect of a cloud of particles between two plates. The first was the least desirable because the characteristics of the surface where the detection device was placed were greatly modified and thus the parallel plate configuration loses much of its significance. Of the eight commercial production detectors of infrared radiation, the three lead salts, PbS, PbSe, and PbTe, indium antimonide, doped germanium, bolometers, thermocouples, and the Golay cell, an uncooled lead sulfide cell and a bolometer arrangement using thermistors was tried. The lead sulfide detector was bonded to the cold plate using a high temperature epoxy. It was one leg of a wheatstone bridge using a Hewlett-Packard 413 A DC Null Voltmeter to amplify and display the response. Instead of using a commercial bolometer with flake element thermistors and the required amplifiers, chopper, and black body reference instrumentation, two Fenwal 1,000,000 ohm type GA61J1 bead thermistors were placed on the face of the cold plate with one of the thermistors exposed directly to the radiant energy and the other one being just under the surface of the cold plate. Thus only the effect of the incident radiant energy could be noted and changes in the environmental temperature are cancelled out as background.

The second approach involved a thermopile or heat flow meter embedded in the cold plate behind the front surface of the plate.

Fiberglas of the Minnesota Mining and Manufacturing Company Type 181 volan A and Shell Chemical Company laminating resin Epon 828 was used in attempts to build a heat flow meter. Minnesota Mining and Manufacturing Company adhesive type AF-110, weight B, was used in bonding the Fiberglas to the front of the mild steel cold plate cover and to the back of the stainless steel sheet. Both of these faces were sandblasted and cleaned with acetone. The Fiberglas was selected because it was available together with the hydraulic press equipped with a heated anvil necessary for bonding the composition. The technical reason for selecting Fiberglas was that it provided the necessary temperature drop for the measurement of the energy flux through the face of the cold plate.

Several arrangements were tried with a thermistor bonded between the stainless steel face and the Fiberglas and a matched thermistor bonded between the Fiberglas and the mild steel plate. Once again these were used as two legs in a bridge to measure a differential temperature across the Fiberglas. The size of the bead thermistor, 0.043 inch, plus the fact that it was encased in glass, made the bead difficult to position accurately without damaging it. Before grooves were milled in the back of the cold plate as in the final version, embedding wires between the two plates without having electrical shorts in either of the metal faces was difficult. Copper-Constantan was used in fabricating a series connection of the wires to form a thermopile of 5 junctions on each side of the Fiberglas. Also, a parallel arrangement of the thermocouple wires was made to measure the mean temperature of each face of the Fiberglas. Both the series and the parallel multiple thermocouples were connected on either side of the Fiberglas. Once again an insulation breakdown resulted in the shorting out of the series thermopile. On one of the last thermopiles built an acrylic spray was used to give additional insulation protection, but it did not provide an adequate coating. A 4 by 4 inch section was removed from the center of the cold plate face to the depth of the mild steel back. The center was then replaced with a thermopile embedded in a square sheet of Fiberglas which had already been formed. It was too difficult to thread a series thermopile in a tacky sheet of preimpregnated Fiberglas or in a fresh mixture of Fiberglas and expoxy; therefore, a cured 4 by 4 inch section was threaded with the series thermopile. Eccobond 104 ultra-high temperature epoxy adhesive was used in place of the Fiberglas adhesive, AF-110 weight B; thus, only a slight increase in the temperature during bonding was needed together with sufficient pressure to bring the stainless steel face into uniform contact with the Fiberglas. This method appeared to be adequate until it was subjected to a vacuum and a temperature of approximately 200°F. Under these conditions the stainless steel sheet with nothing to constrain it but the adhesive, upon reaching a moderate temperature, wrinkled and separated in the center area from the mild steel. This parting caused a failure of the parallel thermocouples for measuring a differential temperature as the stainless steel sheet now acted as a shield and reached an intermediate temperature between that of the hot plate and the cold plate. Because of the light gauge of the stainless sheet, its temperature became almost uniform throughout.

The next version was just like the last one except that the 4 by 4 inch center section which contained the thermocouple junctions of the heat flow meter was bonded to both metal surfaces with a silicone rubber produced by Dow Corning and called Silastic. This material vulcanizes at room temperature. Silastic contains its own catalyst and is a thick, paste-like material which when squeezed from a tube remains in the shape in which it is extended without sag or slump. Because of its good thermal conductivity, adhesion is maintained through a temperature range of -100°F to as high as 500°F. Silastic cures in 24 hours by reacting with the moisture in the air. In addition to the silicon rubber to hold the heat flow meter in place, four No. 8-32 flat head stainless steel screws were placed in the corners of the meter being careful not to disturb the junctions. These screws were threaded into the mild steel plate. The heads were sandblasted to reduce their disturbing effect.

After analysis of experimental data using this arrangement it was apparent that the stainless steel acted as an excellent heat sink together with the silicon rubber. With an energy flux at the hot plate of 1385 Btu per hour per square foot, the center of the cold plate indicated a temperature of 113°F, while the border read 247°F. A thermal gradient of this magnitude could not be tolerated as the maximum gradients allowed on the hot plate were 10°F. The operating version of the cold plate is described in the chapter on equipment.

APPENDIX B

LIST OF SYMBOLS

Alphabetic Symbol	Meaning	Dimentional Units
A	Area	ft^2
a	Measure of edge of square	ft
h	Spacing of walls	ft
I	Intensity of radiation	Btu ft^{-2} $stearad^{-1}$
L	Length	ft
Q	Energy flux	Btu hr^{-1} ft^{-2}
R	Radiosity	Btu hr^{-1} ft^{-2}
r	Variable distance	ft
T	Temperature	$^{\circ}R$
W	Width	ft
x	Coordinate distance	ft
y	Coordinate distance	ft

Greek Symbol	Meaning	Dimensional Units
ϵ	Surface emittance	none
θ	Polar angle for variable radiosity	radians
λ	Wavelength	microns
π	3.1416	none
ρ	Surface reflectivity	none
σ	Stefan-Boltzmann constant (0.17213×10^{-8})	Btu hr^{-1} ft^{-2} $^{\circ}R^4$
φ	Polar angle for variable radiosity	radians

Subscripts	Meaning	Dimensional Units
b	Black body	none

Subscripts	Meaning
i	Refers to surface i
j	Refers to surface j
p	Coordinate
q	Coordinate
r	Coordinate
s	Coordinate
ν	Refers to monochromatic value of term
1	Refers to surface 1
2	Refers to surface 2
3	Refers to surface 3
4	Refers to surface 4
5	Refers to surface 5
6	Refers to surface 6
7	Refers to surface 7

APPENDIX C

SPECTRAL EMITTANCE OF SURFACES

	Sample A		Sample B	
Wavelength λ (microns)	Reflectance ρ	Emittance $\epsilon = 1 - \rho$	Reflectance ρ	Emittance $\epsilon = 1 - \rho$
2.50	0.395	0.605	0.395	0.605
2.00	0.385	0.615	0.385	0.615
1.50	0.375	0.625	0.375	0.625
1.00	0.350	0.650	0.345	0.655
0.80	0.340	0.660	0.330	0.670
0.70	0.330	0.670	0.325	0.675
0.60	0.320	0.680	0.295	0.705
0.50	0.300	0.700	0.290	0.710
0.40	0.270	0.730	0.250	0.750
0.32	0.230	0.770	0.215	0.785

These measurements were made by Avco Corporation of Tulsa, Oklahoma, on April 4, 1965, using an integrating sphere. The samples supplied by the author were Type 302 stainless steel sheet 0.020 inch thick and 1 3/16 inches square. The surfaces were prepared in accordance with the procedures outlined in the text.

APPENDIX D

SAMPLE CALCULATION OF SPECTRAL EMISSIVE POWER OF SURFACES AND TABULATED VALUES

$$W_\lambda = \frac{\epsilon_\lambda 2\pi c^2 h}{\lambda^5 (e^{ch/\lambda kT} - 1)}$$

W_λ = spectral flux density

ϵ_λ = spectral emittance

c = velocity of light

h = Planck's quantum constant

λ = wavelength

k = Boltzmann constant

T = temperature

	$T = 1000^\circ R$	$T = 1500^\circ R$
Wavelength λ (microns)	Spectral Flux Density W_λ (Btu/hr ft^2 - μ)	Spectral Flux Density W_λ (Btu/hr ft^2 - μ)
2	5.35	107.00
3	16.05	248.77
3.5	21.40	262.15
4	26.75	254.12
5	34.77	195.27
6	37.45	139.10
7	32.10	96.30
8	24.07	72.22
9	18.72	56.17
10	13.37	45.47
11	8.02	26.75

APPENDIX E

SAMPLE CALCULATION OF CONVECTIVE HEATING EFFECTS AND TABULATED VALUES

$$Q = m_i\left[\frac{1}{2} v^2 + \frac{5}{2} R(T_i - T_w)\right]$$

$$m_i = \rho_i \sqrt{\frac{RT_i g_c}{2\pi}} \left[e^{-n^2} + \sqrt{\pi}\, n(1 + \text{erf } n)\right] ; \qquad \rho_i = p/RT$$

where Q = net energy flux at a surface

m_i = molecular mass flux incident on a surface

v = gas velocity (assume small, i.e., $v^2 = 0$)

R = universal gas constant

ρ_i = gas density at incident surface

T = gas temperature

T_i = temperature of incident surface

T_w = temperature of cold wall

g_c = 32.2 lbm ft/lb$_f$ sec^2

n = velocity ratio (n = 0 plate aligned in the direction of motion)

p = pressure

Run No. 1

Point	A	B	C	D	E
p (mm Hg)	Q	Q	Q	Q	Q
1	2.52×10^{4}	2.01×10^{4}	1.215×10^{4}	0.956×10^{4}	0.758×10^{4}
10^{-1}	2.52×10^{3}	2.01×10^{3}	1.215×10^{3}	0.956×10^{3}	0.758×10^{3}
10^{-2}	2.52×10^{2}	2.01×10^{2}	1.215×10^{2}	0.956×10^{2}	0.758×10^{2}
10^{-3}	2.52×10	2.01×10	1.215×10	0.956×10	0.758×10
10^{-4}	2.52×1	2.01×1	1.215×1	0.956×1	0.758×1
10^{-5}	2.52×10^{-1}	2.01×10^{-1}	1.215×10^{-1}	0.956×10^{-1}	0.758×10^{-1}
10^{-6}	2.52×10^{-2}	2.01×10^{-2}	1.215×10^{-2}	0.956×10^{-2}	0.758×10^{-2}
10^{-7}	2.52×10^{-3}	2.01×10^{-3}	1.215×10^{-3}	0.956×10^{-3}	0.758×10^{-3}

APPENDIX F

EQUIPMENT

Description	Identification
NRC Equipment Corporation Vacuum Pumping System Number 3307	O.U.R.I. 35610 0097
Variable Auto Transformer-A Standard Electrical Products Co. 230 Volts, 9.0 Amps., 2.4 KVA	Serial Number 12711
Variable Auto Transformer-B Superior Electric Co. 240 Volts, 9.0 Amps., 2.5 KVA	Serial Number 8102
Variable Auto Transformer-C General Radio Co. 115 Volts, 6.0 Amps.	Serial Number 666062-039
Wattmeter-A General Electric Co. Amps. 2.25/4.5, Volts 75/150 Calibrated 5/65	Serial Number 3917764
Wattmeter-B General Electric Co. Amps. 5/10, Volts 100/200 Calibrated 5/65	O.U. 1015-0497
Ammeter Weston Co. Volts 110, Amps. 1-50 Calibration 6/27/64	Serial Number 18344
Voltmeter Heath Company Volts 1.5-1500	U.S.A.F. 36790032
Potentiometer Leeds and Northrup Co. 8686 Portable Millivolt Potentiometer	O.U.R.I. 36110 0313
Rotary Selector Switch Leeds and Northrup Co. 8248-16 Switch	Serial Number 4179

APPENDIX G

SAMPLE CALCULATION OF PERMEATION RATE OF HELIUM AND TABULATED VALUES

$F = KAP/d$ $\qquad A = \pi DL + \pi D^2/2$

$D = 18$ in.

$L = 20$ in.

$A = 10{,}600\ cm^2$

$d = 0.635$ cm

From Steinherz (21) $K = 9.1 \times 10^{-11}\ cm^2/sec$ at 101°C for glass

$K = 8.4 \times 10^{-9}\ cm^2/sec$ at 492°C for glass

$P = 3 \times 10^{-3}$ mm Hg partial pressure of helium in the atmosphere

$F = 9.06 \times 10^{-7}$ std atm cm^3/sec for Viton carbon black film

	Glass F(std atm cm^3/sec)	(std atm liters/sec)
At 101°C	3.8×10^{-12}	3.8×10^{-15}
At 492°C	3.515×10^{-10}	3.515×10^{-13}
	Gasket	
Viton	9.06×10^{-7}	9.06×10^{-10}

$F_{total} = 9.064 \times 10^{-10}$ std atm liters/sec

APPENDIX H

ESTIMATED ENERGY LOSSES

Note: All Temperatures °F

Point A
(0.5 inch spacing)

Hot Plate

Time Before Final Reading Hours	Center T_9	Steady State Variation	Back T_{10}	Steady State Variation	$(T_{10}-T_9)$
Run No. 1, No Foil					
1.0	981	---	986		5
0.5	980	-1.0	985	-0.5	5.5
0.0	979	-1.0	985	-0.5	6
Run No. 3, Foil					
1.0	982		993.5		11.5
0.5	982	-0.0	994	0.5	12
0.0	982	-0.0	994	0.0	12

Time Before Final Reading Hours	Center T_2	Steady State Variation	Border T_1	Steady State Variation	(T_1-T_2)
Run No. 1, No Foil					
1.0	770		777		7
0.5	771	1.0	775	-2.0	4
0.0	771	0.0	774	-1.0	3
Run No. 3, Foil					
1.0	776.5		764		-12.5
0.5	777	0.5	765	1.0	-12
0.0	765	-1.0	765	0.0	-11

Cold Plate

Time Before Final Reading, hours	Center T_4	Steady State Variation	Middle T_3
Run No. 1, No Foil			
1.0	65		--
0.5	66	1.0	--
0.0	65	-1.0	55

Time Before Final Reading, hours	Center T_4	Steady State Variation	Middle T_3
	Run No. 3, Foil		
1.0	85.5		--
0.5	86	0.5	--
0.0	85	-1.0	58

A. The estimated energy exchange through the back of the heater was computed by assuming no contact resistance at the interface of the glass and the stainless steel sheet.

$$Q\ \text{back} = \frac{A\ \Delta T}{\dfrac{1}{\frac{k_{ss}}{x_{ss}}} + \dfrac{1}{\frac{k_p}{x_p}} + \dfrac{1}{\frac{k_{ss}}{x_{ss}}}} \qquad \begin{aligned} x_{ss} &= 0.001666\ \text{ft} \\ x_p &= 0.01042\ \text{ft} \end{aligned}$$

k_{ss} = 13 Btu $hr^{-1} ft^{-1}\ {}^{\circ}F^{-1}$ for 18-8 stainless steel at 1112°F

k_p = 0.63 Btu $hr^{-1}\ ft^{-10}\ {}^{\circ}F^{-1}$ for borosilicate glass at 86° - 167°F

Q back = 12.5 ΔT

B. The actual material configuration involved ceramic heaters covered by a sheet of stainless steel. The thermocouples measuring T_1 and T_2 were located approximately 4 inches apart on the outside surface of stainless steel sheet. By assuming that the center and border heaters were entirely stainless steel and that spacing of the thermocouples was 1 inch rather than 4 inches, an upper limit on the estimated energy exchange was established.

$$Q\ \text{border} = \frac{k_{ss}\ \Delta T\ A}{L} \qquad L = 0.0883\ \text{ft}$$

Q border = 10.95 ΔT

Q computed output = $\pm$ Q border $\pm$ Q back + Q measured

$$\text{Estimated correction} = \frac{(\text{Q measured} - \text{Q computed output})(100)}{\text{Q measured}}$$

Aaron and Blum (27) in a study conducted for the Aerospace Group of Hughes Aircraft Company in 1963, considered the effect of ambient pressure changes on the heat transfer rate across surfaces in contact. As part of their work, Aaron and Blum (27) reviewed the experimental findings of Fenech and Rohsenow (28). In summary, Fenech and Rohsenow (28) showed that the important modes of heat transfer across a metallic joint at sea level ambient pressure are fluid conduction and metallic conduction. Radiation was negligible unless the joint temperature exceeded 1100°F. According to their findings, 58 percent of the total heat transfer rate was by fluid conduction. Hence, if all the air was removed from the voids in the surfaces by exposure to zero ambient pressure, the thermal conductance would be reduced 58 percent. As the mode of energy transfer between the heating elements of the hot plate was neither completely conduction nor radiation, the 58 percent reduction estimate was applied.

Estimated Correction

	Conduction	58% Reduction
Point A, Run No. 1	8.93%	3.76%
	7.23%	3.04%
	6.92%	2.91%
Point A, Run No. 3	-0.42%	-0.18%
	-1.16%	-0.487%
	-1.86%	-0.78%

APPENDIX I

SAMPLE CALCULATION FOR INFINITE PARALLEL PLANE METHOD

Run No. 1, Point A

$$Q_2 = Q_4 = \sigma \frac{(T_2^4 - T_4^4)}{(1/\epsilon_2) + (1/\epsilon_4) - 1} \qquad (3.1)$$

$\sigma = 0.17123 \times 10^{-8}$ Btu/hr ft^2 °R

$T_2 = 1231$°R $\qquad \epsilon_2 = 0.556$

$T_4 = 525$°R $\qquad \epsilon_4 = 0.556$

$Q_2 = Q_4 = 1463.89$ Btu/hr ft^2

APPENDIX J

SAMPLE CALCULATION FOR LUMPED PARAMETER METHOD

Run No. 1, Point A

$$R_i = \epsilon_i \sigma T_i^4 + \rho_i \sum_{j=1}^{n} R_j F_{ij} \qquad (3.4)$$

$$Q_i = R_i - \sum_{j=1}^{n} R_j F_{ij} \qquad (3.6)$$

$$n = 5$$

$$\epsilon_1 = \epsilon_2 = \epsilon_3 = \epsilon_4 = 0.556 \qquad \epsilon_5 = 1$$

$$\rho_1 = \rho_2 = \rho_3 = \rho_4 = 0.444 \qquad \rho_5 = 0$$

$$T_1 = 1234°R$$

$$T_2 = 1231°R$$

$$T_3 = 515°R$$

$$T_4 = 525°R$$

$$T_5 = 612°R$$

F_{ij} from Table 11

Equation 3.4 results in five equations with five unknowns which when solved simultaneously yields:

R_1 = 2683.39 Btu hr^{-1} ft^{-2}
R_2 = 2741.81 Btu hr^{-1} ft^{-2}
R_3 = 1154.88 Btu hr^{-1} ft^{-2}
R_4 = 1277.62 Btu hr^{-1} ft^{-2}
R_5 = 240.21 Btu hr^{-1} ft^{-2}

Substituting the radiosity terms in equation 3.6 gives

Q_1 = 1611.73 Btu hr^{-1} ft^{-2}
Q_2 = 1490.40 Btu hr^{-1} ft^{-2}
Q_3 = -1295.37 Btu hr^{-1} ft^{-2}
Q_4 = -1437.00 Btu hr^{-1} ft^{-2}
Q_5 = -1559.00 Btu hr^{-1} ft^{-2}

A negative net radiant flux means that the energy is entering the surface.

APPENDIX K

SAMPLE CALCULATION FOR QUADRATURE METHOD

Run No. 1, Point A

$$B_2(X_p,Y_q) = 1 + \frac{\rho_2 a^4 H^2}{\pi} \sum_{r=1}^{n} \sum_{s=1}^{n} \frac{W_r W_s B_4(X_r,Y_s)}{[a^2(X_p - X_r)^2 + a^2(Y_q - Y_s)^2 + H^2]^2} \tag{3.10}$$

$$B_4(X_r,Y_s) = \frac{\rho_4 a^4 H^2}{\pi} \sum_{p=1}^{n} \sum_{q=1}^{n} \frac{W_p W_q B_2(X_p,Y_q)}{[a^2(X_p - X_r)^2 + (Y_q - Y_s)^2 + H^2]^2} \tag{3.11}$$

$$R_2 = \epsilon_2 \sigma T_2^4 B_2(X_p,Y_q) + \epsilon_4 \sigma T_4^4 B_4(X_r,Y_s) \tag{3.12}$$

Because of the similarity of the computations regardless of the value of n, only the n = 1 case will be discussed.

n = 1 $\quad X_1 = 0.5$, $Y_1 = 0.5$, $W_1 = 1$

$H = 1$ ft
$a = 1$ ft
$\epsilon_1 = \epsilon_2 = 0.556$
$\rho_1 = \rho_2 = 0.444$
$T_1 = 1231°R$
$T_2 = 525°R$

Because of symmetry resulting from the fact that both plates are square, the (n = 2) case with eight equations and eight unknowns reduces to the (n = 1) case with two equations and two unknowns.

$$B_2(X_1,Y_1) = 1 + \frac{\rho_2}{\pi} B_4(X_1,Y_1) \tag{3.10}$$

$$B_4(X_1,Y_1) = \frac{\rho_4}{\pi} B_2(X_1,Y_1) \tag{3.11}$$

$$R_2 = \epsilon_2\sigma\, T_2^4 B_2(X_1,Y_1) + \epsilon_4\sigma T_4^4 B_4(X_1,Y_1) \qquad (3.12)$$

Solving equation 3.10 and equation 3.11 for $B_2(X_1,Y_1)$ and $B_4(X_1,Y_1)$ and substituting in equation 3.12 for H = 1.0 gives

$$R_2 = 2241.17 \text{ Btu hr}^{-1} \text{ ft}^{-2}$$
$$R_4 = 389.07 \text{ Btu hr}^{-1} \text{ ft}^{-2}$$

Substituting these results in equation 3.7

$$\begin{aligned} Q_2 &= \frac{\epsilon_2}{\rho_2}(\sigma T_2^4 - R_2) \\ Q_4 &= \frac{\epsilon_4}{\rho_4}(\sigma T_4^4 - R_4) \end{aligned} \qquad (3.7)$$

yields the radiant flux at Plane 2 and Plane 4

$$Q_2 = 2117.33 \text{ Btu hr}^{-1} \text{ ft}^{-2}$$
$$Q_4 = -324.32 \text{ Btu hr}^{-1} \text{ ft}^{-2}$$